THE UNIVERSITY OF MICHIGAN

COLLEGE OF ENGINEERING
Department of Nuclear Engineering

Technical Report

RAYLEIGH SCATTERING OF RUBY LASER LIGHT IN NEUTRAL GASES

Ralph R. Rudder
David R. Bach

ORA Project 07599

sponsored by:

Advanced Research Projects Agency
Project DEFENDER
ARPA Order No. 675

under contract with:

U.S. ARMY RESEARCH OFFICE-DURHAM
CONTRACT NO. DA-31-124-ARO(D)-403
DURHAM, NORTH CAROLINA

administered through:

OFFICE OF RESEARCH ADMINISTRATION ANN ARBOR

November 1967

This report was also a dissertation submitted by the first author in partial fulfillment of the requirements for the degree of Doctor of Philosophy in The University of Michigan, 1967.

ACKNOWLEDGMENTS

The author wishes to acknowledge the many stimulating and helpful discussions with his thesis advisor, Associate Professor David R. Bach. The assistance of several other faculty members is warmly appreciated: Professor Richard K. Osborn, with whom many hours were profitably spent discussing theoretical aspects of this dissertation, Associate Professor Glenn F. Knoll, and Professor Paul F. Zweifel, who elevated many discussions to a high plane. Much gratitude is due to Dr. Carl M. Penney, who suggested this problem and whose guidance through the early days of this research was invaluable. Thanks go to many fellow students, including Kenneth Ware, Helmut Koehler, George Darling, and Donald Gillespie, and also to Miss Julie Calver for typing the manuscript.

Without the encouragement, understanding, and love of his family, the author would never have progressed this far.

The author is grateful to the Ford Foundation—Phoenix Memorial Fund and the U.S. Atomic Energy Commission, who provided financial assistance in the form of fellowships for graduate study. The latter stages of the research and publication were supported by the Advanced Research Projects Agency (Project DEFENDER) and were monitored by the U.S. Army Research Office-Durham under Contract No. DA-31-124-ARO-D-403.

TABLE OF CONTENTS

LIST OF TABLES

LIST OF FIGURES

LIST OF FIGURES (Concluded)

ABSTRACT

Measurements are described of Rayleigh scattering from atoms and molecules in the gaseous state at one atmosphere. The use of a Q-switched ruby laser of 8 MW average power and care in minimizing spurious light permitted the determination of very small depolarizations. In agreement with theoretical predictions, the depolarization ratio ρ_v (for linearly polarized light) or argon was found to be vanishingly small ($\rho_v \lesssim 4.10^{-5}$). Similarly, for helium, $\rho_v \lesssim 3.10^{-3}$. However, xenon and methane exhibited nonzero depolarization ratios: 1.55 ($\pm$.25) x10^{-4} and 1.27 ($\pm$.23)x10^{-4}, respectively. It is found that departures from ideal gas behavior provide the most plausible explanation for these findings. Calculations from currently available theory* are presented to support this assertion. The effect of nuclear spin in xenon-129 is considered and shown to contribute negligibly to the measured depolarization.

Depolarization ratios were also measured in hydrogen, deuterium, nitrogen, and nitrous oxide, and found to be lower than generally accepted values.

Measured differential scattering cross sections at 60° for He, Ar, Xe, CH_4, H_2, D_2, N_2, and N_2O were within experimental error of values calculated from known indices of refraction. Previous measurements** at 6943Å had indicated the cross sections were approximately twice as large as the calculated ones. The angular dependence of Rayleigh scattering in N_2 as a function of the polarization states of both incident and scattered radiation was studied from 30° to 150°, and found to be in excellent agreement with theory.

*S. Kielich, Acta. Phys. Polonica 19, 149 (1960).

**T. V. George, L. Goldstein, L. Slama, and M. Yokoyama, Phys. Rev. 137, A369 (1965).

CHAPTER I

INTRODUCTION

The unshifted Rayleigh scattering* of light by atoms and molecules has long been the object of experimental inquiry. This is amply evidenced by the large number of articles that have appeared in the scientific literature of the past fifty years. Although interest had waned somewhat in recent years, the development of the laser as an intense, monochromatic, highly collimated light source stimulated a vigorous renewal of research activity. The major aim of this dissertation has been to make use of the unique properties of the laser to resolve a number of previously unanswered and provocative questions regarding Rayleigh scattering, and to shed new light on several intriguing facets of the phenomenon.

In this introductory chapter a brief review of previous experimental undertakings is first presented. Then the scope of this research is summarized and the more significant findings are pointed out in some detail.

---

*The well-known phenomenon of Rayleigh scattering is an elastic event involving bound electrons. This may be contrasted with the inelastic Raman scattering, in which an energy exchange with the scattering molecule occurs. Of interest in numerous recent laser scattering experiments with plasmas has been Thomson scattering, in which free electrons are involved.

The work undertaken in this dissertation was confined specifically to nonresonant Rayleigh scattering of optical radiation by atoms and molecules in the gaseous state at or near the conditions of STP (temperature 273°K and pressure 29.92 in. Hg). Consequently we shall often, for the sake of brevity, refer to this rather special phenomenon with the single term scattering. When other types of scattering are considered, suitable delineating phrases will be employed. Hopefully no confusion will be caused by this procedure.

1.1 HISTORICAL REVIEW

The first successful observation of Rayleigh scattering in a pure, dust-free gas, reported by Cabannes[11] in 1915, confirmed Lord Rayleigh's contention[47] that the blue color of the sky is primarily due to molecular scattering. Rayleigh's theory, derived on a classical basis, had predicted that the scattering should vary inversely with the fourth power of wavelength.[48] Further corroborating evidence of this was provided by independent experiments of Smoluchowski[54] and Strutt.[55]

Although the original Rayleigh theory had indicated that transversely scattered light should be linearly polarized perpendicular to the plane of observation, regardless of the polarization state of the incident radiation, Strutt[56] and subsequent experimentalists found otherwise. For example, Strutt[56] observed that 3.0% of the light scattered by nitrogen was depolarized; i.e., polarized parallel to the plane of observation. By modifying his theory to include the effects of molecular asymmetry, Rayleigh[49] was able to qualitatively account for this originally unpredicted effect.

Now recognizing the nature of its origin, researchers actively investigated the phenomenon of depolarization for many substances with the hope of furthering the knowledge of molecular structure. Unfortunately these researchers were limited by various experimental difficulties, as evidenced by the wide dispersion of depolarization ratios (the ratio of the weak, depolarized component to the strong one) measured in independent

studies. To illustrate this remark, consider the depolarization ratios measured for CO_2 by Strutt[56,57] (8.0 and 11.7%), Gans[21] (7.3%), Raman and Rao[43] (10.6%), Cabannes and Granier[13] (9.8%), Rao[46] (9.7%), Volkman[60] (7.24%), and Parthasarathy[38] (9.22%) between 1919 and 1951.

Particularly perplexing has been the situation of scatterers possessing spherically symmetric charge structures and zero total angular momentum. According to Rayleigh theory, the depolarization ratios of such molecules should vanish. However this has never been adequately demonstrated, and consequently has long been a source of argument and frustration.[5]

Although the study of depolarizations is the most potentially fruitful area of scattering research, there has been substantial interest in measuring cross sections for various gases and in investigating the angular behavior of scattering. The primary motivation for these studies has been to test the validity of the Rayleigh theory.

Owing to their difficulty, very few absolute measurements of differential scattering cross sections have been undertaken. Much more common have been experiments to determine relative scattering intensities for various gases. The original Rayleigh theory predicted that the ratio of scattering intensities from two gases "A" and "B" should depend only on their indices of refraction as $(\mu_A-1)^2/(\mu_B-1)^2$. This dependence was verified approximately by Rayleigh himself.[56] Later, when the theoretical cross section was modified to include depolarization effects, even better agreement with experimental values was obtained.[49]

Although experiments to directly measure scattering cross sections are quite difficult, a few have been attempted. Cabannes[12] performed the first absolute measurement, using his experimental cross section for argon to determine a value for Avogardo's number of 6.90×10^{23}. A later measurement by Daure[17] in ethyl chloride vapor achieved a somewhat higher degree of accuracy. However, T. V. George and co-workers at the University of Illinois, who performed the first laser-scattering experiment, reported the startling result that the cross sections they measured at 6943Å were approximately twice as large as calculated ones.[22] Neither coherence effects nor departures from linearity appear to account adequately for this factor of two, and these measurements have been a source of mystery.

Quite early it was recognized that an investigation of the angular distribution of scattering would be a valuable addition to the inventory of knowledge concerning Rayleigh scattering. However, until the appearance of the laser, an experiment to determine this angular dependence was not considered feasible. The prime reason for this was that with conventional light sources, it was necessary to use condensing lenses to strongly focus the light through the scattering volume. The finite convergence angle of the incident radiation did not permit a successful interpretation of angular data. For this and other reasons, all scattering experiments were originally performed at 90°.

Using a ruby laser, George et al.,[22] performed the first scattering measurements at angles differing from 90°. They examined the scattering

from 45° to 135° in argon and xenon for vertically and horizontally polarized incident light.* Although the results for horizontally polarized light agreed with theoretical predictions, a striking departure was observed for the case of vertical polarization. This was a surprising and completely unforseen result, and consequently provoked a good deal of controversy and conjecture.[30,58,59]

However, most of this controversy was laid aside when Watson and Clark[61] reported the results of their studies of scattering in nitrogen from 40° to 140°. Also using a ruby laser, they could detect no departures from theory for either polarization state of the ruby light. Furthermore, studies of the angular dependence of Rayleigh and Raman scattering in liquids were in accord with theory.[16,30,42]

1.2 SCOPE OF THIS RESEARCH

During the past several years, we have carried out a number of Rayleigh scattering experiments using a high-power pulsed ruby laser. The many questions raised by the discrepancies in measured cross sections, depolarizations, and the angular distribution of scattering prompted experimental studies in all of these areas of research.

Probably the most important contributions of this work have been in the realm of depolarization measurements. Of main interest have been

*Since all angular experiments have been performed about the horizontal plane, we shall refer to the two polarization states of interest—perpendicular and parallel to the plane—as vertical and horizontal, respectively.

spherically symmetric scatterers, in particular the atoms helium, argon and xenon and the tetrahedral molecule methane. There has never been a truly conclusive experimental demonstration that these particles do not depolarize, as is stipulated by theory. Most nonzero measurements have been explained away as being due to various instrumental defects. Those experiments which reported "zero" values had confidence levels which were too high to completely erase the continuing doubts. By gaining almost a full order of magnitude in the capability of measuring very small depolariaztions, this experiment demonstrated that spherically symmetric scatterers do not, in themselves, depolarize. However, it has also been found that in their departure from true ideal gas behavior, assemblies of spherical molecules can produce measureable, though very small, depolarizations. For example, the depolarization ratio of xenon gas at one atmosphere was measured to be $1.55(\pm.25) \times 10^{-4}$.

A few nonspherical molecules—hydrogen, deuterium, nitrogen, and nitrous oxide—were also studied, the prime motivation having been supplied by the wide dispersion in the depolarization ratios previously measured for these gases. It was felt that this experiment could establish reliable, accurate depolarization ratios as it had reduced or eliminated many early sources of difficulty. Probably the biggest problem in the past was the competing presence of Raman scattered light. Since Raman light may be strongly depolarized, it can contribute appreciably to the measured anisotropy. Almost all previous experiments either failed

to exclude the Raman scattering or only partially reduced it. By using a narrow bandwidth interference filter this experiment succeeded in eliminating all vibrational Raman scattering and in substantially reducing the contribution from pure rotational Raman. As a result, depolarization ratios have been measured which are smaller that those reported in the literature. For example, our value for nitrogen is a factor of 2.8 lower than the average of six previous representative experiments. Although it is not certain that all of the obscuring effects of rotational Raman scattering were removed, at the least new upper limits for Rayleigh depolarization ratios have been determined. More positively, there is evidence which indicates that these upper limits are not far removed from the true values.

The large scattering cross sections found by George et al.,[22] prompted the performance of a similar measurement with nitrogen. Close agreement with the calculated value was obtained. The relative scattering intensities of hydrogen, deuterium, nitrous oxide, helium, argon, xenon, and methane were also studied. In each case, no appreciable departure from the calculated intensity was discovered.

Although it now appears that the validity of Rayleigh theory for the angular distribution of scattering has been established, we nevertheless have included in this thesis the results of our confirming experiment with nitrogen. The main reason for doing this is that this experiment was done not only as a function of the polarization state of incident light but also for that of the scattered light.

In the next chapter the theoretical aspects of Rayleigh scattering pertinent to the experimental work of this thesis will be discussed. Specifically, the classical derivation of the scattering cross section and depolarization will be briefly presented at first. Then in Section 2.2 the quantum mechanical approach will be outlined. Section 2.3 makes use of the quantum mechanical theory to calculate the depolarizing effect of the nonzero nuclear spin of Xe^{129}. It is found that this mechanism cannot account for the measured depolarization in xenon gas.

Chapter III deals with the experimental design. The success of this experiment was due in good measure to the incorporation into the design of a number of recent technological advances. There have been, for example, significant advances in optical sources, optical detectors, optical filters, and gas purities. The laser is a distinct improvement over previously available light sources, particularly in terms of the parallelism and excellent collimation of its output beam. Also its high power and monochromacity make the laser a logical choice for scattering experiments. The development of electronic photodetection devices has also proven a boon to the experimentalist working in the area. These devices exhibit extremely high gains, some more than 10^7, and a wide range of linearity extending over many decades. Consequently the photographic method, long a part of Rayleigh scattering measurements, has largely been rendered obsolete. Multilayer interference filters have now reached a stage of perfection such that they may be used to discriminate effectively against

Raman scattered light without severly reducing the Rayleigh component. Finally there are now commercially available ultrapure gases whose impurity levels are so low that they cause no detectible scattering effects.

In Chapter IV the experimental methods employed are elucidated. Since our methods differed in several aspects from those of previous experiments, they are presented in detail. It is hoped this will enable future experimenters to avoid some of the many pitfalls encountered during the course of this research. Of particular interest should be Section 4.1, in which the techniques employed to reduce spurious light are described. Spurious light is light measured when the scattering volume is evacuated, and hence places a lower limit on the intensity of scattering that can be detected. Other topics covered in Chapter IV are the general procedure followed in scattering measurements (Section 4.2), and the calibration method employed to measure absolute values for scattering cross sections (Section 4.3).

The fifth chapter presents final results for cross sections (5.2), the angular distribution in nitrogen (5.3) and depolarization ratios (5.4). These results are analyzed in terms of presently available theory, and the contributions of various experimental errors are calculated.

Finally in Chapter VI, the conclusions of this work are summarized and proposals for possibly interesting future work are suggested.

CHAPTER II

THEORY

In this chapter, of prime concern will be those aspects of Rayleigh scattering theory that are most directly applicable to the experimental research carried out. Our efforts in presenting this material are not in any way intended to provide a complete analysis of the process, and the interested reader is referred to the more substantive works of Rayleigh,[48] Cabannes,[14] Born,[6] Placzek,[41] Penney,[40] and others.

The classical approach is first presented as it yields essentially all of the "right" answers and also gives free rein to physical insight and intuition. The quantum mechanical derivation is somewhat more rigorous and aesthetically pleasing. It also contains in its formulation the mechanism for calculating depolarizations directly. Consequently the effect of the nonzero nuclear spin of xenon-129 has been computed.

2.1 CLASSICAL THEORY

The classical approach to the scattering process is a straightforward one requiring only a few assumptions:

(a) The incident wavelength is large compared to molecular dimensions.

(b) The incident frequency is far removed from any resonances of the scattering system.

(c) The ideal gas law holds so that scattering intensity from individual particles may be added arithmetically. This implies that no coherent interference of scattered waves occurs.

The classical view of a scattering event is pictured in Fig. 2.1. An electromagnetic wave is incident in the y direction and linearly polarized such that its electric vector is

$$\underline{E} = \hat{\underline{z}}\, E_o \cos(\omega_1 t) \tag{2.1}$$

This wave causes the bound electron to oscillate with identical frequency ω_1, the dipole moment induced being

$$\underline{p} = \alpha \underline{E} \tag{2.2}$$

where the polarizability α is a scalar for the simple case (initially assumed) of spherically symmetric electronic charge distribution.

By employing the classical rules for the radiation emitted by an oscillating dipole, a scattering cross section can be computed. The far field of the emitted (scattered) radiation is

$$E_s = \frac{\omega_1^2 p}{c^2 r} \sin\xi \tag{2.3}$$

where c is the speed of light in vacuum, r is the distance from the electron to the detector, and ξ is the polar scattering angle shown in the figure. The Poynting vector $\underline{S}$ is readily calculated for the scattered radiation:

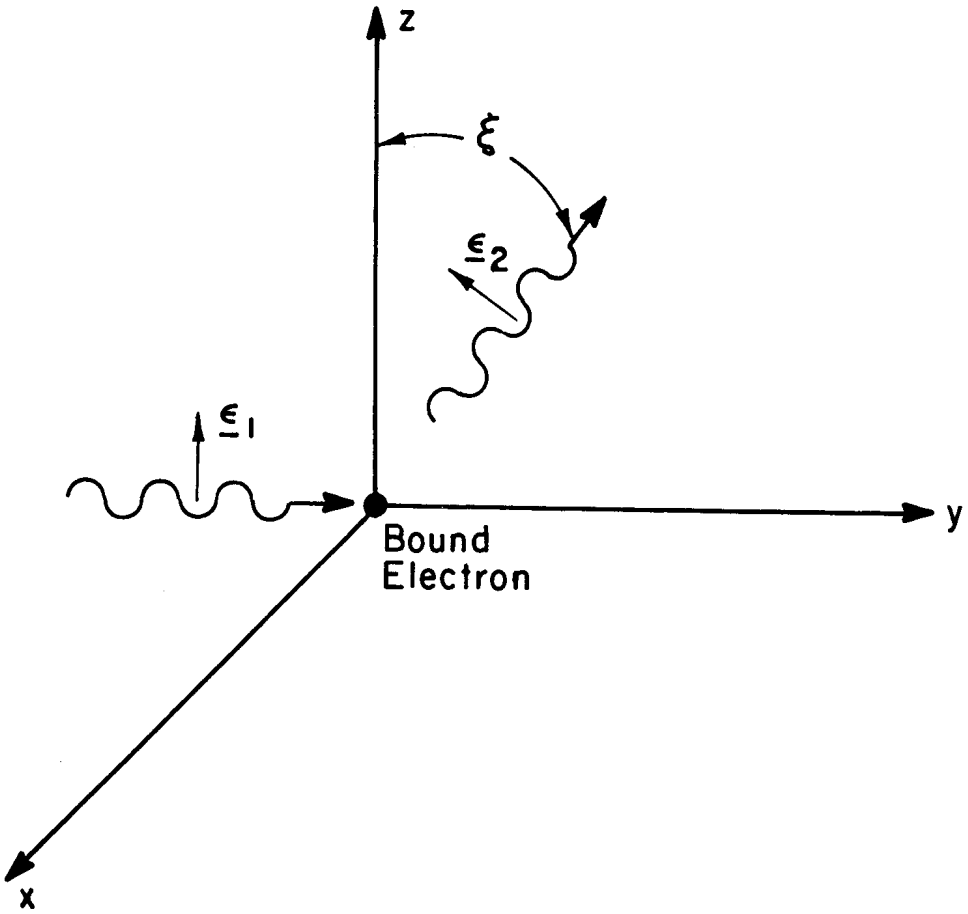

Fig. 2.1. Schematic of Rayleigh scattering process for classical analysis.

$$\underline{S} = \frac{c}{4\pi} \underline{E}_s \times \underline{H}_s = \frac{\omega_1^4 p^2 \sin^2\xi}{4\pi r^2 c^3} \hat{\underline{r}}$$

Multiplying by $r^2 d\Omega_2$, using Eq. (2.2) for p, and averaging over a period of oscillation, the average energy $\mathcal{E}_S$ radiated into solid angle $d\Omega_2$ is obtained:

$$\mathcal{E}_S d\Omega_2 = \frac{\omega_1^4 \alpha^2 E_o^2 \sin^2\xi}{8\pi c^3} d\Omega_2$$

Since the differential scattering cross section is defined as the ratio:

$$\sigma d\Omega_2 = \frac{\text{energy scattered into solid angle } d\Omega_2/\text{mol}}{\text{incident energy/cm}^2} \qquad (2.4)$$

one need merely divide $\mathcal{E}_S d\Omega_2$ by the average incident energy/cm^2, $cE_o^2/8\pi$:

$$\sigma d\Omega_2 = \frac{\omega_1^4 \alpha^2 \sin^2\xi}{c^4} d\Omega_2 \qquad (2.5)$$

The Lorentz-Lorenz relation may be used to express the polarizability in terms of the refractive index μ:

$$\alpha = \frac{\mu^2 - 1}{4\pi N_o} \qquad (2.6)$$

where N_o is the number density of scatterers. Since for most gases $\mu \simeq 1$, one may closely approximate μ^2-1 as $2(\mu-1)$. Employing this relation and expressing the cross section in terms of the incident wave-

length λ_1 rather than frequency, one finds:

$$\sigma d\Omega_2 = \frac{4\pi^2(\mu-1)^2 \sin^2\xi}{\lambda_1^4 N_o^2} d\Omega_2 \qquad (2.7)$$

One may observe the characteristic $1/\lambda^4$ dependence of the cross section, which, for example, is responsible for the blue appearance of the sky. This also demonstrates that the choice of a ruby laser operating in the red portion of the spectrum is less than ideal. However the many advantages of the ruby laser compensate for this detraction.

The direct connection of the scattering cross section with the refractive index illustrates the intimate relationship of the two phenomena; in fact refraction may be treated as forward scattering.

The angular nature of the scattered light is fully described by the $\sin^2\xi$ factor. Thus for vertically polarized incident light, the scattering intensity along the horizontal plane is constant, while for horizontally polarized light, the scattering varies as $\cos^2\theta$, where θ is the angle of scattering with respect to the forward beam.

The transversely scattered light should be completely (vertically) polarized, independent of the polarization state of the incident wave. As previously mentioned, this part of the theory was not borne out by early experiments. It was subsequently realized that most scatterers are not spherically symmetric in their optical properties and that the scattering consequently depends on the orientation of the molecule.

Introduction of this into the theory is done via the polarizability, which becomes a tensor of second order rather than a simple scalar.

With the scattering molecule in some arbitrary orientation, the induced moment is generally in some other direction than the incident field. Its i^{th} component is given by:

$$P_i = \sum_j \alpha_{ij} E_j \tag{2.8}$$

Each molecule has a set of principal axes for which α is diagonal. By convention:

$$\begin{aligned} \alpha_{xx} &\equiv A \\ \alpha_{yy} &\equiv B \\ \alpha_{zz} &\equiv C \\ \alpha_{ij} &= 0 \qquad i \neq j \end{aligned} \tag{2.9}$$

Using this information, one can now calculate the depolarization ratio ρ_v for z-polarized incident light. This is simply the ratio for transverse scattering of the y-polarized component to the z-polarized one. Recalling that the scattering cross section varies as p^2, ρ_v is obtained by averaging over all molecular orientations* to find $< p_z^2 >$ and $< p_y^2 >$. The result is:

$$\rho_v = \frac{\langle P_y^2 \rangle}{\langle P_z^2 \rangle} = \frac{A^2 + B^2 + C^2 - AB - BC - AC}{3(A^2+B^2+C^2) + 2(AB+BC+AC)} \tag{2.10}$$

It is convenient to define a mean polarizability α for the molecule and an anisotropy factor γ^2 as:

$$\alpha \equiv \frac{1}{3}(A + B + C) \tag{2.11}$$

*Again the ideal gas assumption must be invoked in order to perform the averaging process.

$$\gamma^2 \equiv A^2 + B^2 + C^2 - AB - BC - AC \qquad (2.12)$$

Then ρ_v may be re-expressed as:

$$\rho_v = \frac{3\gamma^2}{45\alpha^2 + 4\gamma^2} \qquad (2.13)$$

Another anisotropic parameter that appears frequently is δ, defined as:

$$\delta \equiv \frac{A^2 + B^2 + C^2 - AB - BC - AC}{(A + B + C)^2} = \frac{\gamma^2}{9\alpha^2} \qquad (2.14)$$

The primary use of the depolarization ratio ρ_v in this dissertation is mainly a matter of personal preference. The depolarization ratio commonly seen in the literature is the one defined for <u>unpolarized</u> incident light, and is simply related to ρ_v:

$$\rho_u = \frac{2\rho_v}{1 + \rho_v} \qquad (2.15)$$

They are entirely equivalent expressions of molecular anisotropy.

There have been a few attempts to calculate depolarization ratios on a classical basis. The model employed postulated that the measured anisotropy was due to the mutual interaction of dipole moments induced in the constituent atoms of the molecule. The first attempts with this approach were those of Silberstein.[53] Ramanathan[45] and Havelock[24] subsequently obtained numerical results. However these classical calculations have never proved to yield any more than qualitative agreement with experimental values.

The scattering cross section of Eq. (2.7) must be modified to include the effects of depolarization. This modification was studied by Born,[6] and his results may be rearranged to yield:

$$\sigma_{12}\, d\Omega_2 = \sigma_{zz} \left[(1 - \rho_v) \cos^2 \psi + \rho_v \right]$$

where (2.16)

$$\sigma_{zz} \equiv \frac{4\pi^2 (\mu - 1)^2}{\lambda_1^4 N_o^2} \left(\frac{3}{3 - 4\rho_v} \right)$$

The cross section σ_{12} is defined for the scattering of an electromagnetic wave from state "1" to state "2," where the initial state is characterized by frequency ω_1, propagation direction $\underline{\Omega}_1$ and polarization vector $\underline{\epsilon}_1$, and the scattered wave propagates in direction $\underline{\Omega}_2$ with polarization $\underline{\epsilon}_2$. The angle between the two polarization vectors is ψ.

The angular dependence of scattering is completely described by Eqs. (2.16). However, it is instructive to express the scattering about the horizontal plane in terms of the scattering angle Θ. Four cross sections are of interest for the four possible combinations of incident and scattered polarizations. The double subscripts on the cross sections refer to the vertical (V) or horizontal (H) polarization states of incident and scattered radiation, respectively:

$$\sigma_{VV}(\Theta) = \sigma_{zz} \tag{2.17a}$$

$$\sigma_{VH}(\Theta) = \sigma_{zz}\, \rho_v \tag{2.17b}$$

$$\sigma_{HV}(\theta) = \sigma_{zz}\,\rho_v \tag{2.17c}$$

$$\sigma_{HH}(\theta) = \sigma_{zz}\left[\cos^2\theta + \rho_v(1-\cos^2\theta)\right] \tag{2.17d}$$

2.2 QUANTUM MECHANICAL TREATMENT

Employing the correspondence principle, Kramers and Heisenberg[28] in 1925 performed the first quantum mechanical analysis of Rayleigh scattering. It is interesting to note that their theory also suggested the possibility of an inelastic scattering event occurring during which the energy state of the scattering molecule changed by a discrete amount. When Raman[44] observed this inelastic scattering in 1928, he made a valuable contribution to the efforts to substantiate quantum mechanics.

Dirac,[20] employing a modern formulation of quantum mechanics, confirmed the results of Kramers and Heisenberg. Later work by Placzek[41] explored numerous facets of both Rayleigh and Raman scattering, particularly the application of group theory to relate scattering phenomena to molecular symmetry properties. Other than studies of scattering near a resonance, there have been relatively few applications of quantum theory to Rayleigh scattering since Placzek's.

In the next several pages will be outlined a quantum mechanical derivation of the important aspects of Rayleigh scattering, following the approach of Penney.[40] The assumptions employed are essentially the

same as those used in the classical derivation. Thus, resonant scattering is ruled out. Also only incident waves are considered which are large compared to molecular dimensions, so that only dipole interactions are of importance. Finally scattering from a single molecule is initially considered; then the ideal gas assumption is invoked so that the effects of scattering from many particles in the gaseous state may be obtained by a simple addition process.

Since the scattering problem cannot be solved rigorously, an approximation approach, based on time-dependent perturbation theory, is necessary. Thus the Hamiltonian for the system is broken into two parts, the zero order contribution H^o and a perturbing part V:

$$H = H^o + V \tag{2.18}$$

H^o, in turn, consists of two parts, the first being a Hamiltonian H^M for the internal motion* of the molecule. Because of the inverse dependence on mass, only the electrons are treated. Thus:

$$H^M = \sum_j^{N_e} \frac{p_j^2}{2m} \tag{2.19}$$

*In the consideration of scattering from a single particle, it is convenient to remove the dependence on external motion by introducing a center-of-mass transformation. Consequently the "internal motion" referred to is that of the electrons and nuclei about the molecular center of mass. Observe that masses m, charges e, and momenta p are reduced electronic masses, charges, and momenta associated with the particular transformation required by the molecule of interest.

where p_j is the (reduced) momentum of the j^{th} (of N_e total) electron. The second part of H^O is a Hamiltonian H^R for the radiation fields in a cubic cell of side L. Using the standard Fourier technique and requiring that periodic boundary conditions on the cell walls be satisfied, one has:

$$H^R = \sum_\lambda \hbar c k_\lambda \alpha_\lambda^+ \alpha_\lambda \tag{2.20}$$

where α^+ and α are the well-known photon creation and destruction operators. The λ summation implies a sum over all propagation vectors $\underrightarrow{k}_\lambda$ allowed by the boundary conditions and over the two orthogonal polarization states $\underrightarrow{\epsilon}_\lambda$ associated with each $\underrightarrow{k}_\lambda$.

The perturbation consists of terms relating to the interaction between the radiation field and the bound electrons:

$$V = V^1 + V^2 \tag{2.21}$$

where

$$V^1 = \sum_j^{N_e} \frac{e}{mc} \underline{A}_j \cdot \underline{P}_j \tag{2.22}$$

$$V^2 = \sum_j^{N_e} \frac{e^2}{2mc^2} \cdot A_j^2 \tag{2.23}$$

The vector potential $\underline{A}_j$ is given by:

$$\underline{A}_j = \sum_\lambda \left(\frac{2\pi\hbar c}{L^3 k}\right)^{1/2} \underline{\epsilon}_\lambda \cdot \left[\alpha_\lambda^+ e^{-i\underline{k}_\lambda \cdot \underline{r}_j} + \alpha_\lambda e^{i\underline{k}_\lambda \cdot \underline{r}_j} \right] \tag{2.24}$$

where $\underline{r}_j$ is the location of the j^{th} electron from the center of mass.

The eigenfunctions of the unperturbed Hamiltonian factor into internal and radiation state functions. That is:

$$H^{\circ}|b\rangle|\eta\rangle = (E_b + E_\eta)|b\rangle|\eta\rangle \tag{2.25}$$

where

$$H^{M}|b\rangle = E_b|b\rangle \tag{2.26}$$

and

$$H^{R}|\eta\rangle = E_\eta|\eta\rangle \tag{2.27}$$

The radiation states further factor:

$$|\eta\rangle = |\eta_1\rangle|\eta_2\rangle \cdots |\eta_\lambda\rangle \cdots \tag{2.28}$$

where η_λ is the number of photons having propagation vector $\underline{k}_\lambda$ and polarization state $\underline{\epsilon}_\lambda$.

An analysis of the scattering event requires a consideration of the transition in the system from an initial state "i" to a final state "f" described by:

$$|i\rangle = |b\rangle|\eta_1\rangle|\eta_2\rangle|\eta_R\rangle \equiv |b\rangle|\eta\rangle \tag{2.29}$$

$$|f\rangle = |b'\rangle|\eta_1 - 1\rangle|\eta_2 + 1\rangle|\eta_R\rangle \equiv |b'\rangle|\eta'\rangle \tag{2.30}$$

Thus in the scattering process the number of photons in state "1" decrease by one, the number in state "2" increase by one, while the remaining photon states (schematically designated $|\eta_R>$) are unchanged. Since Raman scattering can be included in this treatment without additional complication, the internal molecular state will be allowed to change from $|b>$ to $|b'>$. Later when the analysis is specialized to Rayleigh scattering, the requirement that $|b'> = |b>$ will be imposed.

The probability per unit time for the scattering transition to take place is given by

$$T_{i\to f} = \frac{2\pi}{\hbar} \left| V_{fi} - \sum_{g}{}' \frac{V_{fg} V_{gi}}{E_{gi}} \right|^2 \delta(E_{fi}) \qquad (2.31)$$

where the summation over all accessible intermediate states "g" is restricted from including the initial and final states. The double subscript notation on the perturbation V implies that matrix elements are taken between the two indicated states. On the other hand, $E_{fi} \equiv E_f - E_i$. Conservation of energy is implied by the delta function $\delta(E_{fi})$. The transition probability of Eq. (2.31) is the result of carrying perturbation theory to second order. This is necessary if the scattering process is to be described with sufficient accuracy.

The calculation of the transition probability is substantially simplified by virtue of the fact that V^1 connects only those radiation states which are identical except for the addition or subtraction of a single photon. Furthermore V^2 only connects those states which are either the same, or for which two occupation numbers are different (each

changing by one), or for which one occupation number increases or decreases by two. Consequently in the first term within the absolute square of Eq. (2.31), all matrix elements of V^1 vanish, and in the second term, products of matrix elements of V^1 with matrix elements of V^2 also vanish. The fourth order corrections due to products of matrix elements of V^2 are neglected in this analysis. Thus the transition probability becomes:

$$T_{b\eta\to b'\eta'} = \frac{2\pi}{\hbar}\,\delta(E_{b'\eta',b\eta}) \left| (V^2)_{b'\eta',b\eta} - \sum_{b''\eta''}{}' \frac{(V')_{b\eta,b''\eta''}\,(V')_{b''\eta'',b'\eta'}}{E_{b''\eta'',b\eta}} \right|^2 \tag{2.32}$$

where b" and η" refer to permissible intermediate particle and photon states, respectively. The matrix elements between photon states of V^1 and V^2 may be calculated in a straightforward manner. Also employing the dipole approximation, one finds:

$$T_{b\eta\to b'\eta'} = \frac{2\pi}{\hbar^2}\left(\frac{e^2}{mc^2}\right)^2\left(\frac{2\pi\hbar c}{L^3}\right)^2 \frac{\eta_1(1+\eta_2)}{k_1 k_2}\left|a_{b'b}\right|^2 \cdot \delta(\omega_{b'b}-\omega_{12}) \tag{2.33}$$

where

$$a_{b'b} \equiv N_e\,\underline{\epsilon}_1\cdot\underline{\epsilon}_2\,\delta_{b'b} - \frac{1}{\hbar m}\sum_{b''}\left[\frac{\langle b'|P_2|b''\rangle\langle b''|P_1|b\rangle}{\omega_{b''b}-\omega_1} + \frac{\langle b'|P_1|b''\rangle\langle b''|P_2|b\rangle}{\omega_{b''b'}+\omega_1}\right] \tag{2.34}$$

$$\omega_{b''b} \equiv \frac{1}{\hbar}(E_{b''}-E_b) \tag{2.35}$$

$$P_\lambda \equiv \sum_{j}^{N_e} \underline{P}_j\cdot\underline{\epsilon}_\lambda \tag{2.36}$$

Observe that the presence of ω_{12}, the difference between the incident and scattered frequencies, results from the earlier generalization to include Raman scattering. For Rayleigh scattering, of course, ω_{12} vanishes.

Following suitable manipulations to remove the explicit dependence on electron momenta, one has:

$$a_{b'b} = \frac{m\omega_1(\omega_1 - \omega_{b'b})}{\hbar} \sum_{b''} \left[\frac{\langle b'|r_2|b''\rangle\langle b''|r_1|b\rangle}{\omega_1 - \omega_{b''b}} - \frac{\langle b'|r_1|b''\rangle\langle b''|r_2|b\rangle}{\omega_1 + \omega_{b''b'}} \right] \tag{2.37}$$

where

$$r_\lambda = \sum_j^{N_e} \underline{r}_j \cdot \underline{\epsilon}_\lambda \tag{2.38}$$

The "quantum" polarizability tensor $(c_{12})_{bb'}$ is simply related to a'_{bb} by

$$(c_{12})_{bb'} = \frac{e^2}{m\omega_1(\omega_1 - \omega_{b'b})} a^*_{b'b} \tag{2.39}$$

or

$$(c_{12})_{bb'} = \frac{1}{\hbar} \sum_{b''} \left[\frac{\langle b|D_1|b''\rangle\langle b''|D_2|b'\rangle}{\omega_{b''b} - \omega_1} + \frac{\langle b|D_2|b''\rangle\langle b''|D_1|b'\rangle}{\omega_{b''b'} + \omega_1} \right] \tag{2.40}$$

where $\underline{D}$ is the dipole moment operator:

$$D_\lambda = e r_\lambda$$

Studies of this polarizability tensor will yield all necessary information regarding the scattering cross section itself. In order to see how c_{12} is related to the cross section, we return to the transition

probability and note that one is really interested in the transition from photon state η to state η'. Consequently the transition probability is averaged over all initial particle states and summed over all final ones:

$$T_{\eta \to \eta'} = \sum_{b b'} P_b \, T_{b\eta \to b'\eta'} \tag{2.41}$$

where P_b is the probability the molecule is initially in state $|b>$.

The cross section σ_{12} for a photon of polarization $\underline{\epsilon}_1$, frequency ω_1, and propagating in direction $\underline{\Omega}_1$ to be scattered into solid angle $d\Omega_2$ about direction $\underline{\Omega}_2$ with polarization $\underline{\epsilon}_2$ and frequency ω_2 is:

$$\begin{aligned} \sigma_{12}\, d\Omega_2 &\equiv \sigma(\underline{\epsilon}_1, \omega_1, \underline{\Omega}_1 \to \underline{\epsilon}_2, \omega_2, \underline{\Omega}_2)\, d\Omega_2 \\ &= \left(\frac{L^3}{n_1 c}\right)\left(\frac{L}{2\pi}\right)^3 T_{\eta \to \eta'} \cdot d\Omega_2 \end{aligned} \tag{2.42}$$

Substituting Eqs. (2.41), (2.33), and (2.39), and using the free space dispersion relation ($\hbar c k_\lambda = \hbar \omega_\lambda$), one has

$$\sigma_{12}\, d\Omega_2 = \sum_{b b'} P_b \, (\sigma_{12})_{bb'}\, d\Omega_2 \tag{2.43}$$

where

$$(\sigma_{12})_{bb'} = \frac{\omega_1 (\omega_1 - \omega_{b'b})^3}{c^4} \left| (C_{12})_{bb'} \right|^2 \tag{2.44}$$

We have set $\eta_2 = 0$ as it otherwise contributes to stimulated scattering, which is not considered in this analysis.

The angular dependence of scattering is derived easily by further consideration of $|c_{12}|^2$, as this is the only part of the cross section

(2.44) depending on angle. To do this, we introduce a coordinate system oriented such that $\underline{\epsilon}_1$ is along the z-axis and $\underline{\epsilon}_2$ is in the xz plane. Then:

$$D_1 = D_z \tag{2.45}$$

$$D_2 = D_x \sin\Psi + D_z \cos\Psi \tag{2.46}$$

where ψ is the angle between $\underline{\epsilon}_1$ and $\underline{\epsilon}_2$. Putting these in Eq. (2.40):

$$(C_{12})_{bb'} = \frac{1}{\hbar} \sum_{b''} \left[\frac{\langle b | D_z | b'' \rangle \langle b'' | D_x \sin\Psi + D_z \cos\Psi | b' \rangle}{\omega_{b''b} - \omega_1} + \frac{\langle b | D_x \sin\Psi + D_z \cos\Psi | b'' \rangle \langle b'' | D_z | b' \rangle}{\omega_{b''b'} + \omega_1} \right] \tag{2.47}$$

In order to further analyze this, it is necessary to make use of pertinent properties of the particle eigenstates $|b>$. The properties derive from the fact that the total internal angular momentum $\underline{J}$ is a constant of the motion. Thus the eigenstates can be chosen to be eigenfunctions of J^2 and J_z, and $|b>$ can be designated $|\tau JM>$:

$$J^2 |\tau JM\rangle = J(J+1) |\tau JM\rangle \tag{2.48}$$

$$J_z |\tau JM\rangle = M |\tau JM\rangle \tag{2.49}$$

and also

$$H^M |\tau JM\rangle = E_{\tau J} |\tau JM\rangle \tag{2.50}$$

The quantum number τ is used to denote all those quantum numbers other than J and M necessary to describe the state of the molecule.

For eigenfunctions of the type $|\tau JM>$, there are well-known selection rules for matrix elements of D_X and D_Z.[15] Specifically:

$$\langle \tau' J' M' | D_z | \tau J M \rangle = 0 \qquad M' \neq M$$

$$\langle \tau' J' M' | D_x | \tau J M \rangle = 0 \qquad M' \neq M \pm 1 \tag{2.51}$$

The eigenfunctions $|\tau JM>$ are now introduced into Eq. (2.47), and the sum over M" is readily accomplished by applying the selection rules above:

$$(c_{12})_{\tau JM \to \tau' J' M'} = \sum_{\tau'' J''} \left[\frac{\langle \tau J M | D_z | \tau'' J'' M \rangle \langle \tau'' J'' M | D_x \sin\Psi + D_z \cos\Psi | \tau' J' M' \rangle}{\omega_{\tau'' J'', \tau J} - \omega_1} \right.$$

$$\left. + \frac{\langle \tau J M | D_x \sin\Psi + D_z \cos\Psi | \tau'' J'' M' \rangle \langle \tau'' J'' M' | D_z | \tau' J' M' \rangle}{\omega_{\tau'' J'', \tau' J'} + \omega_1} \right] \tag{2.52}$$

Upon taking the absolute square of c_{12}, one observes that coefficients of sin ψ vanish when M' = M while coefficients of cos ψ vanish when $M' \neq M$. Thus no cross products of sin ψ with cos ψ survive, and one simply has:

$$\left| (c_{12})_{\tau JM \to \tau' J' M'} \right|^2 = \cos^2\Psi \left| (c_{zz})_{\tau JM \to \tau' J' M'} \right|^2 + \sin^2\Psi \left| (c_{zx})_{\tau JM \to \tau' J' M'} \right|^2 \tag{2.53}$$

Using Eq. (2.44):

$$(\sigma_{12})_{\tau JM \to \tau' J' M'} = \cos^2\Psi \, (\sigma_{zz})_{\tau JM \to \tau' J' M'} + \sin^2\Psi \, (\sigma_{zx})_{\tau JM \to \tau' J' M'} \qquad (2.54)$$

Recalling the definition of the depolarization ratio ρ_v, it is clear that:

$$(\rho_v)_{\tau JM \to \tau' J' M'} = \frac{(\sigma_{zx})_{\tau JM \to \tau' J' M'}}{(\sigma_{zz})_{\tau JM \to \tau' J' M'}} \qquad (2.55)$$

Using this in Eq. (2.54), employing a simple trigonometric identity, and returning to more compact notation, one arrives at:

$$(\sigma_{12})_{bb'} = \left\{ [\, 1 - (\rho_v)_{bb'} \,] \cos^2\Psi + (\rho_v)_{bb'} \right\} (\sigma_{zz})_{bb'} \qquad (2.56)$$

This is exactly the same angular dependence calculated in Section 2.1, demonstrating that classical mechanics and quantum mechanics are equally valid in describing this portion of the scattering process.

By employing a quantum mechanical expression for the refractive index μ,[34,7] and proceeding from the theory outlined in this section, it is possible to show that the scattering cross section is proportional to $(\mu-1)^2$, just as was found classically.[40] Although the explicit dependence on the refractive index is the same, the two cross sections are not identical. However, it appears that the so-called quantum correction is negligible away from resonance and in the visible part of the spectrum.

2.3 DEPOLARIZATION THEORY

The applicability of quantum mechanics to the calculation of Rayleigh depolarization ratios has primarily been confined to pinpointing those cases for which ρ_v should vanish. One of the few nonzero calculations is due to Penney,[40] who expressed the depolarization ratio in terms of the emission oscillator strength, and then performed the computation for cesium, whose oscillator strengths are known.

It is easily demonstrated that if the total angular momentum J of a scatterer is zero, then the Rayleigh depolarization vanishes. Since Rayleigh scattering is being considered, $J' = J = 0$, and then necessarily $M' = M = 0$. Recalling the selection rules (2.51), one sees that c_{zx} (and consequently both σ_{zx} and ρ_v) must vanish. This is the basis of the contention that atoms such as helium, argon, and xenon should not depolarize.

In attempting to explain our measured nonzero value for the depolarization ratio of xenon, we have investigated the effect of the nonzero nuclear spin ($\frac{1}{2}\hbar$) of Xe^{129}.* To do this, we note that H^M consists of three parts: Hamiltonians for the electronic motion (H^e), for the nucleus (H^N), and for the interaction between the electrons and the nucleus (H^{eN}):

$$H^M = H^e + H^N + H^{eN} \tag{2.57}$$

*The possibility of atomic depolarization arising from nuclear spin effects has been considered by Placzek.[41] He has indicated that except near resonance, no depolarization from these effects should be observable.

The total angular momentum of the atom, here designated $\underline{F}$, is the sum of the nuclear spin $\underline{I}$ and the total angular momentum of the electrons $\underline{K}$:

$$\underline{F} = \underline{K} + \underline{I} \tag{2.58}$$

Since F^2, F_z, K^2, and I^2 are constants of the motion, the particle eigenstates can be chosen to be $|fmkia\rangle$, where

$$F^2|fmkia\rangle = f(f+1)|fmkia\rangle \tag{2.59}$$

$$F_z|fmkia\rangle = m\,|fmkia\rangle \tag{2.60}$$

$$K^2|fmkia\rangle = k(k+1)|fmkia\rangle \tag{2.61}$$

$$I^2|fmkia\rangle = i(i+1)|fmkia\rangle \tag{2.62}$$

and also

$$H^H|fmkia\rangle = E_{fkia}|fmkia\rangle \tag{2.63}$$

The quantum number a plays the same role as τ of the previous section in representing all the unspecified quantum numbers. The polarizability of Eq. (2.40) now is:

$$(C_{\alpha\tau})^{fkia}_{m\to m'} = \frac{1}{\hbar}\sum_{\substack{f''m''k''\\ i''a''}}\left[\frac{\langle fmkia|D_\alpha|f''m''k''i''a''\rangle\langle f''m''k''i''a''|D_\tau|fm'kia\rangle}{\omega_{b''b}-\omega_1}\right.$$

$$\left. + \frac{\langle fmkia|D_\tau|f''m''k''i''a''\rangle\langle f''m''k''i''a''|D_\alpha|fm'kia\rangle}{\omega_{b''b}+\omega_1}\right] \tag{2.64}$$

Observe we have specialized to the case of Rayleigh scattering, where the final state differs from the initial state at most in the quantum number m. The compact notation b, b" for the frequency subscripts has been retained.

It is now convenient to make use of vector coupling coefficients (here Wigner 3j symbols, as defined, for example, in Messiah[35]) to decompose the eigenvector $|fmkia\rangle$ as follows:

$$|f\,m\,k\,i\,a\rangle = (-1)^{k-i+m}(2f+1)^{1/2}\sum_{\mu}\begin{pmatrix} k & i & f \\ m-\mu & \mu & -m \end{pmatrix}|i\mu\rangle|k\,m-\mu\,a\rangle \qquad (2.65)$$

where

$$\begin{aligned} I_z|i\mu\rangle &= \mu|i\mu\rangle \\ K_z|i\mu\rangle &= (m-\mu)|i\mu\rangle \end{aligned} \qquad (2.66)$$

Then, for example:

$$\langle f\,m\,k\,i\,a|\,D_\alpha\,|f''m''k''i''a''\rangle = \sum_{\mu\mu''}(-1)^{k-i+m}(-1)^{-k''+i''-m''}(2f+1)^{1/2}(2f''+1)^{1/2}$$

$$(x)\begin{pmatrix} k & i & f \\ m-\mu & \mu & -m \end{pmatrix}\begin{pmatrix} k'' & i'' & f'' \\ m''-\mu'' & \mu'' & -m'' \end{pmatrix}\langle i\mu|i''\mu''\rangle\langle k\,m-\mu\,a|\,D_\alpha\,|k''\,m''-\mu''\,a''\rangle \qquad (2.67)$$

The well-known Wigner-Eckart theorem is now employed to express the dipole moment matrix elements in terms of reduced matrix elements, which are independent of magnetic quantum numbers:

$$\begin{aligned} &\langle k\,m-\mu\,a|\,D_\alpha\,|k''\,m''-\mu\,a''\rangle \\ &\quad = (-1)^{k-m+\mu}\langle a\,k\|D\|a''k''\rangle\begin{pmatrix} k & 1 & k'' \\ -m+\mu & \alpha & m''-\mu \end{pmatrix} \end{aligned} \qquad (2.68)$$

The subscript α may take on values 0, ±1, where by definition:

$$D_0 \equiv D_z$$
$$D_{\pm 1} \equiv \mp \frac{\sqrt{2}}{2} (D_x \pm i D_y) \tag{2.69}$$

Using the Wigner-Eckart theorem and also the orthonormality of the $|i\mu\rangle$ eigenstates, Eq. (2.67) becomes:

$$\langle f\, m\, k\, i\, a | D_\alpha | f''\, m''\, k''\, i''\, a'' \rangle = \sum_{\mu} (-1)^{2k - k'' - m'' + \mu} (2f+1)^{1/2} (2f''+1)^{1/2}$$
$$(x)\ \delta_{ii''} \begin{pmatrix} k & i & f \\ m-\mu & \mu & -m \end{pmatrix} \begin{pmatrix} k'' & i & f'' \\ m''-\mu & \mu & -m'' \end{pmatrix} \begin{pmatrix} k & 1 & k'' \\ -m+\mu & \alpha & m''-\mu \end{pmatrix}$$
$$(x)\ \langle a\, k \| D \| a''\, k'' \rangle \tag{2.70}$$

In analyzing Eq. (2.64) it is convenient to define the following:

$$\zeta_{\alpha\sigma} \equiv \sum_{m''} \langle f\, m\, k\, i\, a | D_\alpha | f''\, m''\, k''\, i''\, a'' \rangle \langle f''\, m''\, k''\, i''\, a'' | D_\sigma | f\, m'\, k\, i\, a \rangle \tag{2.71}$$

Using (2.70), this becomes:

$$\zeta_{\alpha\sigma} = \sum_{m''\mu\mu'} (-1)^{\sigma + \mu - \mu'} (2f+1)(2f''+1)\, \delta_{ii''} \left| \langle a\, k \| D \| a''\, k'' \rangle \right|^2$$
$$(x) \begin{pmatrix} k & i & f \\ m-\mu & \mu & -m \end{pmatrix} \begin{pmatrix} k & i & f \\ m'-\mu' & \mu' & -m' \end{pmatrix} \begin{pmatrix} k'' & i & f'' \\ m''-\mu & \mu & -m'' \end{pmatrix}$$
$$(x) \begin{pmatrix} k'' & i & f'' \\ m''-\mu' & \mu' & -m'' \end{pmatrix} \begin{pmatrix} k & 1 & k'' \\ -m+\mu & \alpha & m''-\mu \end{pmatrix} \begin{pmatrix} k & 1 & k'' \\ -m'+\mu' & -\sigma & m''-\mu' \end{pmatrix} \tag{2.72}$$

Now specializing to the case of xenon, one notes the ground state electronic angular momentum vanishes ($k = 0$). The only allowed intermediate state is $k'' = 1$. The following familiar properties[50] of the 3j symbol $\begin{pmatrix} a_1 & a_2 & a_3 \\ b_1 & b_2 & b_3 \end{pmatrix}$ may be used to simplify $\zeta_{\alpha\sigma}$:

$$b_1 + b_2 + b_3 = 0$$
$$|a_1 - a_2| \leq a_3 \leq a_1 + a_2$$
$$b_i \leq a_i$$

$$\begin{pmatrix} 0 & a & a \\ 0 & b & -b \end{pmatrix} = \frac{(-1)^{a-b}}{(2a+1)^{1/2}} \tag{2.73}$$

Thus the first and second 3j symbols of (2.70) require that $m = \mu$, $m' = \mu'$, and $i = f$, and $\zeta_{\alpha\sigma}$ becomes:

$$\zeta_{\alpha\sigma} = \sum_{m''} (-1)^{\sigma} (2f''+1)\, \delta_{if}\, \delta_{i''i}\, |\langle a0 \| D \| a''1 \rangle|^2 \begin{pmatrix} 1 & f & f'' \\ m''-m & m-m'' \end{pmatrix} \begin{pmatrix} 1 & f & f'' \\ m''-m' & m'-m'' \end{pmatrix}$$
$$\times \begin{pmatrix} 0 & 1 & 1 \\ 0 & \alpha & -m''+m \end{pmatrix} \begin{pmatrix} 0 & 1 & 1 \\ 0 & -\sigma & m''-m' \end{pmatrix} \tag{2.74}$$

It is a simple matter to again apply the 3j symbol properties when specific values are assigned to α and σ. Thus:

$$\zeta_{00} = \frac{1}{3}(2f''+1)\, \delta_{ii''}\, \delta_{if}\, \delta_{m'm}\, |\langle a0 \| D \| a''1 \rangle|^2 \begin{pmatrix} 1 & f & f'' \\ 0 & m & -m \end{pmatrix}^2$$

$$\zeta_{0-1} = \frac{1}{3}(2f''+1)\, \delta_{ii''}\, \delta_{if}\, \delta_{m',m+1}\, |\langle a0 \| D \| a''1 \rangle|^2 \begin{pmatrix} 1 & f & f'' \\ 0 & m & -m \end{pmatrix} \begin{pmatrix} 1 & f & f'' \\ -1 & m+1 & -m \end{pmatrix}$$

$$\zeta_{01} = \frac{1}{3}(2f''+1)\, \delta_{ii''}\, \delta_{if}\, \delta_{m',m-1}\, |\langle a0 \| D \| a''1 \rangle|^2 \begin{pmatrix} 1 & f & f'' \\ 0 & m & -m \end{pmatrix} \begin{pmatrix} 1 & f & f'' \\ 1 & m-1 & -m \end{pmatrix}$$

$$\zeta_{10} = \frac{1}{3}(2f''+1)\, \delta_{ii''}\, \delta_{if}\, \delta_{m',m-1}\, |\langle a0 \| D \| a''1 \rangle|^2 \begin{pmatrix} 1 & f & f'' \\ 0 & m-1 & -m+1 \end{pmatrix} \begin{pmatrix} 1 & f & f'' \\ -1 & m & -m+1 \end{pmatrix}$$

$$\zeta_{-10} = \frac{1}{3}(2f''+1)\, \delta_{ii''}\, \delta_{if}\, \delta_{m',m+1}\, |\langle a0 \| D \| a''1 \rangle|^2 \begin{pmatrix} 1 & f & f'' \\ 0 & m+1 & -m-1 \end{pmatrix} \begin{pmatrix} 1 & f & f'' \\ 1 & m & -m-1 \end{pmatrix}$$

(2.75)

One can now use these to calculate c_{zz} and c_{zx}:

$$c_{zz} = \frac{1}{\hbar} \sum_{\substack{f'' k'' \\ i'' a''}} \left[\frac{G_{00}}{\omega_{b''b} - \omega_1} + \frac{G_{00}}{\omega_{b''b} + \omega_1} \right]$$

or

$$c_{zz} = \frac{2}{3\hbar} \sum_{f'' a''} (2f''+1) |\langle a_0 \| D \| a'' 1 \rangle|^2 \delta_{m'm} \times \frac{\omega_{b''b}}{\omega_{b''b}^2 - \omega_1^2} \begin{pmatrix} 1 & f & f'' \\ 0 & m & -m \end{pmatrix}^2 \tag{2.76}$$

and

$$c_{zx} = \frac{\sqrt{2}}{2} (c_{0-1} - c_{01})$$

$$= \frac{\sqrt{2}}{2\hbar} \sum_{\substack{f'' k'' \\ i'' a''}} \left[\frac{G_{0-1} - G_{01}}{\omega_{b''b} - \omega_1} + \frac{G_{-10} - G_{10}}{\omega_{b''b} + \omega_1} \right]$$

or

$$c_{zx} = \frac{\sqrt{2}}{6\hbar} \sum_{f'' a''} (2f''+1) |\langle a_0 \| D \| a'' 1 \rangle|^2 \times \left[\frac{\delta_{m', m+1} \begin{pmatrix} 1 & f & f'' \\ 0 & m & -m \end{pmatrix} \begin{pmatrix} 1 & f & f'' \\ -1 & m+1 & -m \end{pmatrix} - \delta_{m', m-1} \begin{pmatrix} 1 & f & f'' \\ 0 & m & -m \end{pmatrix} \begin{pmatrix} 1 & f & f'' \\ 1 & m-1 & -m \end{pmatrix}}{\omega_{b''b} - \omega_1} \right.$$

$$\left. - \frac{\delta_{m', m+1} \begin{pmatrix} 1 & f & f'' \\ 0 & m+1 & -m-1 \end{pmatrix} \begin{pmatrix} 1 & f & f'' \\ 1 & m & -m-1 \end{pmatrix} - \delta_{m', m-1} \begin{pmatrix} 1 & f & f'' \\ 0 & m-1 & -m+1 \end{pmatrix} \begin{pmatrix} 1 & f & f'' \\ -1 & m & -m+1 \end{pmatrix}}{\omega_{b''b} + \omega_1} \right] \tag{2.77}$$

In order to determine the cross sections σ_{zz} and σ_{zx}, one returns to Eqs. (2.43) and (2.44), noting that $P_b = 1/(2f+1)$ and $\omega_{b'b} = 0$. Thus

$$\sigma_{ij} = \frac{\omega_1^4}{(2f+1)\, c^4} \sum_{mm'} |c_{ij}|^2 \tag{2.78}$$

and

$$\sigma_{zz} = \frac{\omega_1^4}{(2f+1)\,c^4}\,\frac{4}{9\hbar^2}\sum_{f''f'''a''a'''}(2f''+1)(2f'''+1)$$

$$(x)\,|\langle a_0\|D\|a''1\rangle|^2\,|\langle a_0\|D\|a'''1\rangle|^2$$

$$(x)\left[\frac{\omega_{b''b}\,\omega_{b'''b}}{(\omega_{b''b}^2-\omega_1^2)(\omega_{b'''b}^2-\omega_1^2)}\right]\delta_1(f,f'',f''') \tag{2.79}$$

where

$$\delta_1(f,f'',f''') \equiv \sum_m \begin{pmatrix} 1 & f & f'' \\ 0 & m & -m \end{pmatrix}^2 \begin{pmatrix} 1 & f & f''' \\ 0 & m & -m \end{pmatrix}^2 \tag{2.80}$$

This sum may be performed via suitable manipulations which make use of the following relation between Wigner 3j symbols and Wigner 6j symbols[50] (designated $\begin{Bmatrix} a_1 & a_2 & a_3 \\ b_1 & b_2 & b_3 \end{Bmatrix}$):

$$\sum_{m_3}\begin{pmatrix} j_1 & j_2 & j_3 \\ m_1 & m_2 & m_3 \end{pmatrix}\begin{pmatrix} \ell_1 & \ell_2 & j_3 \\ n_1 & n_2 & -m_3 \end{pmatrix} = \sum_{\ell_3 n_3}(-1)^{j_3+\ell_3+m_1+n_1}(2\ell_3+1)$$

$$(x)\begin{Bmatrix} j_1 & j_2 & j_3 \\ \ell_1 & \ell_2 & \ell_3 \end{Bmatrix}\begin{pmatrix} \ell_1 & j_2 & \ell_3 \\ n_1 & m_2 & n_3 \end{pmatrix}\begin{pmatrix} j_1 & \ell_2 & \ell_3 \\ m_1 & n_2 & -n_3 \end{pmatrix} \tag{2.81}$$

Using this relation and the orthogonality properties of 3j symbols, one can show:

$$\sum_{MM'M''M'''}\begin{pmatrix} J'' & 1 & J' \\ -M'' & a & M' \end{pmatrix}\begin{pmatrix} J'' & 1 & J \\ -M'' & b & M \end{pmatrix}\begin{pmatrix} J''' & 1 & J' \\ -M''' & c & M' \end{pmatrix}\begin{pmatrix} J''' & 1 & J \\ -M''' & d & M \end{pmatrix}$$

$$= \sum_S (-1)^{J'-J-c+d}(2S+1)\begin{Bmatrix} J'' & 1 & J' \\ 1 & J''' & S \end{Bmatrix}\begin{Bmatrix} J'' & 1 & J \\ 1 & J''' & S \end{Bmatrix}$$

$$(x)\begin{pmatrix} 1 & 1 & S \\ -c & a & c-a \end{pmatrix}\begin{pmatrix} 1 & 1 & S \\ -d & b & d-b \end{pmatrix} \tag{2.82}$$

Equation (2.80) can be rearranged in this form by employing appropriate properties of the 3j symbols, with the result:

$$\mathcal{S}_1(f, f'', f''') = \sum_{S=0}^{2} (2S+1) \begin{Bmatrix} f''' & 1 & f \\ 1 & f''' & S \end{Bmatrix}^2 \begin{pmatrix} 1 & 1 & S \\ 0 & 0 & 0 \end{pmatrix}^2$$

The sum over the dummy variable S is performed by substituting tabulated values for the three 3j symbols:

$$\mathcal{S}_1(f, f'', f''') = \frac{1}{3}\left[\begin{Bmatrix} f'' & 1 & f \\ 1 & f''' & 0 \end{Bmatrix}^2 + 2 \begin{Bmatrix} f'' & 1 & f \\ 1 & f''' & 2 \end{Bmatrix}^2 \right] \qquad (2.83)$$

At this point, we specialize to the case of Xe^{129}. In order to permit a numerical calculation of the cross sections (and hence the depolarization ratio), we shall only include two intermediate electronic states in the sum over a". Although many other states are also accessible with reasonable probability, it would be impossible to include them and still obtain numerical results. Clearly this approach will not yield the correct values for the cross sections. On the other hand, it should give a reasonable order of magnitude estimate of the depolarization ratio.

The two intermediate states considered here, designated a_1" and a_2", are the two possible $5p^5 6s$ electronic states. The energy level diagram[36] of Fig. 2.2 gives the wave numbers for the transitions from the $5p^6$ ground state. Each of the levels is hyperfine split into two lines because of the $i = \frac{1}{2}$ nuclear spin.[27] Consequently the transition frequency may be written:

$$\omega_{b''b} \equiv \omega_{a''f'', af} = \omega_{a''a} + (\delta\omega)_{a''f''} \qquad (2.84)$$

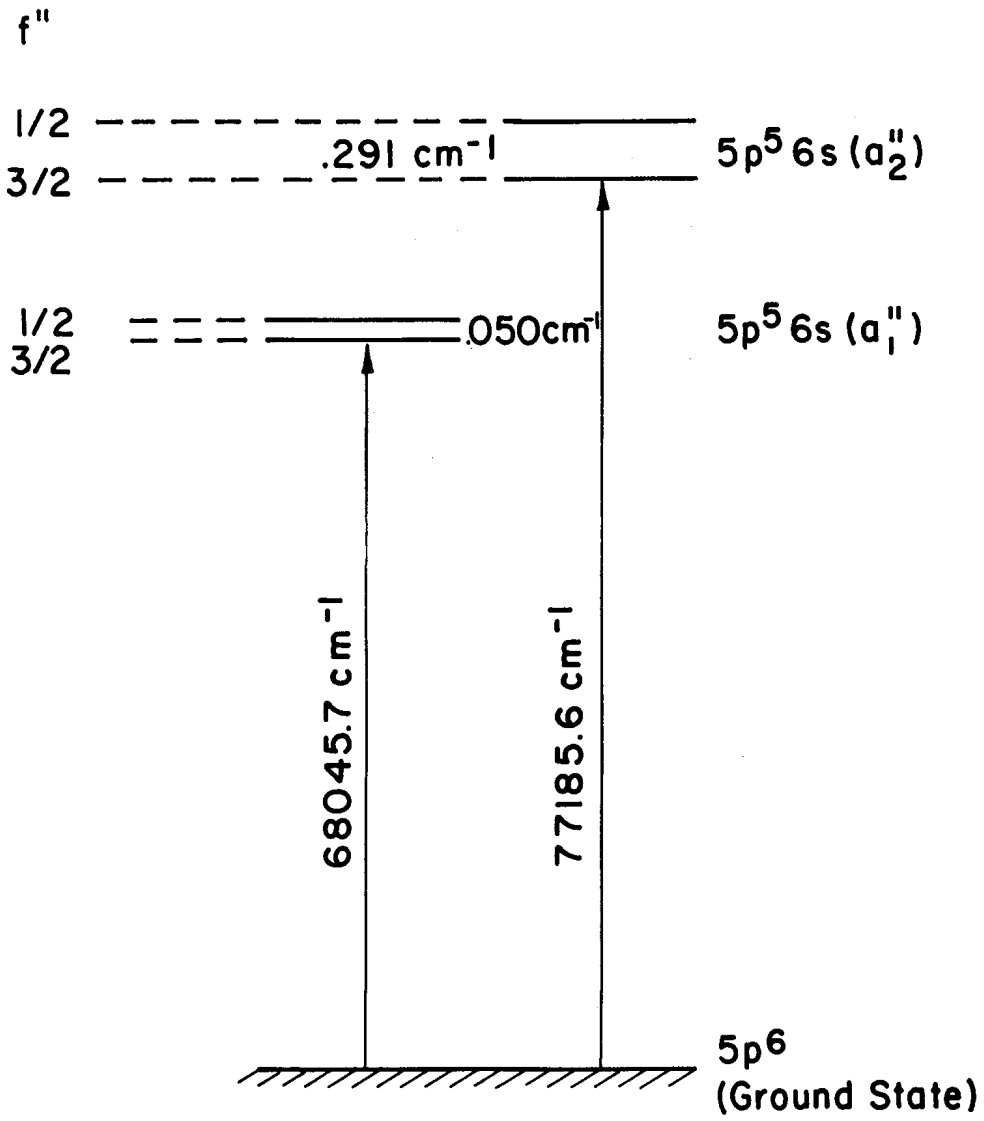

Fig. 2.2. Energy level diagram for transitions in Xe^{129} from $5p^6$ ground state to $5p^56s$ excited states.

where, by definition:

$$(\delta\omega)_{a''f''} \equiv \begin{cases} 0 & f'' = 3/2 \\ (\delta\omega)_{a''} & f'' = 1/2 \end{cases} \tag{2.85}$$

Since $(\delta\omega)_{a''}$ is much smaller than both ω_1 and $\omega_{a''a}$, it can be completely neglected in the calculation of σ_{zz}, so that upon substituting Eq. (2.83) into (2.79), one finds:

$$\sigma_{zz} = \frac{2\omega_1^4}{27\hbar^2 c^4} \sum_{f''f'''a''a'''} |\langle a_0 \| D \| a'' 1\rangle|^2 |\langle a_0 \| D \| a''' 1\rangle|^2 \times \left[\frac{\omega_{b''b}\,\omega_{b'''b}}{(\omega_{b''b}^2 - \omega_1^2)(\omega_{b'''b}^2 - \omega_1^2)}\right] \times \left\{(2f''+1)(2f'''+1)\left[\begin{Bmatrix} f'' & 1 & f \\ 1 & f''' & 0 \end{Bmatrix}^2 + 2\begin{Bmatrix} f'' & 1 & f \\ 1 & f''' & 2 \end{Bmatrix}^2\right]\right\} \tag{2.86}$$

Using the following property of 6j symbols:[50]

$$\sum_{l} (2l+1) \begin{Bmatrix} j_1 & j_2 & j' \\ l_1 & l_2 & l \end{Bmatrix} \begin{Bmatrix} j_1 & j_2 & j'' \\ l_1 & l_2 & l \end{Bmatrix} = \frac{\delta_{j'j''}}{(2j''+1)} \tag{2.87}$$

one can show:

$$\sigma_{zz} = \frac{4\omega_1^4}{9\hbar^2 c^4} \sum_{a''a'''} |\langle a_0 \| D \| a'' 1\rangle|^2 |\langle a_0 \| D \| a''' 1\rangle|^2 \times \frac{\omega_{a''a}\,\omega_{a'''a}}{(\omega_{a''a}^2 - \omega_1^2)(\omega_{a'''a}^2 - \omega_1^2)} \tag{2.88}$$

The reduced matrix elements are related to emission oscillator strengths $f_{a''k'',ak}$ by the following relation:[15]

$$f_{a''k'',ak} = \frac{2m}{3e^2\hbar}\left(\frac{\omega_{a''k'',ak}}{2k+1}\right) |\langle ak \| D \| a''k''\rangle|^2 \tag{2.89}$$

Thus:

$$\sigma_{zz} = r_0^2 \sum_{a'' a'''} f_{a'' 1, a0}\, f_{a''' 1, a0}\, \frac{\omega_1^4}{(\omega_{a'' a} - \omega_1^2)(\omega_{a''' a} - \omega_1^2)} \tag{2.90}$$

where r_0 is the classical radius of the electron:

$$r_0 = \frac{e^2}{m c^2} \tag{2.91}$$

To calculate σ_{zx}, one returns to Eqs. (2.77) and (2.78):

$$\sigma_{zx} = \frac{\omega_1^4}{18(2f+1)c^4\hbar^2} \sum_{f'' f''' a'' a'''} (2f''+1)(2f'''+1)\, |\langle a0 \| D \| a'' 1 \rangle|^2 \, (\times) |\langle a0 \| D \| a''' 1 \rangle|^2 \, \mathcal{S}_2(f, f'', f''') \tag{2.92}$$

where

$$\mathcal{S}_2(f, f'', f''') \equiv \sum_m \left[\frac{\begin{pmatrix} f'' & 1 & f \\ -m & -1 & m+1 \end{pmatrix}\begin{pmatrix} f'' & 1 & f \\ -m & 0 & m \end{pmatrix}\begin{pmatrix} f''' & 1 & f \\ -m-1 & 1 & m+1 \end{pmatrix}\begin{pmatrix} f''' & 1 & f \\ -m & 0 & m \end{pmatrix} + \begin{pmatrix} f'' & 1 & f \\ -m & 1 & m-1 \end{pmatrix}\begin{pmatrix} f'' & 1 & f \\ -m & 0 & m \end{pmatrix}\begin{pmatrix} f''' & 1 & f \\ -m+1 & -1 & m \end{pmatrix}\begin{pmatrix} f''' & 1 & f \\ -m & 0 & m \end{pmatrix}}{(\omega_{b'' b} - \omega_1)(\omega_{b''' b} - \omega_1)} \right.$$

$$- \frac{\begin{pmatrix} f'' & 1 & f \\ -m & -1 & m+1 \end{pmatrix}\begin{pmatrix} f'' & 1 & f \\ -m & 0 & m \end{pmatrix}\begin{pmatrix} f''' & 1 & f \\ -m-1 & 0 & m+1 \end{pmatrix}\begin{pmatrix} f''' & 1 & f \\ -m-1 & 1 & m \end{pmatrix} + \begin{pmatrix} f'' & 1 & f \\ -m & 1 & m-1 \end{pmatrix}\begin{pmatrix} f'' & 1 & f \\ -m & 0 & m \end{pmatrix}\begin{pmatrix} f''' & 1 & f \\ -m+1 & 0 & m-1 \end{pmatrix}\begin{pmatrix} f''' & 1 & f \\ -m+1 & -1 & m \end{pmatrix}}{(\omega_{b'' b} - \omega_1)(\omega_{b''' b} + \omega_1)}$$

$$- \frac{\begin{pmatrix} f'' & 1 & f \\ -m & -1 & m+1 \end{pmatrix}\begin{pmatrix} f'' & 1 & f \\ -m & 1 & m \end{pmatrix}\begin{pmatrix} f''' & 1 & f \\ -m-1 & 1 & m+1 \end{pmatrix}\begin{pmatrix} f''' & 1 & f \\ -m & 0 & m \end{pmatrix} + \begin{pmatrix} f'' & 1 & f \\ -m & 1 & m-1 \end{pmatrix}\begin{pmatrix} f'' & 1 & f \\ -m+1 & -1 & m \end{pmatrix}\begin{pmatrix} f''' & 1 & f \\ -m & 1 & m-1 \end{pmatrix}\begin{pmatrix} f''' & 1 & f \\ -m & 0 & m \end{pmatrix}}{(\omega_{b'' b} + \omega_1)(\omega_{b''' b} - \omega_1)}$$

$$\left. + \frac{\begin{pmatrix} f'' & 1 & f \\ -m & -1 & m+1 \end{pmatrix}\begin{pmatrix} f'' & 1 & f \\ -m & 1 & m \end{pmatrix}\begin{pmatrix} f''' & 1 & f \\ -m-1 & 0 & m+1 \end{pmatrix}\begin{pmatrix} f''' & 1 & f \\ -m & 1 & m \end{pmatrix} + \begin{pmatrix} f'' & 1 & f \\ -m+1 & 0 & m-1 \end{pmatrix}\begin{pmatrix} f'' & 1 & f \\ -m+1 & -1 & m \end{pmatrix}\begin{pmatrix} f''' & 1 & f \\ -m+1 & 0 & m-1 \end{pmatrix}\begin{pmatrix} f''' & 1 & f \\ -m+1 & -1 & m \end{pmatrix}}{(\omega_{b'' b} + \omega_1)(\omega_{b''' b} + \omega_1)} \right] \tag{2.93}$$

Using Eq. (2.82):

$$\mathcal{S}_2 = \sum_S (2S+1) \begin{Bmatrix} f'' & 1 & f \\ 1 & f''' & S \end{Bmatrix}^2 \left[\frac{\begin{pmatrix} 1 & 1 & S \\ 1 & -1 & 0 \end{pmatrix}\begin{pmatrix} 1 & 1 & S \\ 0 & 0 & 0 \end{pmatrix} - \begin{pmatrix} 1 & 1 & S \\ -1 & 1 & 0 \end{pmatrix}\begin{pmatrix} 1 & 1 & S \\ 0 & 0 & 0 \end{pmatrix}}{(\omega_{b''b} - \omega_1)(\omega_{b'''b} - \omega_1)} \right.$$

$$+ \frac{\begin{pmatrix} 1 & 1 & S \\ 0 & -1 & 1 \end{pmatrix}\begin{pmatrix} 1 & 1 & S \\ -1 & 0 & 1 \end{pmatrix} + \begin{pmatrix} 1 & 1 & S \\ 0 & 1 & -1 \end{pmatrix}\begin{pmatrix} 1 & 1 & S \\ 1 & 0 & -1 \end{pmatrix}}{(\omega_{b''b} - \omega_1)(\omega_{b'''b} + \omega_1)} + \frac{\begin{pmatrix} 1 & 1 & S \\ 1 & 0 & -1 \end{pmatrix}\begin{pmatrix} 1 & 1 & S \\ 0 & 1 & -1 \end{pmatrix} + \begin{pmatrix} 1 & 1 & S \\ -1 & 0 & 1 \end{pmatrix}\begin{pmatrix} 1 & 1 & S \\ 0 & -1 & 1 \end{pmatrix}}{(\omega_{b''b} + \omega_1)(\omega_{b'''b} - \omega_1)}$$

$$\left. - \frac{\begin{pmatrix} 1 & 1 & S \\ 0 & 0 & 0 \end{pmatrix}\begin{pmatrix} 1 & 1 & S \\ -1 & 1 & 0 \end{pmatrix} + \begin{pmatrix} 1 & 1 & S \\ 0 & 0 & 0 \end{pmatrix}\begin{pmatrix} 1 & 1 & S \\ 1 & -1 & 0 \end{pmatrix}}{(\omega_{b''b} + \omega_1)(\omega_{b'''b} + \omega_1)} \right]$$

Carrying out the sum over S and using known values of 3j symbols:

$$\mathcal{S}_2 = \frac{2}{3} \left[\frac{1}{(\omega_{b''b} - \omega_1)(\omega_{b'''b} - \omega_1)} + \frac{1}{(\omega_{b''b} + \omega_1)(\omega_{b'''b} + \omega_1)} \right]$$

$$(x) \left[\begin{Bmatrix} f'' & 1 & f \\ 1 & f''' & 0 \end{Bmatrix}^2 - \begin{Bmatrix} f'' & 1 & f \\ 1 & f''' & 2 \end{Bmatrix}^2 \right] - \left[\frac{1}{(\omega_{b''b} - \omega_1)(\omega_{b'''b} + \omega_1)} + \frac{1}{(\omega_{b''b} + \omega_1)(\omega_{b'''b} - \omega_1)} \right]$$

$$(x) \left[\begin{Bmatrix} f'' & 1 & f \\ 1 & f''' & 1 \end{Bmatrix}^2 - \begin{Bmatrix} f'' & 1 & f \\ 1 & f''' & 2 \end{Bmatrix}^2 \right] \qquad (2.94)$$

Making use of the 6j property of Eq. (2.87), one can show:

$$\sum_{f''} (2f''+1) \left[\begin{Bmatrix} f'' & 1 & f \\ 1 & f''' & 0 \end{Bmatrix}^2 - \begin{Bmatrix} f'' & 1 & f \\ 1 & f''' & 2 \end{Bmatrix}^2 \right] = 0$$

$$\sum_{f''} (2f''+1) \left[\begin{Bmatrix} f'' & 1 & f \\ 1 & f''' & 1 \end{Bmatrix}^2 - \begin{Bmatrix} f'' & 1 & f \\ 1 & f''' & 2 \end{Bmatrix}^2 \right] = 0 \qquad (2.95)$$

As a consequence of the vanishing of these sums over f'' (and also similar sums over f') many terms in the equation for σ_{zx} drop out. This is seen by making the following definitions and recalling (2.84):

$$W^{\pm}_{a''} \equiv \omega_{a''a} \pm \omega_1$$

$$(\Delta\omega)^{\pm}_{a''f''} \equiv \frac{(\delta\omega)_{a''f''}}{W^{\pm}_{a''}} \tag{2.96}$$

Expanding the two frequency dependent factors in Eq. (2.94) and keeping only terms to second order, one has:

$$\frac{1}{(\omega_{b''b} - \omega_1)(\omega_{b'''b} - \omega_1)} + \frac{1}{(\omega_{b''b} + \omega_1)(\omega_{b'''b} + \omega_1)}$$

$$\simeq \frac{1}{(W^{-}_{a''})(W^{-}_{a'''})} \left\{ 1 - (\Delta\omega)^{-}_{a''f''} - (\Delta\omega)^{-}_{a'''f'''} + (\Delta\omega)^{-}_{a''f''}(\Delta\omega)^{-}_{a'''f'''} + [(\Delta\omega)^{-}_{a''f''}]^2 + [(\Delta\omega)^{-}_{a'''f'''}]^2 + \cdots \right\}$$

$$+ \frac{1}{(W^{+}_{a''})(W^{+}_{a'''})} \left\{ 1 - (\Delta\omega)^{+}_{a''f''} - (\Delta\omega)^{+}_{a'''f'''} + (\Delta\omega)^{+}_{a''f''}(\Delta\omega)^{+}_{a'''f'''} + [(\Delta\omega)^{+}_{a''f''}]^2 + [(\Delta\omega)^{+}_{a'''f'''}]^2 + \cdots \right\}$$

(2.97)

and

$$\frac{1}{(\omega_{b''b} - \omega_1)(\omega_{b'''b} + \omega_1)} + \frac{1}{(\omega_{b''b} + \omega_1)(\omega_{b'''b} - \omega_1)}$$

$$\simeq \frac{1}{(W^{-}_{a''})(W^{+}_{a'''})} \left\{ 1 - (\Delta\omega)^{-}_{a''f''} - (\Delta\omega)^{+}_{a'''f'''} + (\Delta\omega)^{-}_{a''f''}(\Delta\omega)^{+}_{a'''f'''} + [(\Delta\omega)^{-}_{a''f''}]^2 + [(\Delta\omega)^{+}_{a'''f'''}]^2 + \cdots \right\}$$

$$+ \frac{1}{(W^{+}_{a''})(W^{-}_{a'''})} \left\{ 1 - (\Delta\omega)^{+}_{a''f''} - (\Delta\omega)^{-}_{a'''f'''} + (\Delta\omega)^{+}_{a''f''}(\Delta\omega)^{-}_{a'''f'''} + [(\Delta\omega)^{+}_{a''f''}]^2 + [(\Delta\omega)^{-}_{a'''f'''}]^2 + \cdots \right\}$$

(2.98)

In light of Eqs. (2.95) it is clear that all the terms indicated above will disappear in the σ_{zx} calculation except for the product terms $(\Delta\omega)^{\pm}_{a''f''}(\Delta\omega)^{\pm}_{a'''f'''}$. Consequently:

$$\sigma_{zx} \simeq \frac{\omega_1^4}{16} r_o^2 \sum_{a''a'''} \frac{f_{a''1,a0}\, f_{a'''1,a0}}{\omega_{a''a}\, \omega_{a'''a}} \sum_{f''f'''} (2f''+1)(2f'''+1)$$

$$(x)\left\{ \frac{2}{3}\left[\frac{(\Delta\omega)^{-}_{a''f''}(\Delta\omega)^{-}_{a'''f'''}}{(w^{-}_{a''})(w^{-}_{a'''})} + \frac{(\Delta\omega)^{+}_{a''f''}(\Delta\omega)^{+}_{a'''f'''}}{(w^{+}_{a''})(w^{+}_{a'''})} \right]\left[\begin{Bmatrix} f'' & 1 & f \\ 1 & f''' & 0 \end{Bmatrix}^2 - \begin{Bmatrix} f'' & 1 & f \\ 1 & f''' & 2 \end{Bmatrix}^2 \right] \right.$$

$$\left. - \left[\frac{(\Delta\omega)^{-}_{a''f''}(\Delta\omega)^{+}_{a'''f'''}}{(w^{-}_{a''})(w^{+}_{a'''})} + \frac{(\Delta\omega)^{+}_{a''f''}(\Delta\omega)^{-}_{a'''f'''}}{(w^{+}_{a''})(w^{-}_{a'''})} \right]\left[\begin{Bmatrix} f'' & 1 & f \\ 1 & f''' & 1 \end{Bmatrix}^2 - \begin{Bmatrix} f'' & 1 & f \\ 1 & f''' & 2 \end{Bmatrix}^2 \right] \right\}$$

(2.99)

The following values for the hyperfine splittings[27] and the oscillator strengths[3] may now be used to calculate the scattering cross sections:

$$\delta\omega_{a''_1} = 0.942 \times 10^{10} \quad \text{sec}^{-1}$$

$$\delta\omega_{a''_2} = 5.48 \times 10^{10} \quad \text{sec}^{-1}$$

$$f_{a''_1,a0} = 0.256$$

$$f_{a''_2,a0} = 0.238$$

The results for 6943Å ruby laser light are:

$$\sigma_{zz} \simeq 2.55 \times 10^{-29} \quad \text{cm}^2$$

$$\sigma_{zx} \simeq 2.01 \times 10^{-42} \quad \text{cm}^2$$

$$\rho_v \simeq 7.9 \times 10^{-14}$$

Observe that, as anticipated, the calculated value for σ_{zz} is appreciably in error: lower than the known cross section by a factor of 45. However the calculated depolarization ratio is so much smaller—approximately eight orders of magnitude—than the minimum measurable depolarization that we can practically conclude $\rho_v = 0$.* Thus the main value of the above analysis is that it lays to rest speculation that nuclear spin might render noble gas atoms optically anisotropic to a measurable extent. Only near resonance does it appear there would be a possibility of observing this effect.

Using a formulation quite similar to that outlined in this section, we have also investigated a possible depolarizing mechanism in methane. The analysis included the interaction between the scattering electrons and the rotational motion of the nuclei of the molecule. Again the estimated depolarization ratio was orders of magnitude too small to have been measured.

*Although Xe^{131} has an isotopic abundance in natural xenon comparable to that of Xe^{129}, there is no reason to believe a calculation of the depolarizing effect of its nuclear spin would lead to any significantly different results nor to a change of our basic conclusion.

CHAPTER III

DESCRIPTION OF EXPERIMENTAL APPARATUS

The experimental arrangement employed in the scattering measurements is schematically depicted in Fig. 3.1 and photographed in Fig. 3.2 The light beam from a Q-switched* ruby laser was focused through an angular filter and polarized by a Glan-Thompson prism. As the beam passed through the scattering chamber, containing a pure, dust-free gas at one atmosphere pressure, scattering events took place. The scattered light was measured by a red-sensitive photomultiplier tube PM_1 in the scattering detector, a series of apertures in the observation port limiting to approximately one centimeter the length of beam viewed. A precision rotatable polarizer and a narrow band interference filter permitted polarization analysis of the unshifted Rayleigh light.

In order to normalize the scattering data for shot-to-shot changes in laser intensity, a second photomultiplier tube PM_2 in the intensity monitor viewed the reflection of the primary beam off a diffuse scattering surface.

3.1 LASER AND ASSOCIATED OPTICS

The laser was a commercially available unit produced by Lear-Siegler Incorporated. It consisted of a separate power-control console and the

*The laser was operated in a single-spike mode by spoiling the "Q" of the resonant optical cavity until a high power density was obtained.

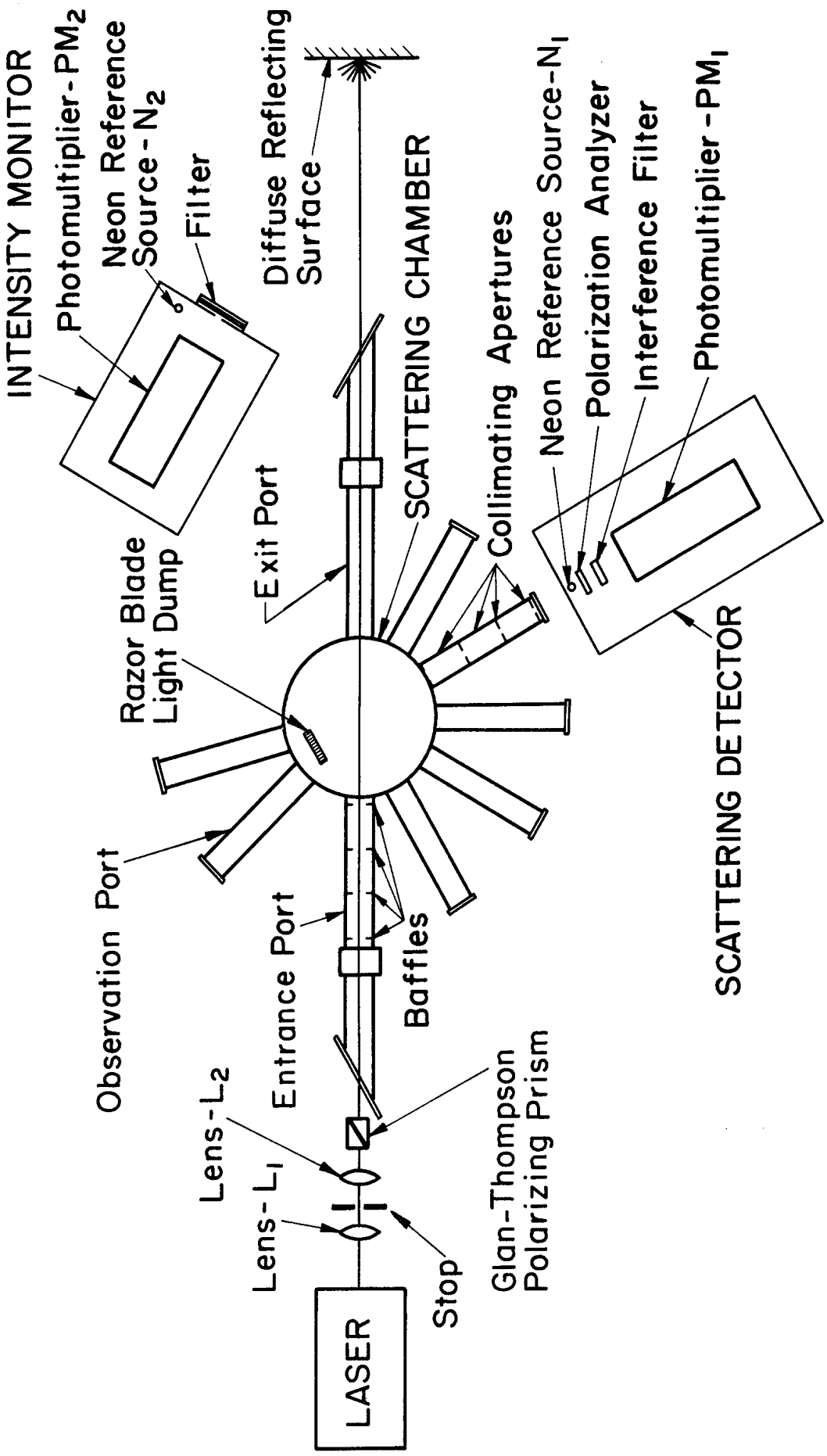

Fig. 3.1. Experimental arrangement for Rayleigh scattering experiments.

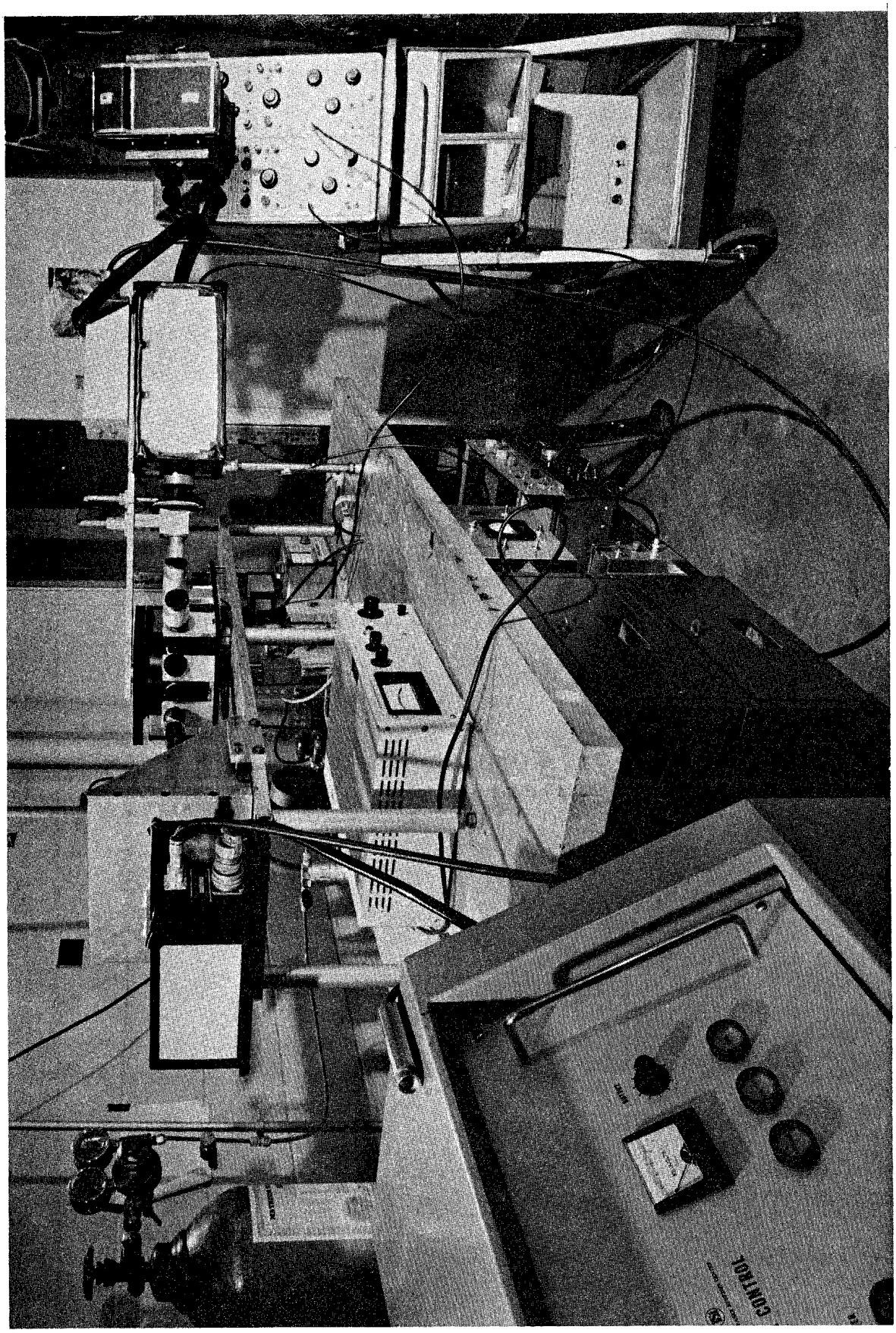

Fig. 3.2. Photograph of experimental arrangement.

laser head, which contained a 1/4 in. diam by 3 in. long ruby rod with Brewster angle faces. Capacitors totaling 4 μf in the power-control console were typically charged to 4000 v and then discharged across a xenon spiral flash lamp to provide laser pumping action. Q-spoiling was performed by a saturable uranyl glass filter.

The laser beam, of 6943Å wavelength, emerged as a pencil of light of elliptical cross section, 1/4 in. by 5/32 in. Divergence was small but finite: approximately 1.5 milliradians full angle divergence. The power output was measured by Lear-Siegler to be typically 8 Mw, with a pulse width of 25 nsec (full width at half maximum). There was a ten per cent shot-to-shot reproducibility of laser energy. Despite the use of a Brewster cut, 90° c-axis ruby rod, the output beam was only about 80% polarized.

The front face of the laser head was mounted flush against a bracket, which, in turn, was rigidly attached to an aluminum table.* As shown in Fig. 3.3, the laser, its associated optics, and the scattering chamber were all mounted on the four foot long aluminum table, which served quite adequately as a poor man's optical bench.

The main function of the angular filter was to suppress the small fraction of laser light that diverged at relatively large angles (greater than one degree). This was accomplished by focusing the beam with lens L_1 (6.3 cm focal length) through a blackened pinhole aperture, .060 in.

*A shim-screw arrangement allowed three-axis positioning of the laser bracket for optical alignment.

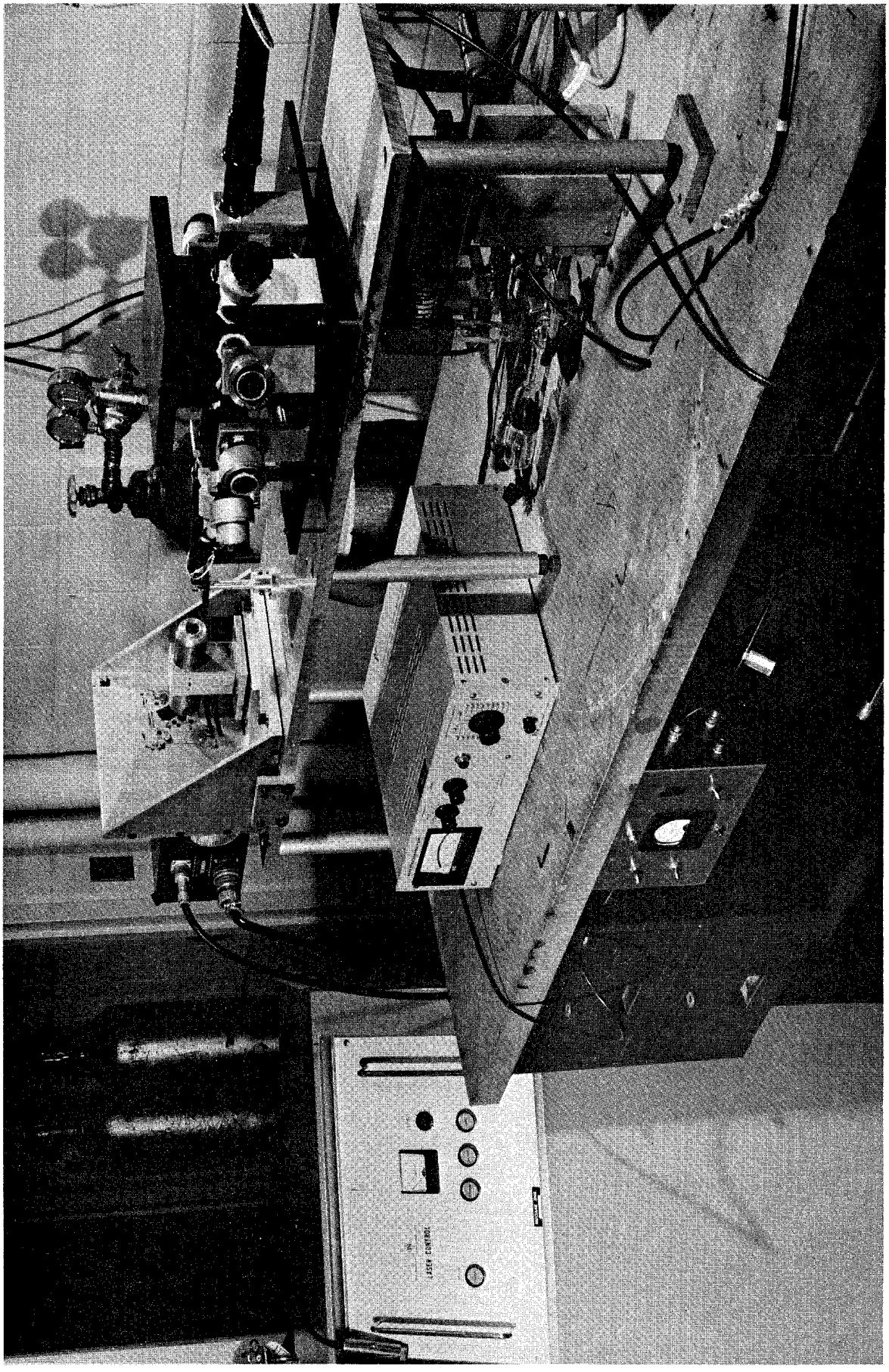

Fig. 3.3. Photograph of laser and associated optics on aluminum mounting table.

diam. In addition the angular filter produced a beam of light which was slightly convergent through the scattering volume, the result of positioning lens L_2 (8.2 cm focal length) approximately 8.8 cm beyond the aperture. The half angle of convergence was 1.6 milliradians, with a nominal beam diameter at the center of the scattering chamber of 0.24 in.

The two lenses and the aperture were held in a cylinder, which maintained centerline alignment, while permitting adjustment of relative positions of the three components. The cylinder could be oriented about all three axes to bring it into alignment with the laser beam.

The Glan-Thompson prism was a specially constructed, air-spaced linear polarizer, designed to transmit, without deterioration, laser pulses up to 25 Mw. The major and minor principal transmittances of the prism for red light were approximately 1.0 and 5.10^{-6}, respectively. Thus the prism produced a highly polarized beam, a prime requirement for experiments of the type undertaken in this research.

3.2 SCATTERING CHAMBER

The scattering chamber was constructed by welding a 14 in. square plate to the bottom and an 8 in. square flange around the top of a six in. length of aluminum pipe. The position of the chamber above the aluminum mounting table was adjustable by means of shim screws in the base plate. A flange-top plate arrangement permitted access to the interior of the chamber, and a viton O-ring seated in a groove in the top plate and bearing against the finished top of the pipe provided a satisfactory

vacuum seal. In order to render the interior of the chamber as optically dark as possible, the sides, bottom and top plate were sandblasted to a matte finish and then the entire chamber black anodized.

Holes for the observation ports were bored in the side of the chamber, the machinist using a 0°01' indexing table to attain the required accuracy. These holes were located on one side at 105° and 135° with respect to the main optical axis, and on the other side at 30°, 60°, 90°, 120°, and 150°. To further ensure accurate positioning of the ports, vertical brackets were mounted around the base plate at appropriate positions. The 6 in. long observation port tubes, which had also been black anodized, were then slid through the brackets and into the bored holes. Torr-Seal, a very low vapor pressure epoxy cement manufactured by Varian Associates, was used to permanently attach and vacuum seal the ports to the scattering chamber.

In order to define the scattering volume viewed by the detection optics, four equally spaced, .250 in. x .375 in. knife edged rectangular apertures were positioned in each observation port, the longer edge of each being vertical. Alignment and spacing of the apertures was accomplished by cementing them with Torr-Seal to the ends of spacer tubes, as shown in the photograph of Fig. 3.4. All apertures and spacer tubes were black anodized. The tight fit of the spacer tubes inside the observation port tubes effectively prevented any vibration present from rotating or moving apertures out of position.

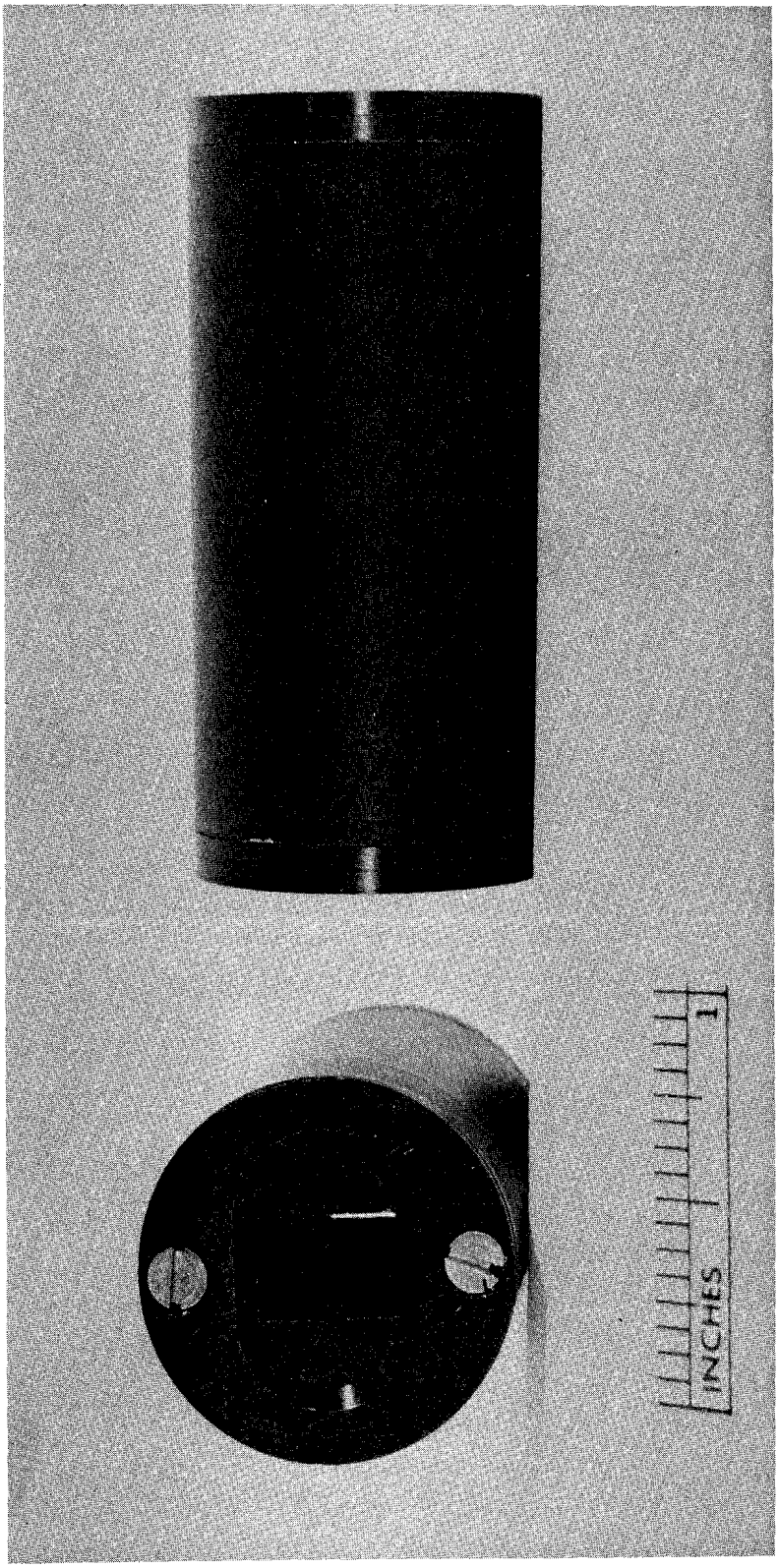

Fig. 3.4. Photograph of rectangular defining apertures and spacer tubes.

Strain-free Pyrex windows were permanently affixed to the end of each observation port, Torr-Seal again being chosen for this task.

The blackened walls of the chamber unfortunately did not provide a sufficiently dark background against which to view the scattered radiation. The normal procedure is to use a tapered glass horn, into which background light makes multiple reflections and is thereby suppressed. For two reasons, this method was rejected. The first reason was that the use of glass horns would have resulted in an unwieldly design that significantly reduced the number of angles at which scattering could be viewed. Of greater importance was the fact that a superior black body of low optical reflectivity and remarkable compactness was available. Pictured in Fig. 3.5, it consisted of a vertical stack of approximately 100 stainless steel razor blades held tightly in a yoke. The yoke was suspended from the scattering chamber top plate in a position opposite whichever observation port was in use. Very little light was reflected from the sharp razor blade edges; most was lost in multiple reflections between adjacent pairs of blades. Measurements with a He-Ne gas laser of the reflectivity of this razor blade assembly showed a factor of two improvement over a blackened glass horn.

The laser beam passed through the scattering chamber via the entrance and exit ports. Holes for these ports were bored in the chamber walls at the same time as the observation port holes. In order to permit rotation of the end window of the entrance port, two Pyrex tubes with mating

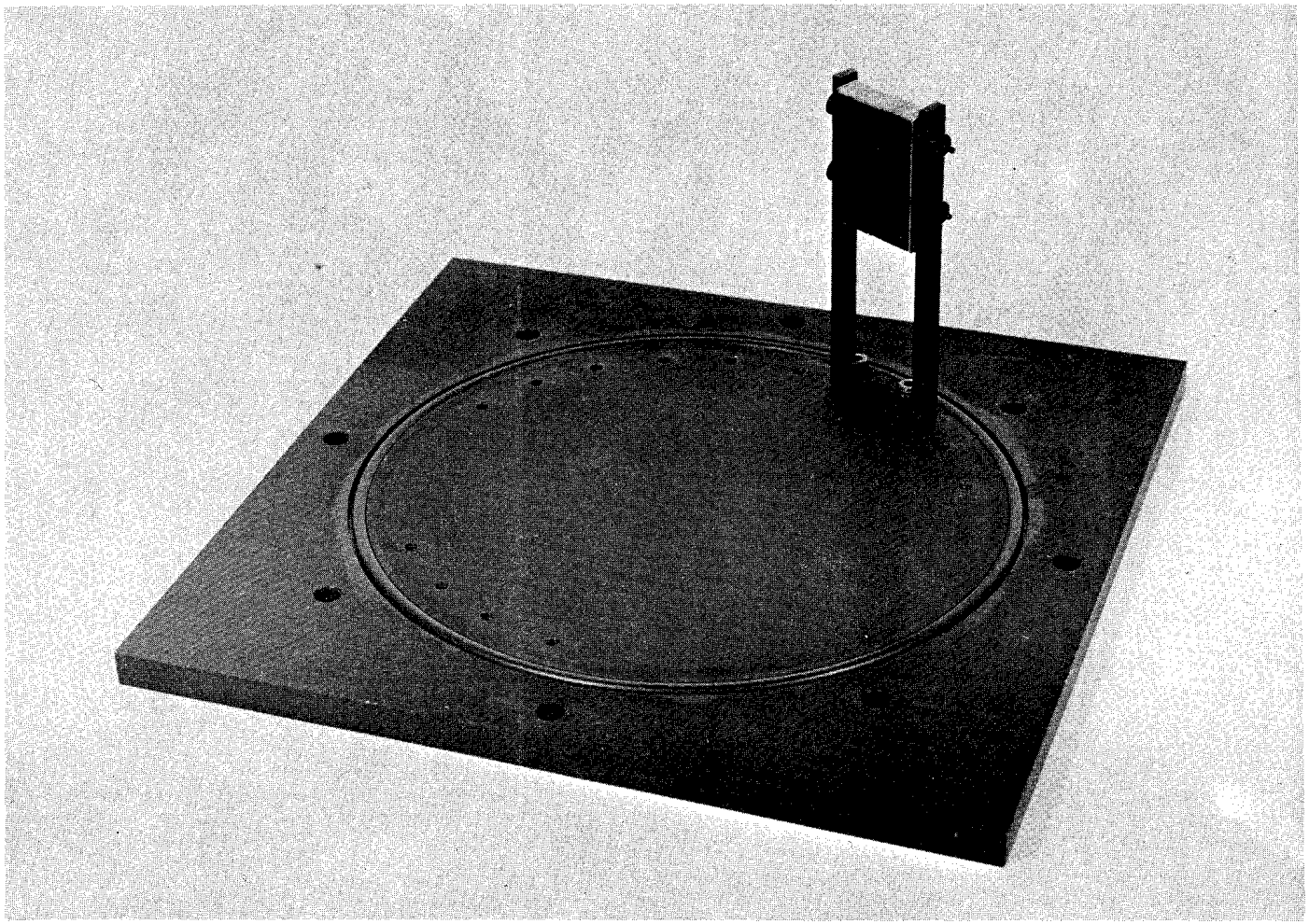

Fig. 3.5. Photograph of razor blade light dump mounted on scattering chamber top plate.

ground glass joints were employed. Low vapor pressure Apiezon "T" vacuum grease was used on the joints. The male tube was cemented to the chamber with Torr-Seal and further held in place by a bracket identical to the ones used with the observation ports. The end of the female tube was cut at Brewster's angle for a strain-free Pyrex window, which was attached with Torr-Seal. Several knife-edged baffles of circular aperture were positioned in the entrance port by means of sliding spacer tubes. With the exception of the baffles, the exit port was identical in design to the entrance port. Both ports were wrapped with black tape to prevent extraneous light from entering the scattering chamber.

3.3 VACUUM-GAS FEED SYSTEM

The vacuum-gas feed system is depicted in Fig. 3.6. The prime consideration in the design and construction of this system was minimizing as far as possible the presence of contaminants in the scattering chamber. Thus, for example, all components were carefully cleansed and degreased by techniques suggested by Guthrie.[23] Also, particular care was exercised to avoid using high vapor pressure materials, particularly above the high vacuum, stainless steel valve, V_1. Tubing was either stainless steel or OFHC copper.

All gases were purchased from the Matheson Company with the highest purity levels consistent with the type of experiments contemplated. In general, these were either their research or ultra-high purity grades. The

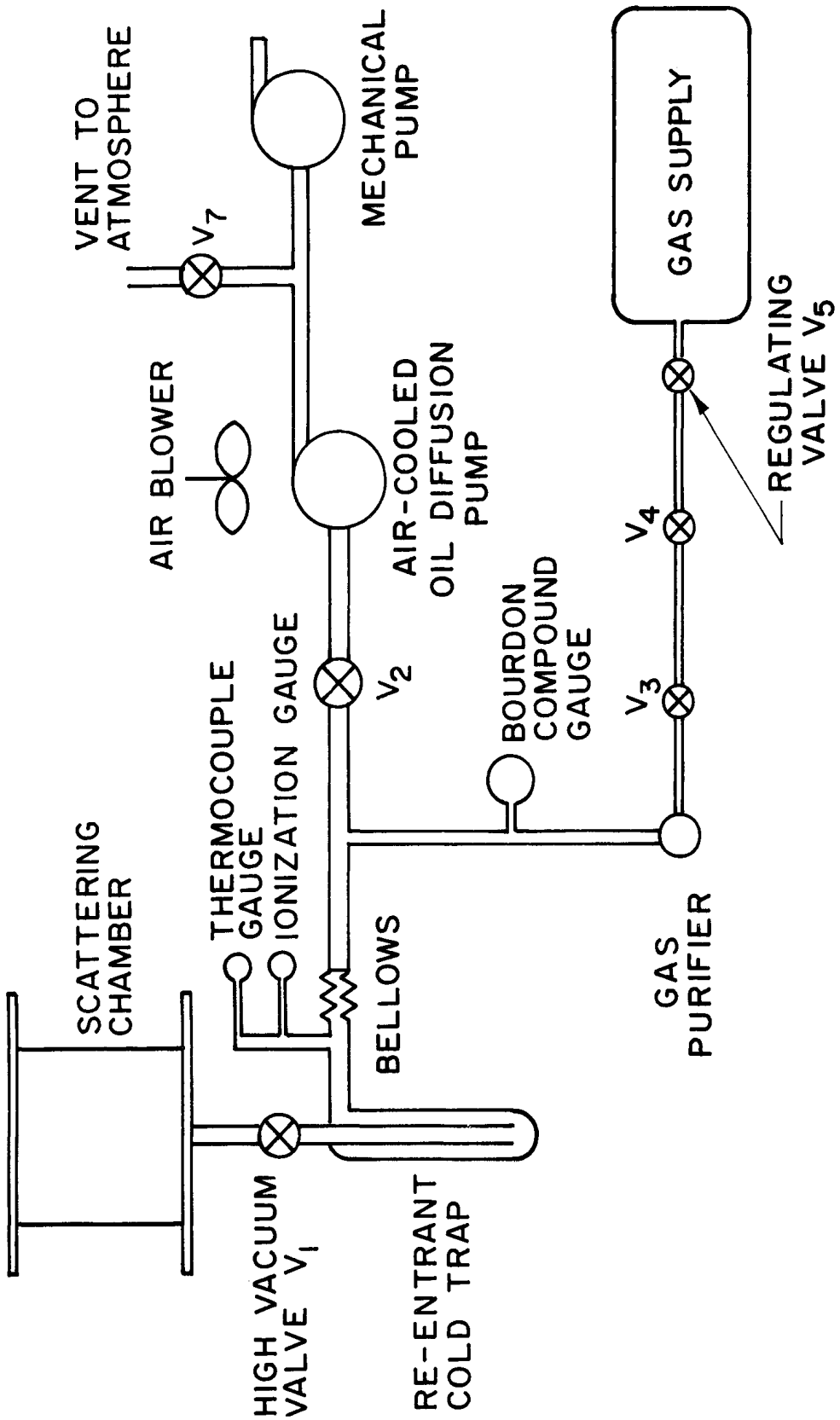

Fig. 3.6. Schematic of vacuum-gas feed system.

double needle valve arrangement (V_3 and V_4) in the gas feed line permitted fine control of the flow rate so that the scattering chamber could be slowly filled to pressure.* Oil, water and any particles approximately 12 microns in size or larger were removed from the fill gas by a Matheson gas purifer containing a molecular sieve desiccant.

Gas pressure was measured by a stainless steel Bourdon gauge. This compound vacuum-pressure gauge had 0.5% full scale accuracy. Evacuation of the system was normally accomplished by a mechanical pump, although an air-cooled oil diffusion pump was available when pressures below one micron were desired. Thermocouple and ionization gauges were used for low pressure measurements.

3.4 SCATTERING DETECTOR

The function of the scattering detector was to measure the intensity and polarization state of the unshifted Rayleigh scattered light. The detection device itself was an RCA 7265 photomultiplier tube (PM_1) with trialkali S-20 photocathode having approximately 2.5% quantum efficiency at 6943Å. Gains up to 2.10^7 were yielded by the 14 stage dynode structure.

The assembly containing the photomultiplier tube and the other detector optics is pictured in Fig. 3.7. In order to assure consistent alignment with each observation port, the assembly pivoted about the vertical centerline of the scattering chamber and was adjustable vertically

*Observe that the use of the Pyrex tubes with ground glass joints precluded filling the scattering chamber to above one atmosphere pressure.

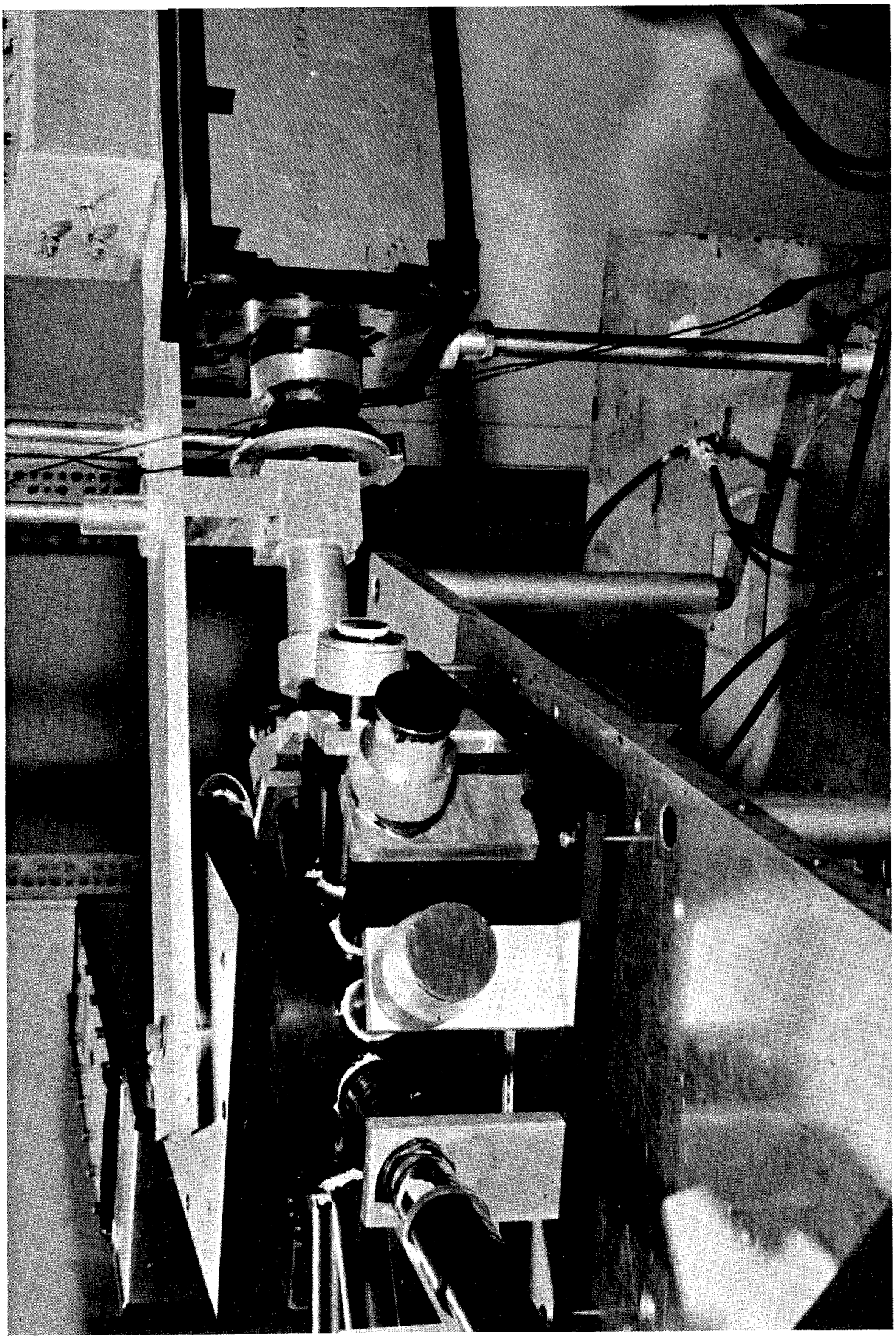

Fig. 3.7. Photograph of scattering detector connected to 60° observation port of scattering chamber.

by means of its support rod.

An O-ring was employed between a sliding aluminum tube and a collar around the observation port in use and light-tight caps were mated to collars around each of the six unused ports. These measures, plus other elements of the scattering detector design, effectively prevented light not emanating from the scattering chamber from reaching the detector. In fact, no increase above photomultiplier dark noise could be detected when lights were turned on inside the experimental dark room.

The polarization analyzer was Polaroid HN22 material laminated in instrument grade glass. Specifications for its major and minor principal transmittances for 6943Å light were 0.59 and 3.10^{-6}. The 1 in. diam analyzer was mounted in a precision divided circle whose angular position was readable by a vernier scale to an accuracy of 0°01'.

In order to reject Raman scattered radiation and light not generated by the laser ruby (particularly light from the xenon flash lamp), a narrow band interference filter was mounted between the analyzer and the photomultiplier. Measurements of the spectral transmission of the filter indicated that it had a peak transmission of 53% at 6942Å and a full width at half maximum of 55Å. At wavelengths below 6775Å, the transmission coefficient was less than 0.1%.

Experience with the operation of S-20 photomultipliers determined that they were subject to variations in sensitivity as a result of temperature changes, photocathode fatigue and previous operating history, and

other uncatalogued effects. This operational characteristic alone necessitated the design of a method of monitoring the photomultiplier response during scattering experiments. However, an equally strong motivating factor became apparent. This was the discovery that in order to accomplish all of the experimental objectives, it was necessary to adjust the photomultiplier gain (by varying the applied voltage) over a significant range. Thus experimental data had to be normalized for these changes in gain.

The monitoring method chosen was a diffuse pinhole light source which could be lowered into position to be viewed by the photomultiplier through the interference filter and the polarization analyzer. A seated keyway arrangement assured that the light was always lowered into the same position. The source of light was a neon bulb N_1, with a rated lifetime of 50,000 hr.

3.5 INTENSITY MONITOR

The intensity monitor, used to compensate scattering data for changes in laser energy, employed a second RCA 7265 photomultiplier tube PM_2. The chassis enclosing this tube was light tight with the exception of a small aperture through which was viewed the diffuse reflection of the direct laser beam. As the diffuse scattering surface was more than two meters from the intensity monitor, alignment problems were negligible; small changes in the position of the laser spot resulted in no measurable changes in the monitored intensity.

A broad-band, low transmitting filter was placed in front of the aperture in order to reduce the light intensity reaching PM_2. At this lower light level, the photomultiplier operated in its linear regime and yet sufficiently large numbers of photoelectrons were generated at the cathode to yield good statistics. Hence the intensity monitor output was always proportional to laser energy.

The sensitivity response of PM_2 was monitored by another diffuse pinhole light source (neon bulb N_2) permanently mounted inside the chassis enclosure.

3.6 ELECTRONICS

The basic components of the electronic circuitry are displayed in Fig. 3.8. Voltage for the photomultiplier tubes was supplied by two Hamner power supplies having very high voltage stability and low ripple. The voltage divider networks were wired according to RCA specifications, with carbon deposited resistors employed because of their low noise characteristics. In order to reduce their heating effects, the resistors were housed in separate chassis. Focusing and accelerating voltages were adjusted by means of trim pots to maximize tube gain.

During scattering experimentation, the anode signal from each photomultiplier was measured by a Tektronix type 555 dual-beam oscilloscope. The 1 M Ω input resistance to the CRO and the lumped parallel capacitance of photomultiplier output, co-axial cable, and CRO input formed an integrating circuit with a decay constant of approximately 130 μsec. Since

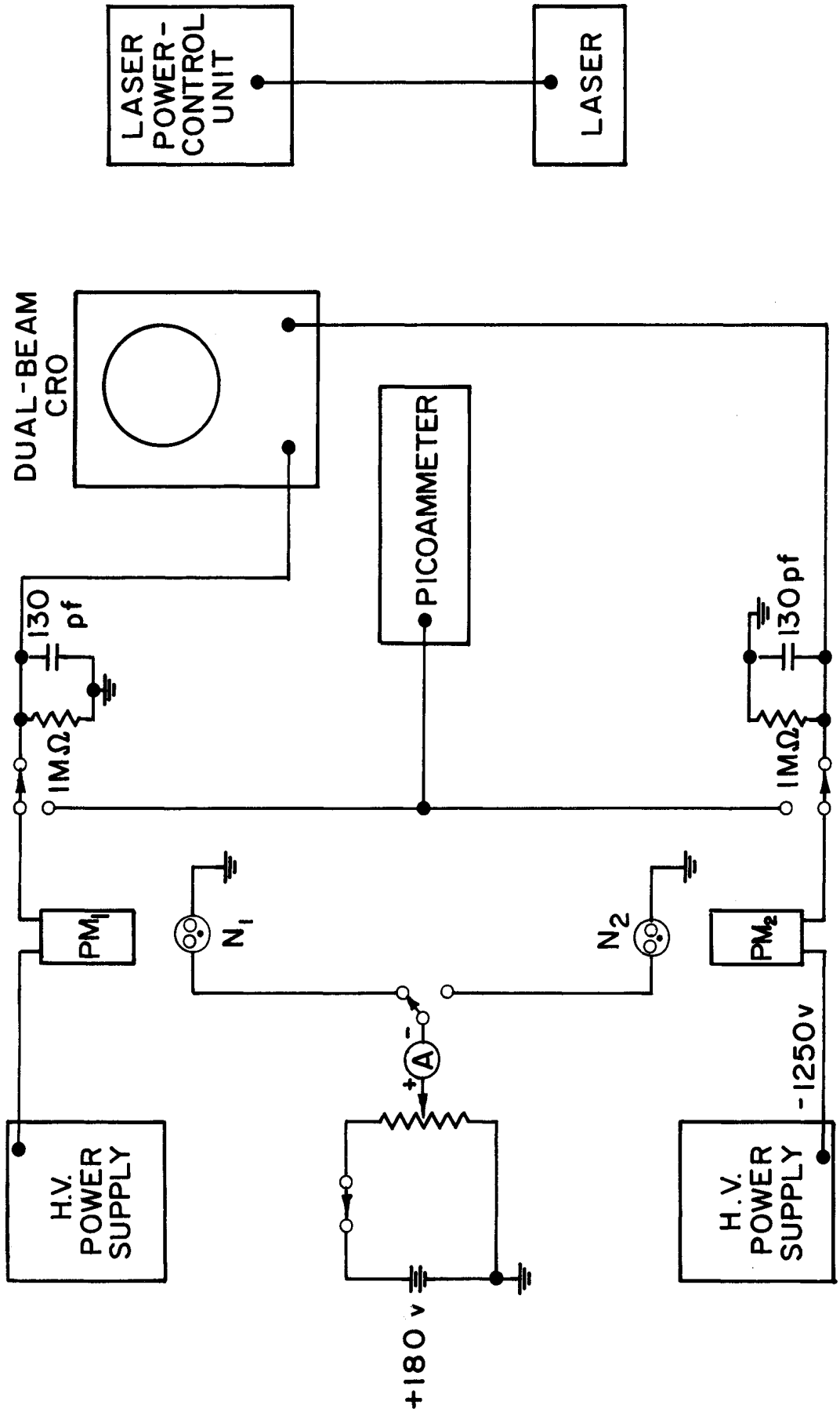

Fig. 3.8. Basic components of electronic circuitry.

this decay constant was much longer than the 50 nsec. laser pulse duration, the anode output appearing on the CRO (with a 100 nsec/cm sweep rate) was a simple step function. Data analysis was consequently the essence of simplicity: one needed only to scale off from a photograph of the CRO trace the magnitude of voltage change. Due to the integrating feature of the circuit, the measured voltage was directly proportional to the total number of photons incident on the photocathode, exactly the information desired.

An important bonus associated with the integral measuring method was that photomultiplier dark noise problems were entirely eliminated. Since there were approximately 6,000 dark noise pulses per second, the probability of one occurring during the total CRO sweep of 1 μsec was very small. However, even when one did occur, it appeared as a small, superimposed step function which was easily discriminated against when the data were analyzed. Thus the experimental problems associated with the usual photomultiplier refrigeration technique of reducing dark noise were completely avoided.

A dc current of 300 μamps was supplied to the neon bulbs by means of a battery-adjustable potentiometer arrangement. Response of the photomultiplier tubes to this steady light was measured by a Keithley picoammeter.

CHAPTER IV

EXPERIMENTAL METHOD

4.1 SUPPRESSION OF SPURIOUS LIGHT

Probably the most troublesome obstacle to be overcome in a Rayleigh scattering experiment is so-called "spurious" or "parasitic" light. This is light which is still registered by the scattering detector after the scattering chamber is evacuated. It is the result of, for example, forward scattering of laser light off the window and/or the baffles of the entrance port and subsequent reflection off the scattering chamber walls into the detection optics.

The success of this experiment in measuring very small depolarizations was predicated upon sufficient suppression of the spurious light. Fortunately this objective was attained, most of the credit being due to the superiority of the Q-switched laser over light sources used in scattering experiments performed prior to 1963. This device represents an unparalleled combination of high power and excellent beam collimation characteristics.

The spurious light suppression was also achieved by a substantial expenditure of effort, mostly of an empirical, trial and error nature. For example, it was found that all optical surfaces had to be religiously maintained clean and free of dust particles. Also, alignment of the laser beam with the scattering chamber axis was quite important. An inexpensive

He-Ne gas laser proved to be a useful aid in accomplishing this. Spotting patterns of the ruby laser on exposed Polaroid film were used to confirm the alignment.

The angular filter described in the previous chapter played a significant role in reducing spurious light resulting from the small, but significant portion of the laser beam which was excessively divergent.

The advantages of using polarized incident light when measuring small depolarizations do not appear to have been fully recognized in the past. Perhaps the most important advantage is that the spurious light retains—to a significant level—the polarization content of the incident beam. Since in this experiment it was approximately 75 per cent polarized, it presented a substantially lower level to be discriminated against when the analyzer was positioned to measure the depolarized scattering.

We found that having the entrance port window positioned at Brewster's angle minimized spurious light. The worst results were obtained with the window normal to the beam. It was also necessary to carefully position the flat so that its normal was in the plane defined by the propagation and polarization vectors of the incident beam. If this was not done, the polarization vector was rotated.

The most time-consuming aspect of the spurious light rejection effort was the proper selection of baffles in the entrance port. All baffles were of circular aperture and were located as illustrated in Fig. 4.1. Definitely superior results were obtained with the knife edges positioned

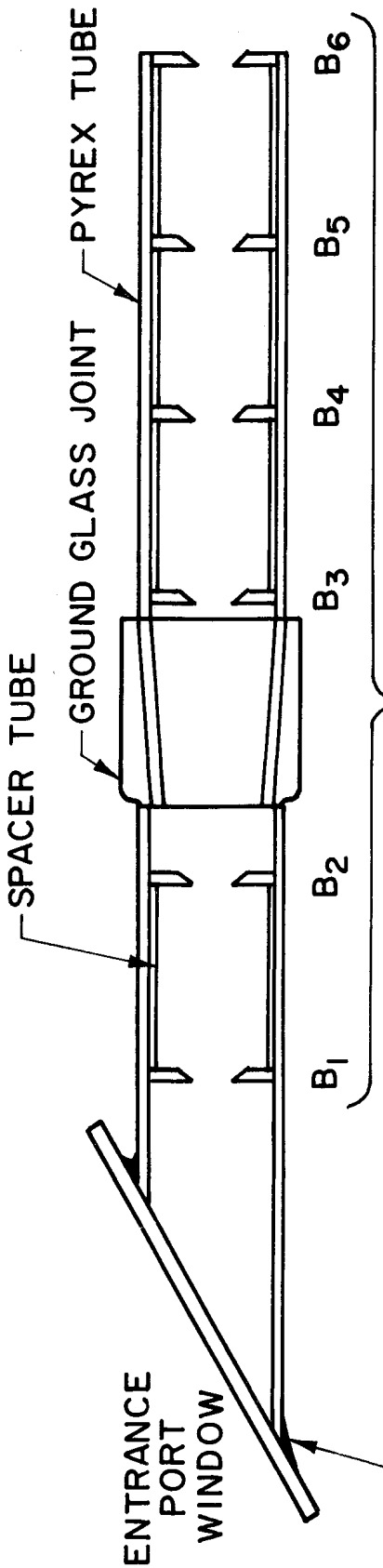

Fig. 4.1. Arrangement of circular baffles in entrance port.

as shown. Also, we found, in agreement with other experimentalists,[18] that the sizes of the last two baffles B5 and B6 were most critical. A change in the diameter of either of these by as little as .005 in. from optimum produced significant increases in the measured spurious light. B5 was the limiting aperture: slightly larger than the beam size with a diameter of 0.350 in. The succeeding aperture B6 was 0.420 in. diam and served to shadow the scattering chamber interior from forward scattering off the edges of B5. The four remaining baffles were .500 in. in diam.

Numerous other techniques, such as using the stacked razor blades and black anodizing the matte interior of the scattering chamber further reduced the parasitic light. The final result was a lowering of measured spurious light to a level at the bounds of detectability. Specifically, this amounted to a spurious intensity $\mathcal{E}_{zx}$ equivalent to the scattering caused by a gas at STP having a differential scattering cross section $\sigma_{zx} = 3.5 \times 10^{-32}$ cm^2. To our knowledge no other experiment has succeeded in eliminating spurious light to such an extent.

4.2 GENERAL SCATTERING MEASUREMENTS

In a typical scattering experiment, first attention was given to the vacuum-gas feed system: the scattering chamber was evacuated below 1 millitorr and then flushed through several times with the gas of interest. Meanwhile all electronic equipment was allowed enough time to warm up and all optical surfaces were cleaned with ethanol and dry air.

The two gas feed line needle valves were partially opened to slowly bleed gas into the scattering chamber. Thus several minutes were taken to fill the chamber, and the possibility of generating any macroscopic dust particles was greatly reduced. An operating pressure 0.5 in. Hg below atmosphere was chosed to maintain a positive pressure on the ground glass joints of entrance and exit ports.

With the completion of the filling process, the high vacuum valve V_1 was closed. This prevented any high vapor pressure contaminants present below the valve from entering the scattering volume.

Current atmospheric pressure was recorded from a corrected mercury barometer readable by vernier to .01 in. Hg, and room temperature* was also measured.

The laser was generally fired several times before measurements were commenced. This allowed the unit to warm up and to stabilize in its output. It also provided a period of time for dust particles, if any, in the scattering chamber to drift downwards.

The precision divided circle was rotated so that the analyzer axis was either vertical or horizontal. Proper settings (to an accuracy of $\pm$ 0°13') had previously been determined by finding the null point for scattering from zero-depolarizing argon. During the several months of experimentation, a number of rechecks were made with argon to detect any

*We have performed an experiment to verify that gas was introduced to the scattering chamber at ambient temperature. No expansion cooling could be detected.

changes in the correct settings. Changes could have been induced by the slight amount of vibration present, but none were ever observed.

High voltage was applied to the phototubes several minutes prior to experimentation. While PM_2 (of the intensity monitor) was always operated at -1250v, the voltage applied to PM_1 differed from experiment, depending on the intensity of scattering being studied. Whenever possible, it was selected (usually in 250v intervals from -1000v to -1750v) so as to place the integrated output pulse in the 50-2000 mv region. As pointed out in Section 3.4, it was necessary to monitor the "sensitivities" of the photomultiplier tubes with neon light sources. The sensitivity of each tube was expressed in terms of the anode current measured by the picoammeter when 300 μamps was supplied to the appropriate neon bulb. The sensitivities of scattering and monitoring phototubes were termed S_1 and S_2, respectively.

Measurements of phototube sensitivity were made at the start of each set of experiments and repeated at intervals of approximately 15 minutes. It was not found necessary to make these measurements with each laser shot, as variations of sensitivity were typically about 1% over an hour's time. Naturally, sensitivity measurements were required each time tube voltage (gain) was changed.

The neon bulbs were turned on—when viewed by an active phototube—only long enough to obtain a stabilized reading on the picoammeter. This minimized phototube fatigue problems, and also had the result of keeping total bulb "on" time very low. This was considered to be extremely important,

as any long term change of bulb intensity would have led to erraneous results.

To determine whether the bulbs were indeed aging, the response to a "standard bulb" of each phototube was measured at the start of the final experiments and compared with the response to the normally used bulbs. Then several times during the run of experiments, the standard bulb was re-inserted as a check against aging: none was ever observed.

The photograph of a typical CRO trace is shown in Fig. 4.2 Sweep rate is 0.1 μsec/cm and the upper and lower beams are the respective outputs ΔV_2 and ΔV_1, from the intensity monitor and the scattering detector. Also shown are the zero level base lines. We may recall that the phototube outputs were electronically integrated and the voltage change displayed was directly proportional to the number of photons incident on the photocathode. Consequently it was simply necessary to scale off the voltages ΔV_1 and ΔV_2 with a steel scale readable to .002 in.

Using these values for ΔV_i and the measured sensitivities S_i, we were able to calculate a dimensionless number $R_{\alpha\beta} \equiv (\Delta V_1/S_1)/(\Delta V_2/S_2)$, which was a measure of the combined intensities of pure scattering and spurious light. The double subscripts α,β have been used to refer, respectively, to polarization states of incident and scattered light.

To measure the portion of $R_{\alpha\beta}$ due to spurious light alone, the scattering chamber was evacuated to 1 millitorr. The procedure then followed was identical to that for scattering measurements, and another dimensionless number, $\mathcal{E}_{\alpha\beta} \equiv (\Delta V_1'/S_1')/(\Delta V_2/S_2)$ was computed. Primes have been

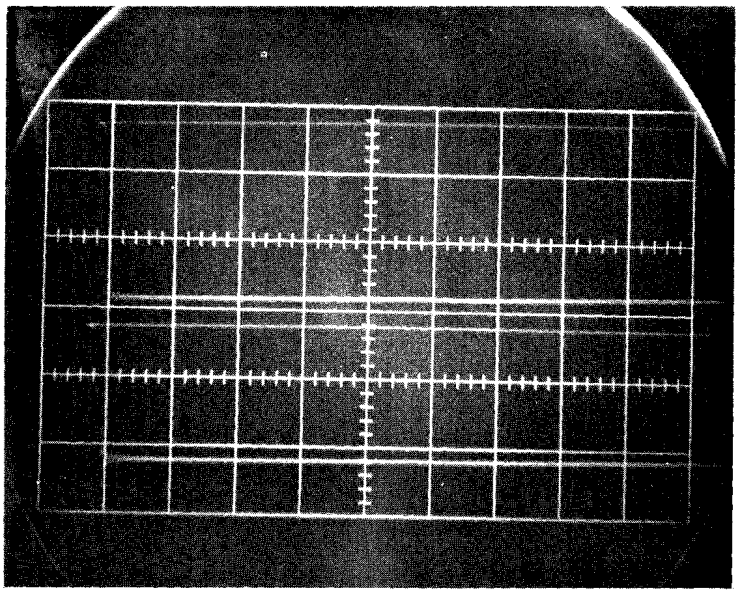

Fig. 4.2. Photograph of typical CRO trace. Upper beam is signal from intensity monitor (50 mv/cm) and lower beam is signal from scattering detector (500 mv/cm); sweep rate of 0.1 μsec/cm. Zero voltage baselines are also shown.

used to indicate that ΔV_1 and S_1 were often substantially different in a spurious light measurement than in a scattering experiment.

A number $I_{\alpha\beta}$ proportional to the fraction of α-polarized incident light scattered by gas molecules into direction Θ with polarization β was next calculated:

$$I_{\alpha\beta} = \left(\frac{29.92}{p}\right)\left(\frac{T}{273}\right)\left(R_{\alpha\beta} - \varepsilon_{\alpha\beta}\right) \qquad (4.1)$$

Corrections were made for departures from STP conditions: p being the scattering chamber pressure (in. Hg) and T, the gas temperature (°K).

Due to the statistical nature of photoelectron generation, multiple laser shots were required for each experimental situation. Then averaged values of $R_{\alpha\beta}$, $\varepsilon_{\alpha\beta}$ and $I_{\alpha\beta}$ were computed. Whenever reasonable, sufficient laser shots were chosen to yield a standard derivation for the averages of 1% or better.* Given the finite lifetimes of both laser and experimenter, however, such good statistics were not reasonably obtainable for cases of very weak scattering, and an arbitrary upper limit of 24 shots was imposed.

The laser was fired at intervals of one minute, this time being sufficient to allow the laser cavity to reach thermal equilibrium. As

*It is instructive to note that the number of photoelectrons generated in the intensity monitor per laser pulse were approximately 7500. Approximate numbers for the electrons ejected from the cathode of PM_1 in a typical nitrogen scattering experiment were 30,000 and 180, respectively for V- and H-polarized scattering and 27 and 3.7 for V- and H-polarized spurious light. The method by which these numbers were obtained is discussed in section 5.1.

a result, laser output displayed a 10% shot-to-shot consistency. (However, the long term stability was poor, the general trend being towards lower powers.)

Cross sections and depolarization ratios for each of the eight gases investigated in this experiment were determined by measuring the polarization-dependent scattering intensities I_{VV} and I_{VH} for vertically polarized incident light. Each I_{VV} measurement was referenced to the I_{VV} value for nitrogen, whose scattering cross section was known from the absolute calibration experiment described in the next section. In this way, σ_{zz} for each gas was determined. As a precaution against any long term changes in the operating characteristics of the experimental apparatus, nitrogen was introduced into the scattering chamber several times during the course of experimentation and I_{VV} was remeasured. No significant changes were observed.

The depolarization ratio ρ_v was simply the ratio I_{VH}/I_{VV}. The general procedure employed was to fill the scattering chamber and take a series of six laser shots to measure I_{VV}. Rotating the polarization analyzer exactly 90° (to the setting previously determined by the argon measurements) quickly permitted the measurement of I_{VH} with a second series of six shots. This method removed any possible errors due to the pressure measurement, as the p-dependence cancelled out when the ratio was taken.

The entire procedure was generally repeated three or four times to improve statistics, the chamber being evacuated and refilled for each set

of measurements. Then a grand average for ρ_v of the gas was determined.

All of the final I_{VV} and I_{VH} measurements were performed at a scattering angle of $\theta = 60°$, as at this angle the relative intensity of spurious light, as expressed by the ratio $\mathcal{E}_{VH}/I_{VH}$, was minimized. To verify that the depolarization measurements were in no way affected by this choice of angle, we also measured ρ_v at 90° for nitrogen and methane, and obtained excellent agreement.

There was some concern that the narrow band interference filter might somehow have contributed to measured depolarizations. This was removed when it was determined that the filter exhibited no birefringence and transmitted all polarizations equally.

The angular dependence of Rayleigh scattering was measured in nitrogen as a function of the polarization states of both incident and scattered radiation. This was first done for vertically polarized light, after which the laser, Glan-Thompson prism, and entrance and exit flats were rotated 90° for the horizontally polarized experiments.

The measurements performed at each observation port followed exactly the same procedure previously described for 60°. The 60° measurements of I_{VV} and I_{VH} were taken as standards, and the scattering detector was moved back to 60° several times during the run of experiments to check for any long term changes in equipment operating characteristics.

Complete measurements (of I_{VV}, I_{VH}, I_{HV}, and I_{HH}) were made at 30°, 60°, 90°, 120°, and 150°, but the 105° and 135° ports were used only to

determine I_{HH}. This procedure was prompted by the great amount of time required to obtain each set of data and by the observation that only the I_{HH} data added significant detail to the measured angular distribution of scattering.

Although a good deal of care had been exercised in machining the holes for the observation ports, a series of experiments were carried out to accurately determine their angular placement.* The nominal and actual angles of each port are indicated in Table 4.1.

TABLE 4.1

MEASURED ANGLES OF OBSERVATION PORTS

Nominal Angle of Port	Measured Angle of Port
30°	30°34'
60°	60°02'
90°	89°54'
105°	104°32'
120°	119°50'
135°	134°16'
150°	150°22'

The end windows of each observation port were selected for uniformity of transmission characteristics: all had transmission coefficients within $\pm$0.3% of 91.5%.

*These measurements were performed by Mr. George D. Darling as part of his Masters' project studies. He employed an arrangement consisting of a He-Ne gas laser, a precision indexing table, and a front surface mirror to determine the observation port angles to an accuracy of 10' or better.

4.3 CROSS SECTION DETERMINATION

In order to determine an absolute number for the differential scattering cross section, it was necessary to obtain a calibration of the detection optics.

Basically this was accomplished by directing an attenuated portion of the main beam into the scattering detector and measuring the resultant response of PM_1. The accuracy of this experiment was strongly dependent upon an accurate knowledge of the very large attenuation coefficient.

We first attempted a method described by T.V. George et al.,[22] in which the attenuation was produced by a thickness of $CuSO_4$ solution. Since the copper sulfate attenuated exponentially, measurements of the response to different levels of solution permitted an extrapolation back to zero thickness and consequent calibration of the system.

In trying this method, we were frustrated by numerous difficulties. These included the inability to compensate for evaporation of the solution, which, owing to the exponential nature of the attenuation, propagated large errors. Additionally, even with the use of a 10 ml burette having .05 ml graduations, it was impossible to fill the long copper tube containing the solution with sufficient accuracy. The addition or deletion of a single droplet produced a significant error. A further complication was the tendency of droplets to cling to the walls of the tube. When these droplets would not be induced to join the remainder of the fluid, the experiment had to be restarted. Due to the meniscus effect of the solution and

the finite cross section of the laser beam, different parts of the beam traversed varying lengths of solution, thus contributing an unknown error to the measurements.

Having noted these and other difficulties and also having been unsuccessful in obtaining consistent extrapolated results for the calibration, we finally abandoned this method.

It was possible to gain one valuable piece of information from the $CuSO_4$ measurements: the range of linearity of response of our photomultiplier tubes to laser pulses. It was quite necessary to obtain this information, as manufacturer specifications for linearity were quoted for steady state conditions and not readily converted to pulsed operation. For laser shots producing a photomultiplier voltage pulse ΔV_i of greater than approximately 5v (absolute value), the exponential response versus $CuSO_4$ length began "kneeing over," thus indicating the onset of nonlinearity. No nonlinear response was observable at low intensities, down to the minimum measurable voltage pulse of approximately 2 mv. To insure linear operation throughout the course of experimentation, photomultiplier gain was adjusted to avoid operation above $|\Delta V_i| = 2v$.

The calibration method eventually chosed consisted of two parts: a "calibration phase" and a "scattering phase." The experimental arrangement for the first phase is depicted in Fig. 4.3 Here the optical axis of the scattering detector was aligned with the direct laser beam, which was attenuated a known amount by a set of three optically dense filters. Since intensity monitoring by the usual method was impossible, a secondary

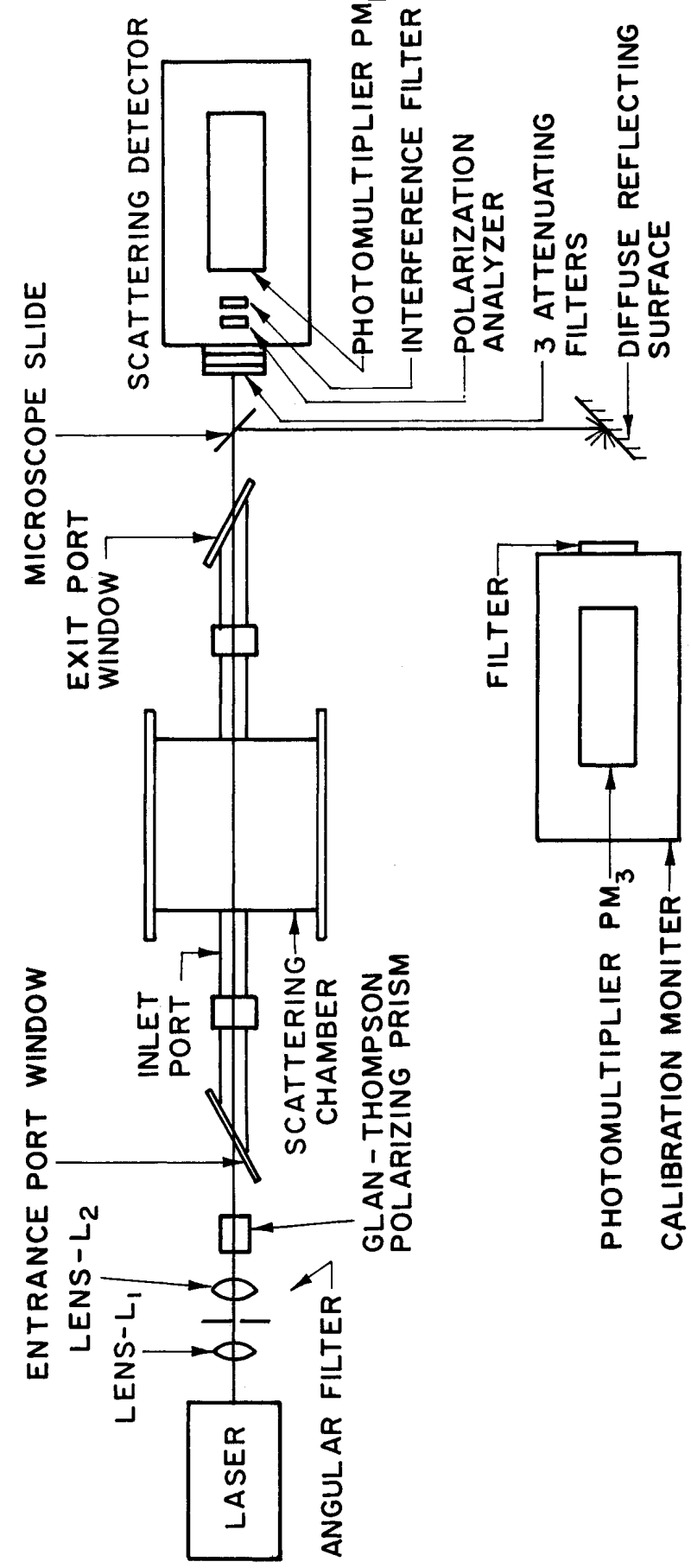

Fig. 4.3. Experimental arrangement for calibration experiment.

monitoring arrangement had to be employed. In this, a portion of the beam was reflected downwards by a microscope slide, and a third photomultiplier tube PM_3 viewed the diffuse scattering of this light. As before, linear operation of PM_3 was achieved by attenuating the reflected light with a pinhole-optical filter combination.

In order to analyze the experimental results, the following definitions have been made:

T_1 = transmission coefficient of angular filter

T_2 = transmission coefficient of Glan-Thompson prism (major axis)

T_3 = transmission coefficient of entrance port window

T_4 = transmission coefficient of exit port window

T_5 = transmission coefficient of microscope slide

T_{6i} = transmission coefficient of i^{th} attenuating filter

T_7 = transmission coefficient of HN22 polarization analyzer (major axis)

T_8 = transmission coefficient of interference filter

T_9 = transmission coefficient of calibration monitor filter

T_{10} = transmission coefficient of observation port window

R_1 = reflectance of microscope slide

R_2 = reflectance of diffuse reflector

$d\Omega_c$ = solid angle subtended by pinhole aperture of calibration monitor

In addition a "conversion efficiency" C_j for each phototube PM_j has been defined as the magnitude of voltage pulse displayed on the CRO per 6943Å photon incident on the photocathode. This conversion efficiency

was a function of the quantum efficiency of the photocathode, the gain of tube, and the characteristics of the integrating electronic circuitry.

Of the n_o photons contained in the laser output, $n_o T_1 T_2 T_3 T_4 T_5 T_6 T_7 T_8$ struck the photocathode of PM_1, where

$$T_6 \equiv \prod_{i=1}^{3} (T_{6i}) \tag{4.2}$$

and thus the voltage pulse displayed by the CRO was

$$\Delta V_1 = n_o T_1 T_2 T_3 T_4 T_5 T_6 T_7 T_8 C_1 \tag{4.3}$$

Similarly, the voltage pulse of the calibrating monitor was

$$\Delta V_3 = n_o T_1 T_2 T_3 T_4 R_1 R_2 d\Omega_c T_9 C_3 \tag{4.4}$$

and the ratio of these two pulses is given by

$$R_c \equiv \frac{\Delta V_1}{\Delta V_3} = \frac{T_5 T_6 T_7 T_8 C_1}{R_1 R_2 d\Omega_c T_9 C_3} \tag{4.5}$$

After this ratio had been experimentally determined, the scattering detector was moved into alignment with the 60° observation port and scattering measurements were performed with pure nitrogen gas. Recalling the definition of the differential scattering cross section, the number of photons n_s scattered into the solid angle $d\Omega_2$ determined by the last of the collimating apertures was

$$n_s = n_1 N_o \ell \sigma_{zz} d\Omega_2 \tag{4.6}$$

where ℓ, the length of beam viewed by the detection optics, was a function of θ. Since the scattering cross section is very small, n_1 was essentially the number of laser photons which passed through the entrance window, or $n_0T_1T_2T_3$.

Clearly the number of photons that reached the cathode of PM_1 was $(n_0T_1T_2T_3)(\gamma\sigma_{zz})T_{10}T_7T_8$ where

$$\gamma \equiv N_0 \ell \, d\Omega_2 \tag{4.7}$$

and thus the scattered voltage pulse ΔV_1 was

$$\Delta V_1 = n_0 T_1 T_2 T_3 T_7 T_8 T_{10} \gamma \tag{4.8}$$

A new ratio R_s of ΔV_1 to ΔV_3 may be computed

$$R_s \equiv \frac{\Delta V_1}{\Delta V_3} = \frac{T_7 T_8 T_{10} \gamma \sigma_{zz} C_1}{T_4 T_9 R_1 R_2 \, d\Omega_c C_3} \tag{4.9}$$

Dividing R_s by R_c and rearranging:

$$\sigma_{zz} = \frac{T_4 T_5 T_6}{T_{10}} \cdot \frac{1}{\gamma} \cdot \frac{R_s}{R_c} \tag{4.10}$$

Thus the cross section was determined by separate measurements of T_4, T_5, T_6, T_{10}, R_s and R_c and a calculation of γ. The transmission coefficients T_4, T_5, and T_{10} were each approximately unity and were quite accurately measured with a He-Ne gas laser operating at 6328Å. As the refractive index of glass changes little in the red region of the spectrum, the values obtained were used without correction for the 6943Å ruby light.

The transmission coefficients T_{6i} of the three attenuating filters were obtained in straightforward fashion by employing the scattering detector in the "calibration" position. Two other filters were placed in front of the detector to reduce the laser intensity to a reasonable level. Then a series of measurements with and without each of the three attenuating filters established their individual transmission coefficients at 6943Å, the laser being fired a sufficient number of times to assure good statistics. In an independent experiment performed with a Cary Model 14 Recording Spectrophotometer, relative values for the three transmission coefficients were obtained and found to be in excellent agreement with absolutely measured ones.

In addition to the transmission measurements, a narrow beam He-Ne laser was used to check the filters for homogeneity and uniformity of transmission. We also verified that the transmissivity was independent of polarization and that the filters displayed no birefringence. Furthermore, no nonlinearity or deterioration of filter transmission characteristics for the high intensity ruby laser light could be detected.

The calculation of γ is outlined in Appendix A, the result being

$$\gamma = \frac{8 N_0 s_1 s_2^2}{L R_0 \sin\theta} \tag{4.11}$$

where s_1, s_2, L, and R_0 are defined in the appendix. Since the geometrical theory used to determine this result is not rigorously correct, we decided to experimentally test the applicability of the theory to our experimental

conditions. One way of doing this was to move a pinhole light source horizontally along the normal laser path and record the scattering detector response as a function of light position. Complementing this experiment was one in which a vertical plane diffuse light source was positioned along the laser beam centerline. The scattering detector was removed so that another photomultiplier, with pinhole aperture, could measure the intensity distribution of light transmitted by the collimating apertures in the observation port. The results of both experiments were predicted by geometrical analysis with small errors. It has thus been concluded that the theory outlined in Appendix A could be used here without correction.

The values of R_s and R_c were obtained by averaging the results of 18 laser shots in each of the two detector positions. These, along with values for T_4, T_5, T_6, T_{10}, and γ, then permitted a calculation of the cross section for Rayleigh scattering in nitrogen according to the prescription of Eq. (4.10).

CHAPTER V

DISCUSSION OF EXPERIMENTAL RESULTS

5.1 EXPERIMENTAL ERRORS

Although some of the experimental errors affected only certain phases of the measurements, there were others which were of concern in all the scattering work performed. These included errors due to statistical processes in the photomultiplier tubes, inaccuracies caused by electronic measuring devices, and the possible presence of undesired macroscopic impurities.

The only purely statistical effects significantly influencing the accuracy of the experiments were those associated with the photodetection devices. In analyzing these statistical effects, it is sufficiently accurate only to consider the electrons generated at the photocathode. Assuming a Poisson distribution in the number n_e of electrons generated, the percentage standard deviation σ of the anode signal was equal to $100/n_e^{1/2}$. In order to determine the relation between the number of photoelectrons and the voltage pulse displayed by the CRO, a series of photographs were taken of the dark noise of the photomultiplier tubes with a sweep rate of 100 μsec/cm and an applied voltage of 2000v. The voltage change due to each dark noise pulse was scaled off and an average of 3.82 mv/pulse computed. Assuming that each pulse was caused by the spurious emission of an electron at the photocathode, this average was exactly the desired relation and will be denoted by the

symbol f. A second determination was accomplished by computing from the same photographs the rate of generation r of noise pulses: 6230 sec^{-1}. Measurements of the capacitance C of the integrating circuitry (130 pf) and of the steady state dark current i_d (2.7×10^{-9} amp) resulted in calculating $f = i_d/rC = 3.35$ mv/pulse. These two values were within experimental uncertainty of each other, and their average, $f = 3.59$ mv/photoelectron, was finally chosen for the analysis of statistics.

It was obvious that at lower tube voltages (lower gains), the voltage/photoelectron was smaller. However relative gains were known from the sensitivity measurements, and hence it was a simple matter to compute, for example, that at the applied voltages of 1750v and 1250v, there were approximately 0.755 and 0.0135 mv/photoelectron, respectively. Changes in photomultiplier operating characteristics due to such phenomena as fatigue and recent operating history were not accounted for. However these changes were sufficiently small that insofar as the analysis of statistics was concerned, they were not important.

The voltage ΔV_i measured by one of the phototubes can be divided by the value of f appropriate to the applied voltage to directly obtain n_e and subsequently the percentage standard deviation. In a nitrogen V-V scattering experiment with both photomultipliers operated at 1250v, ΔV_1 and ΔV_2 were typically 400 mv and 100 mv, respectively, and resulted from the generation of 30,000 and 7500 photoelectrons at their respective cathodes. Consequently, the individual percentage standard

deviations were 0.58% and 1.16%, respectively, and the ratio $\Delta V_1/\Delta V_2$ had a percentage standard deviation σ_R of 1.3%. Twelve laser shots improved σ_R to 0.38%, a highly acceptable figure. All of the other gases had similarly low standard deviations, with the exception of weakly scattering helium, for which σ_R = 1.1%.

For depolarization measurements, the situation was not as good because of the low intensity of light reaching the photocathode. For example, the values of σ_R for nitrogen, hydrogen, and methane (which have successively lower values of σ_{zx} cross section) were 1.2%, 4.1%, and 5.1%, respectively. For very small depolarizations, relatively poor statistics were the biggest single source of error.

The sensitivity measurements were designed to eliminate errors caused by changes in photomultiplier operating characteristics. In this capacity they succeeded quite well. However, their simultaneous use carried the disadvantage that any error in their measurement produced a similar error in the final scattering result. There were two main sources of error: the microammeter, by which the current to the neon bulbs was set, and the picoammeter, which recorded the response of each photomultiplier tube to the light source. The manufacturers of both instruments stated their accuracies to be 2% of full scale. However since these specifications referred to the capability of the instrument to measure absolute currents, it was likely that relative current measurements, upon which the results were actually based, were done with substantially better accuracy. Actual experience indicated

that the neon bulb current could be set to an accuracy of better than 1%. On the other hand, the fluctuations in the anode current prevented a reading of the picoammeter with similar accuracy. The most reasonable conclusion was that each sensitivity measurement resulted in a total uncertainty of approximately 1.7%.

Another electronic device responsible for some error was the cathode ray oscilloscope. While specifications for the accuracy of vertical deflection (absolute voltage) were 3%, relative voltages were certainly displayed with much better accuracy. However, it is interesting to note that many of our early experimental results had to be discarded when it was discovered that the vertical deflection of the Tektronix Type 551 Dual Beam CRO, which was originally employed, was nonlinear.* The Type 555 CRO did not exhibit this nonlinear behavior and hence was used for all subsequent experimental work.

The method employed to scale off the Polariod traces likely led to errors equal to or greater than those of the CRO itself. Since the typical measured deflection was .3 in. and since a steel scale graduated in .005 in. intervals was used, it was not probable that an accuracy superior to 1.0% was obtained.

A constant concern during the initial phases of experimentation was that complete assurance be obtained that no nonlinear effects were entering into the measurements. It was for this reason, for example,

*The nonlinear behavior was discovered by observing that a calibrating square wave of 1 cm amplitude was significantly compressed near the top and bottom of the CRO face. For measurements such as ours, this was completely unacceptable.

that the results of the basically unsuccessful $CuSO_4$ calibration experiments proved worthwhile; they provided vital information regarding the range of linearity of the S-20 phototubes.

Furthermore, tests of phototube linearity with respect to the sensitivity monitoring procedure were conducted. These included a series of measurements of phototube response as a function of neon bulb current (from 50 to 500 μamps) for various applied voltages from 1000 to 1750v. As expected, the response exhibited a strictly linear behavior. In another experiment, the V-V scattering from nitrogen was studied at several different voltages applied to PM_1. It was found that measured values of ΔV_1 varied directly with S_1 (more accurately, all calculated values of I_{VV} were the same; i.e., well within experimental error of each other). Finally, the depolarization ratio in nitrogen was measured in two separate experiments. In the first, applied voltages of 1250 and 1750v were used, respectively, to measure I_{VV} and I_{VH}. In the second, an intermediate voltage was chosen such that both I_{VV} and I_{VH} could be measured without changing phototube gain. Again both depolarization ratios agreed closely. It thus was evident that the sensitivity measuring method correctly compensated data for changes in phototube gain and that nonlinear effects played no discernable role in this portion of the experimental procedure.

The high power of the ruby laser made it suspect as a possible source of nonlinear scattering phenomena. This suspicion was erased when the intensities of both V-V and V-H scattering in nitrous oxide

were studied as a function of laser intensity. The intensity was attenuated in three steps by placing successive cobalt-blue glass slides in front of the laser, with final total attenuation being a factor of 15. The results are displayed graphically in Fig. 5.1. They conclusively demonstrated linearity of the scattering.

However, as an additional verification, the V-V scattering in nitrogen was measured as a function of gas pressure. As may be seen from the graph in Fig. 5.2, no departures from linearity were found.

The presence of macroscopic particles (e.g., dust and macromolecules), owing to their large scattering cross sections, would have introduced large errors in the measurements. Consequently, all conceivable measures were taken to eliminate such particles from the scattering volume. These measures included efforts to clean the vacuum and gas feed systems as thoroughly as possible, the use of the molecular sieve desiccant in the gas feed line, and the allowance of time for potential dust particles to settle out in the scattering chamber.

Various experimental results have indicated that success was obtained. Had the density of macroscopic particles been appreciable, they would have caused the measured scattering cross section to exceed calculated values, the smaller the actual cross section, the greater the deviation. No such trend was observed. Also, since it is unlikely that the macroscopic particle distribution would depend directly on the background gas pressure, the influence of these particles should have been detected in the variable pressure experiment previously described.

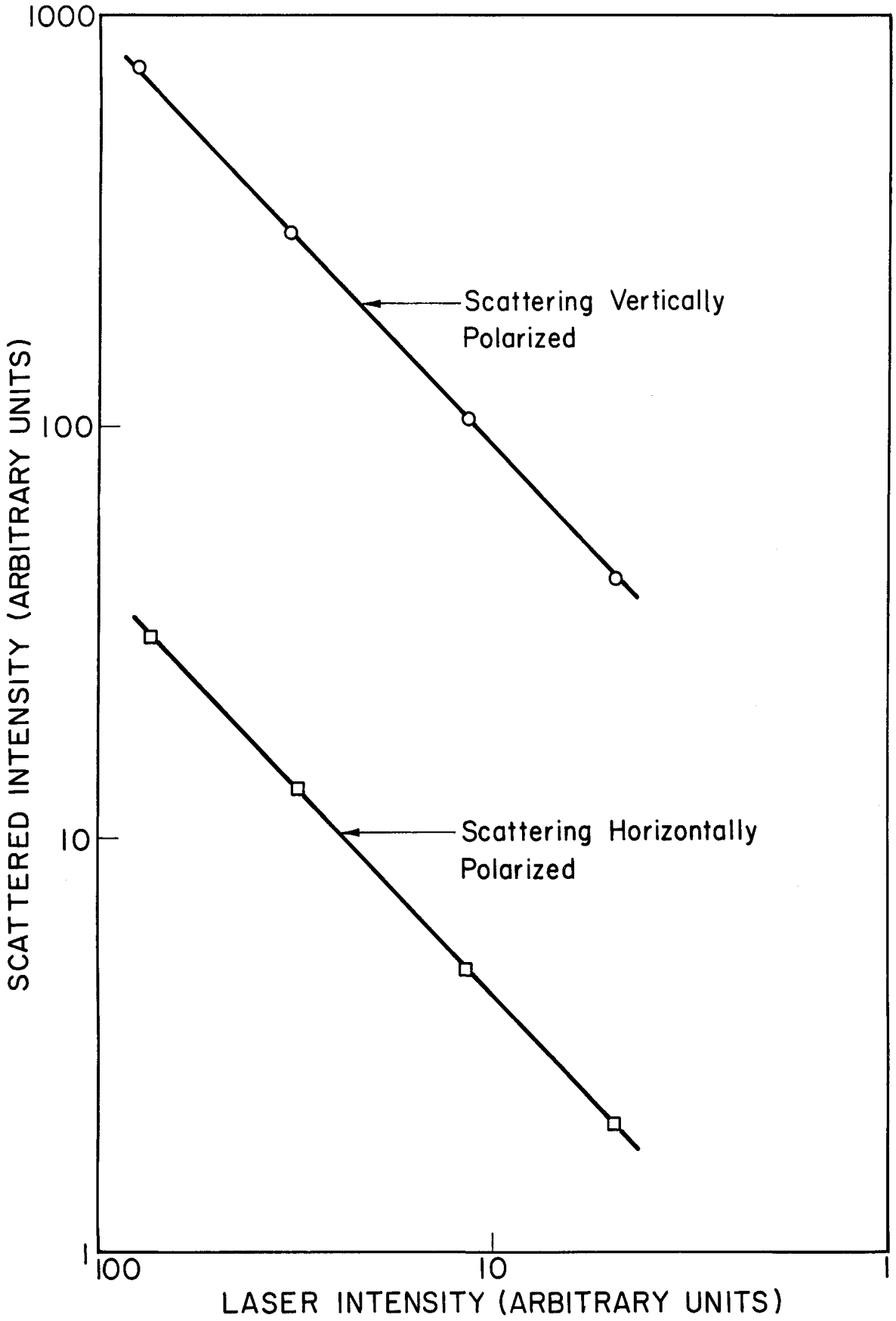

Fig. 5.1. Intensities of V-V and V-H scattering in nitrous oxide as function of incident beam intensity.

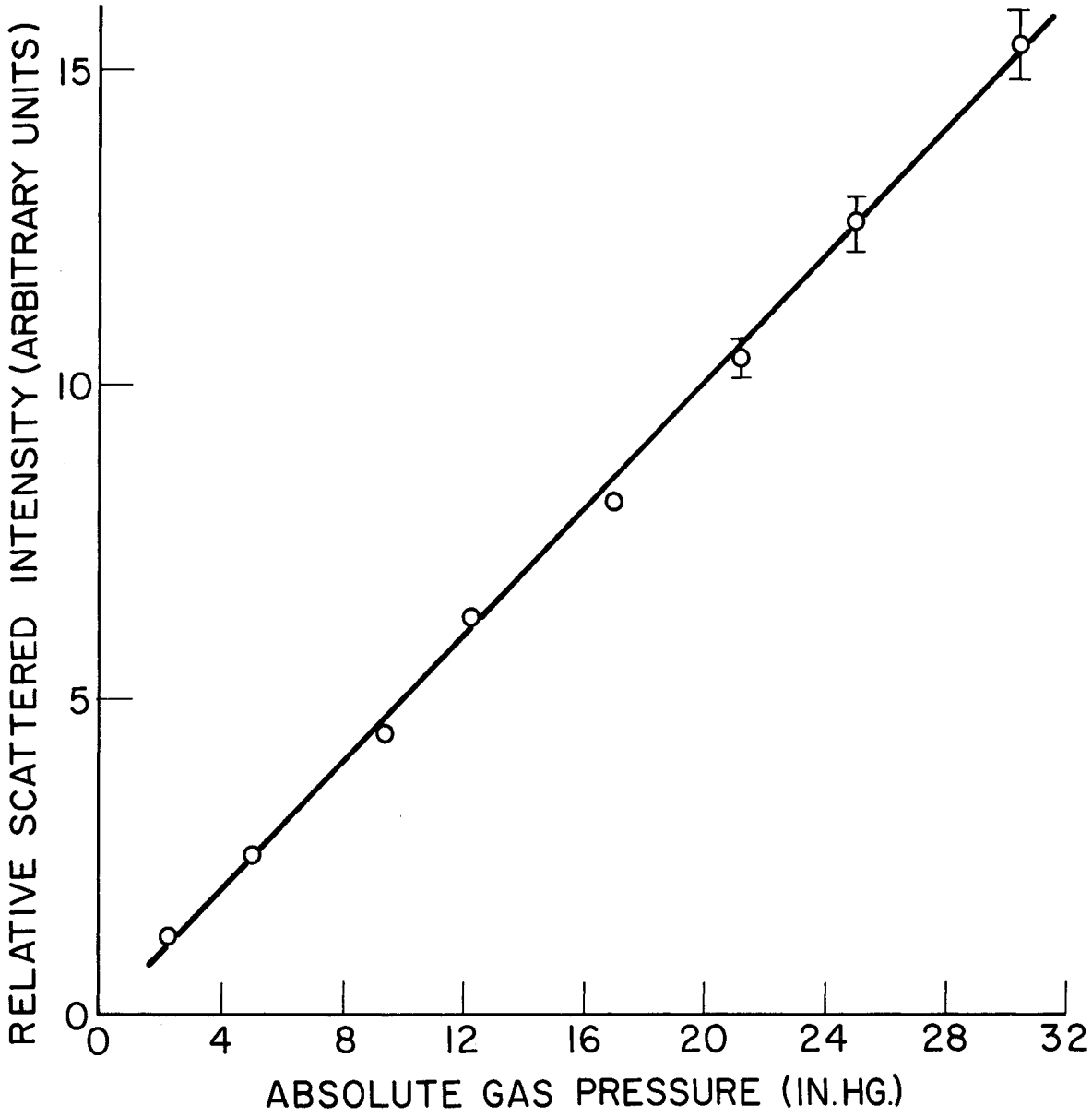

Fig. 5.2. Intensity of V-V scattering in nitrogen as function of gas pressure.

As a final check, the scattering from argon was studied over a period of 1 hr, beginning immediately after the scattering chamber was filled. Only the normal statistical scatter of data was evident when the results were plotted as a function of time.

As pointed out in Section 4.3, the measurement of the scattering cross section in nitrogen depended upon separate measurements of the parameters T_4, T_5, T_6, T_{10}, R_s, and R_c and a calculation of γ. The transmission coefficients T_4, T_5, and T_{10}, each of which was greater than 90%, were measured to a high degree of accuracy with a helium-neon gas laser. Even after the simple extrapolation from 6328Å to 6943Å, it is unlikely these measurements contributed any important errors to the final result. On the other hand, it was impossible to measure the transmission coefficients T_{6i} of the three attenuating filters to comparable accuracy. The main difficulty was caused by the statistical nature of the photodetection process. The type of analysis previously discussed determined the uncertainty of each transmission coefficient to be 1.3%. Thus the total transmission coefficient T_6 (1.99×10^{-11}) was only known to an accuracy of ±2.3%.

Statistical considerations also affected the determinations of R_s and R_c, but to a lesser extent. The percentage standard deviation of the ratio R_s/R_c was computed to be 0.8%.

It was possible to calculate the parameter γ with a relatively high degree of precision. Since the Bourdon gauge used for pressure measurements had an absolute accuracy of 0.5% and since the gas tempera-

ture was well known, the number density N_o was determined quite accurately. The angle of the 60° port was known to within ±10', and the geometrical factors s_1 and s_2 were measured by a vernier caliper to accuracies of better than 1%. Thus, assuming the validity of the geometrical analysis outlined in Appendix A, the uncertainty in the calculated value of γ was probably less than 1.5%.

As previously indicated, statistically generated errors became more and more important as the intensity of light reaching the photodetector decreased. Consequently, except for relatively strong depolarizing N_2 and N_2O, it was not possible to measure the I_{VH} (depolarized) component of scattering as accurately as the primary I_{VV} component.

Two interconnected difficulties were at the root of this problem. The first, of course, was that for very weak depolarizers, the quantity R_{VH} (defined in Section 4.2) could not be determined with a statistical accuracy of better than 4%. Additionally, the standard deviation of the spurious parameter ε_{VH} was approximately 10%. Thus the familiar problem of calculating the difference of two ill-defined, comparable numbers further reduced the experimental accuracy. For example, in the scattering experiments with hydrogen, ε_{VH} amounted to 24% of R_{VH}, with the result that the standard deviation of $I_{VH}(= R_{VH} - \varepsilon_{VH})$ was 6.3%, while that for R_{VH} alone was 4.1%. For the spherically symmetric scatterers, the situation was even worse.

It was possible to correct the experimental data for the facts that the minor principal transmittance of the Glan-Thompson polarizer

was not vanishingly small and that the entrance window had a slight depolarizing effect. Thus the laser beam traversing the scattering chamber was not completely polarized, having a horizontally polarized intensity I_{OH} which was a fraction β of the vertical component I_{OV}:

$$I_{OH} = \beta I_{OV} \tag{5.1}$$

Equations (2.17) can be used to show that I_{SV} and I_{SH}, the scattered intensities polarized vertically and horizontally respectively were:

$$I_{SV} = A(1 + \rho_V \beta)$$

$$I_{SH} = A[\rho_V + \beta \cos^2\theta + \rho_V \beta(1 - \cos^2\theta)]$$

where A is a proportionality factor. Since $\beta \ll 1$ and $\rho_V \ll 1$, the last term in each equation can be neglected with little error. Consequently:

$$\begin{aligned} I_{SV} &= A \\ I_{SH} &= A(\rho_V + \beta \cos^2\theta) \end{aligned} \tag{5.2}$$

The Polaroid analyzer also had a finite minor principal transmittance, so that even if it was set perfectly to measure the horizontally polarized component, some of the vertically polarized scattering was transmitted. The transmitted intensity in this case was:

$$I_H = k_1 A(\rho_V + \beta \cos^2\theta) + k_2 A$$

or

$$I_H = k_1 A\left(\rho_V + \beta \cos^2\theta + \frac{k_2}{k_1}\right) \tag{5.3}$$

where k_1 and k_2 were the major and minor transmittances, respectively.

When the analyzer was oriented so that its major axis was vertical, the transmitted intensity was:

$$I_V = k_1 A \left[1 + \frac{k_2}{k_1} (\rho_V + \beta \cos^2\theta) \right]$$

Because k_2, ρ_V, and β were all small:

$$I_V = k_1 A \tag{5.4}$$

Consequently the measured depolarization ratio was:

$$\rho_V^{Meas} = \frac{I_H}{I_V} = \rho_V + \left(\frac{1}{4}\beta + \frac{k_2}{k_1}\right) \tag{5.5}$$

where the experimental condition of $\theta = 60°$ has been assumed.

By performing a series of crossed polarizer experiments, it was possible to determine that $\frac{1}{4}\beta + k_2/k_1 = 4.0 \times 10^{-5}$. The measured depolarizations were then corrected for the finite values of k_2 and β by subtracting this quantity.

The assumption that the analyzer could be oriented with absolute accuracy was clearly not valid. Conservatively estimating that in the measurements with argon it was possible to detect a 25% increase above the minimum signal (due to the spurious component $\mathcal{E}_{VH}$ plus the intensity from the $\frac{1}{4}\beta + k_2/k_1$ factor), the null position was determined with an accuracy of ±0°13'. It then follows that the uncertainty in the measurement of a depolarization ratio ρ_V due to this inaccuracy was $\pm 1.7 \times 10^{-5}/\rho_V$. For xenon, this contributed an 11% error, while for nitrogen the re-

sultant error was an insignificant 0.3%. Note that in measurements of the σ_{zz} cross section, the analyzer setting was not nearly as critical.

Previous experiments using conventional optical sources required condensing lenses to focus the light at the center of the scattering volume. The ideal situation of a parallel incident beam obviously did not exist, and there were significant components propagating in the z and x directions in addition to the nominal y direction. Classical calculations[12] showed that this caused an apparently larger depolarization ratio to be measured; therefore a "convergence correction" had to be applied to the data to remove this effect.

The effect of convergence in this experiment has been investigated. A somewhat different, but straightforward, analysis was required, as previous computations had been done for unpolarized incident light. The basic result for polarized light was the same: the correction was proportional to the square of the semi-angle of convergence. A series of measurements, using a phototube and pinhole aperture combination, were performed to determine the beam intensity distribution at various distances from the laser. It was determined that 98% of the laser beam power was contained in a convergent cone of semi-angle 1.6 milliradians when focused by the angular filter arrangement. The convergence correction computed from this information was 2.6×10^{-7} and entirely negligible insofar as the measurements were concerned.

The possibility that the finite angular view of the scattering detector contributed an instrumental depolarization factor has also been considered and found negligible.

Since relatively low levels of molecular impurities could significantly affect depolarization measurements, it was deemed important to introduce and maintain the gas in the scattering chamber in as pure a state as possible. This was accomplished partially by preventive techniques such as avoiding high vapor pressure materials in the construction of the experimental apparatus, thoroughly degreasing and cleaning the system, flushing the scattering chamber through several times before the final fill, and valving off the scattering chamber from the remainder of the system as soon as it was filled. Since, however, the limiting purity was that of the gas supply itself, gases of the highest purity levels reasonably obtainable and necessary for the measurements undertaken were procured. The purities, as specified by the supplier (The Matheson Company) are listed in Table 5.1.

TABLE 5.1

PURITY LEVELS OF GASES

Gas	Purity, %
Helium	99.999
Argon	99.999
Xenon	99.995
Methane	99.95
Hydrogen	99.999
Deuterium	99.5
Nitrogen	99.997
Nitrous Oxide	98.0

The first four had been spectroscopically analyzed so that specific information regarding identity and concentration of the impurities was

available. Using known cross sections and depolarizations, it was possible to compute the effect of these contaminants: there were no cases in which the impurity level was high enough to have caused a measurable increase in the depolarization ratio.*

5.2 CROSS SECTION MEASUREMENTS

Following the procedure outlined in Section 4.3, the scattering cross section σ_{zz} for nitrogen was measured, and subsequently cross sections for several other gases were determined by measuring their scattering powers relative to nitrogen. These values are compared in Table 5.2 with cross sections calculated from Eq. (2.16) using our measured depolarization ratios ρ_v and tabulated[29] refractive indices (extrapolated graphically to 6943Å).

TABLE 5.2

MEASURED AND CALCULATED RAYLEIGH SCATTERING CROSS SECTIONS

Gas	Measured Cross Section ($\sigma_{zz} \times 10^{28}$ cm^2)	Computed Cross Section
Helium He	.0296 ± .0014	.0284
Deuterium D_2	.431 ± .021	.449
Hydrogen H_2	.438 ± .021	.449
Argon Ar	1.88 ± .09	1.85
Nitrogen N_2	2.12 ± .09	2.10
Methane CH_4	4.56 ± .22	4.49
Nitrous Oxide N_2O	6.40 ± .31	6.40
Xenon Xe	11.55 ± .55	11.38

*The relatively low purity of N_2O caused no difficulty because the primary constituent has such a large cross section and depolarization ratio.

The uncertainties indicated for the experimental cross sections were determined in accord with the error analysis of the previous section. The measured values agreed with the calculated ones to within experimental error for each of the gases studied.

In view of this close agreement, it is difficult to understand the results of T. V. George et al.,[22] who measured cross sections approximately twice as large as the calculated values. Although it might be postulated that special properties of the laser (for example, its coherence) could lead to anomolous scattering effects, it was our experience that moderately high powered lasers of the type employed in this experiment do not cause the scattering to depart in any measurable detail from the predictions of Rayleigh theory.

The results of this experiment should be of some interest to the plasma physicist employing a ruby laser as a diagnostic tool to determine electron number densities from the intensity of Thomson scattering. He can avoid having to perform a difficult, time-consuming calibration experiment of the type employed here to determine absolute cross sections. Instead he can perform a Rayleigh scattering measurement with a neutral gas,* and confidently employ our experimental cross sections to completely calibrate his optical system.

*Preferably he should use a noble gas such as argon, for which no experimental corrections for Raman scattering or depolarization are necessary.

5.3 ANGULAR DEPENDENCE OF SCATTERING IN NITROGEN

The experiment of Watson and Clark[61] appears to have established the validity of Rayleigh theory in describing the angular behavior of scattering. Nevertheless, it was decided to perform another angular measurement. The main reason was that, to our knowledge, no previous experiment had measured the angular dependence of Rayleigh scattering in a gas as a function of the polarization state of the scattered light as well as that of the incident light. Secondly, in view of the discrepancies observed by George et al.,[22] in the first angular measurement, another independent measurement seemed worth doing.

Nitrogen was selected for these measurements primarily because of its relatively high σ_{zz} cross section and moderately low depolarization ratio. Consequently it was possible for the significant θ-variation of σ_{HH} to be amply displayed.

The results of our studies of the angular dependence of Rayleigh scattering in nitrogen are graphically displayed in Fig. 5.3. Since only relative scattered intensities were of importance, the measured values of $S_{\alpha\beta}(\theta) = I_{\alpha\beta}(\theta)\sin\theta$ were plotted. The quantity $I_{\alpha\beta}$ was defined in Eq. (4.1) and the factor $\sin\theta$ was necessary—according to the theory outlined in Appendix A—to compensate for the different lengths of beam viewed at each of the observation ports.

In order to fit theoretical curves based on Eqs. (2.17) to the experimental results, all of the angular data obtained with vertically polarized incident light were combined to determine averaged values for

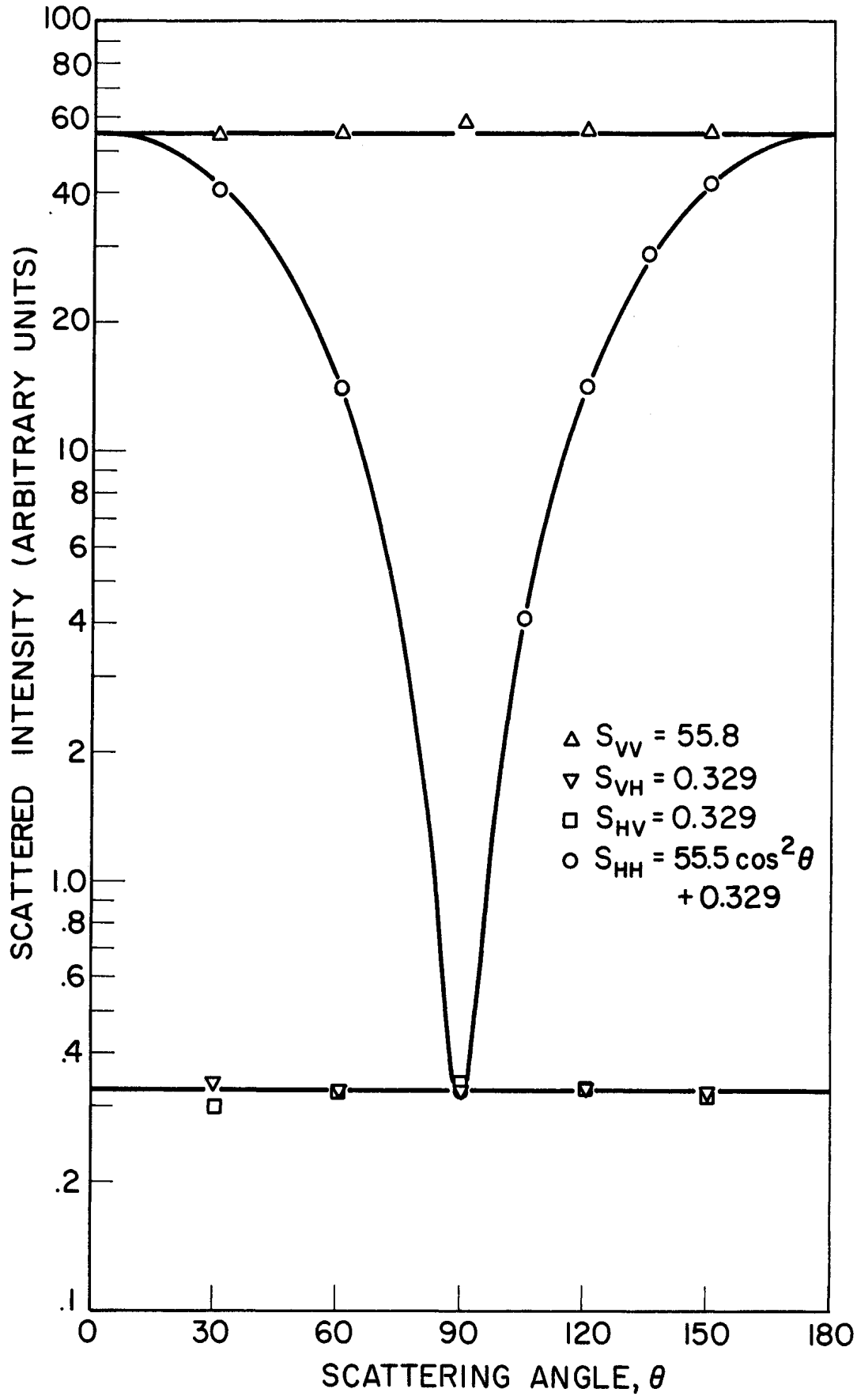

Fig. 5.3. Angular dependence of Rayleigh scattering in nitrogen as a function of the polarization states of incident and scattered light.

S_{VV} and ρ_v (55.8 and 0.00590, respectively). The resultant equations for S_{VV}, S_{VH}, S_{HV}, and S_{HH} were indicated in the figure and were also graphed.

No error bars were indicated, as they were approximately the size of the symbols used to denote the data points. The standard deviations for all values of S_{VV} and S_{HH} (except at $\theta = 90°$) were 3.0%, while S_{VH} and S_{HV} were measured somewhat less accurately (due to poorer statistics) and had an average uncertainty of 3.9%. Although a few of the experimental points did not lie within one standard deviation of the theoretical curves, the departures were not large and appear explainable in terms of statistical error.

The most reasonable conclusion to be drawn from the data is that the actual angular dependence of Rayleigh scattering does not differ significantly from the predictions of theory. This is in agreement with the findings of Watson and Clark.[61] While it does not change this basic conclusion, it is interesting to note that the depolarization ratio measured in this experiment was a factor of 2.8 lower than that reported by Watson and Clark for nitrogen. Our low value will be further discussed in the next section.

5.4 DEPOLARIZATION MEASUREMENTS

The success of this experiment in obtaining reliable values for depolarization ratios most likely resulted from the use of improved equipment and from the choice of certain experimental techniques.

The prime example of improved equipment was the use of the laser. It is apparent that the laser is superior to previously available light

sources for Rayleigh experiments. The high intensities achievable with lasers are particularly important to light scattering experiments, which are so strongly limited by the small scattering cross sections of most molecules.

Through the mid-1930's, most experiments employed sunlight, with all of its attendant disadvantages. The more modern work, up to 1964, was generally done with mercury arcs. Both of these sources required large condensing lenses to focus the light into the scattering volume. Owing to the large angle of convergence of the incident light, an appreciable fraction of the measured depolarization was due to convergence error. Although Cabannes[12] in 1921 recognized the necessity for applying a convergence correction, a number of experimentalists, including Rao[46] and Parthasarathy,*[37] failed to correct their data. Moreover, there was a long dispute[5,1] over the proper analytical form for the correction, and it has never been adequately demonstrated that the correction finally accepted completely removes the convergence error, particularly for very small depolarizations. The primary difficulty was that in order to obtain a valid correction, the intensity distribution of the converging beam had to be well known. With this not available, the gross character of the beam (namely, the semi-angle of convergence) had to be used at the sacrifice of desirable accuracy. The use of a laser beam in our experiments required such a small angle of convergence that

*Parthasarathy in 1951 published a note[38] correcting his earlier 1932 results[37] for convergence effects.

the correction was negligible, thus making our incomplete knowledge of the beam distribution irrelevant.

The extremely short duration of the laser pulse (50 nsec) was particularly important to this experiment, as it made possible a method of collecting data which avoided the many problems generated by phototube dark noise. The technique of integrating the output pulse from each phototube, displaying it on a CRO, and discriminating against any dark noise pulses was described in Section 3.6. Had dark noise been a problem, it might have been necessary to refrigerate each phototube. Refrigeration is not without its practical difficulties, and, furthermore, it generally results in a decrease in quantum efficiency. Thus, being able to avoid the problems of phototube cooling was considered worthwhile.

The laser was probably the single most important contributor to the success in reducing spurious light to a level such that, on the average, it generated in the photocathode of the detector only three or four electrons per laser pulse. This spurious intensity effectively established a lower limit to the intensity of scattering which could be observed. Only with this unprecedented low background was it possible to adequately study the question of whether or not spherically symmetric atoms and molecules indeed depolarize, as has been suggested by the results of numerous previous experiments.[2,8,12,19,31,33,38]

Performing depolarization measurements with polarized incident light, rather than unpolarized, had certain distinct advantages. We

established the fact that the spurious light retained, to an appreciable extent, the polarization content of the incident beam. Consequently there was a much smaller spurious background to be contended with when small depolarized components of scattering were measured. Also with the laser beam polarized, it was not necessary to correct data for the finite angular view of the scattering detector.*

The capability of this experiment to observe scattering at various angles permitted the selection of the angle at which maximum suppression of spurious light occurred. This turned out to be $\theta = 60°$, thus illustrating the versatility of the experimental arrangement. Virtually all previous depolarization measurements were performed solely at 90°.

It is generally recognized that photomultiplier tubes are superior to other possible scattering detectors, such as photographic film and the human eye. The phototube has an extremely wide range of linear response, extending over many decades. In addition, with gains as high as 2×10^7 attainable, it can amply detect and amplify the feeble intensities of scattering. Consequently, most recent Rayleigh experiments have used photomultiplier tubes.[8,19,22,61,62]

It is possible for an impurity content as low as 0.1% (or even less in some cases) to contribute significantly—perhaps completely—to the

*This statement, together with the previous one regarding convergence corrections, points out a major philosophy of this research: wherever possible, the experiment was arranged so that corrections to data were negligible. Clearly such an arrangement is superior to one in which finite corrections, with finite errors, must be applied.

depolarization measured for a spherically symmetric scatterer. Since it was difficult to accurately correct for the presence of contaminants, impurities may well have produced the nonzero depolarizations reported in previous experiments. Only recently have gases become available with sufficiently high purity levels. Consequently, as discussed in Section 5.1, the use of ultra pure gases in this experiment eliminated the need to correct the data for gas impurities.

The results of our experimental determinations of depolarization ratios are summarized in Table 5.3. The indicated confidence limits were determined according to the analysis of Section 5.1. Statistical effects, the finite intensity of spurious light, and inaccuracies in setting the polarization analyzer were the main determinants of experimental error. The lower the value of σ_{zx}, the less accurate was the measurement of the depolarization ρ_v.

TABLE 5.3

MEASURED DEPOLARIZATION RATIOS

Gas	$\rho_v \times 10^4$
Asymmetric Scatterers	
Hydrogen H_2	33.9 ± 2.5
Deuterium D_2	38.1 ± 2.9
Nitrogen N_2	59.0 ± 3.0
Nitrous Oxide N_2O	$469. \pm 17.$
Spherically Symmetric Scatterers	
Helium He	$\leq 30.$
Argon Ar	≤ 0.4
Xenon Xe	$1.55 \pm .25$
Methane CH_4	$1.27 \pm .23$

The experimental results have been arranged in two groups, the first consisting of the four asymmetric scatterers studied: hydrogen, deuterium, nitrogen, and nitrous oxide. The basic motivation for studying such scatterers was the wide dispersion in the results of previous depolarization measurements. For example, five representative measurements of $\rho_v(\%)$ in hydrogen performed between 1927 and 1963 varied from 0.45 to 1.36,[2,33,38,46,60] with an average of 0.93. The average of seven measurements with nitrogen was 1.32 (ranging from 0.60 to 1.76),[8,12,19,33,38,46,62] while for N_2O the average of four experiments was 5.56 (±.70).[2,38,46,60]

The specific selection of the gases studied resulted from the desire to deal with relatively simple molecules that exhibited differing degrees of asymmetry. Since N_2O, N_2, and H_2 were known to have, respectively, relatively high, moderate, and low depolarizations, they were appropriately logical choices. Although there was no reason to believe that deuterium would depolarize differently than hydrogen, we felt it would nevertheless be interesting to experimentally investigate the possibility of an isotopic effect. Within the confines of experimental accuracy, it was not possible to detect a significant difference in the scattering behavior of deuterium, either with regard to the depolarization or the scattering cross section σ_{zz}.

The experimental depolarizations for H_2, N_2 and N_2O were lower than the generally accepted values (based on the averages cited above) by factors of 2.7, 2.2 and 1.2, respectively. These results are most plausibly explained in terms of our experimental efforts to isolate Ray-

leigh scattering from Raman. Since many Raman lines are strongly depolarized, failure to exclude them can lead to the measurement of an apparently larger depolarization ratio. This happens despite the fact that Raman scattering cross sections are generally a factor of 10^3 or more smaller than those for Rayleigh scattering.[62]

Until the discovery of the Raman effect in 1928, it was obviously not considered necessary to experimentally discriminate against the Raman-shifted radiation. Even afterwards the continuous spectrum of sunlight precluded any experimental corrections. Use of mercury arcs permitted the inclusion of colored filters into the optical design. However, since these filters reduced the overall intensity of scattered light, often to the limit of detectibility, they were not used in many experiments. The few experiments which were successful in employing filters generally measured smaller depolarization ratios. A typical example was the work of Dintzis and Stein[19] in which filtering reduced their measured depolarization ratio in N_2 from 1.08 to 0.89, approximately a 20% decrease. Obviously the intensity of the depolarized Raman scattering was sufficiently high in this experiment to cause an observable effect in the measurements without a filter.

The recent work of Weber, Porto, Cheesman and Barrett[62] nas provided the most significant confirmation of our results. Using a He-Ne laser and observing the scattering with a high-resolution spectrograph, they were able to completely isolate the Rayleigh line in N_2, O_2, and CO_2 and measure its depolarization. In each case, they measured sub-

stantially smaller depolarization ratios than those commonly accepted, and asserted this was due to their elimination of Raman scattering.

Since we did not employ a high resolution spectroscopic device in our detection scheme, but rather used an interference filter of finite bandwidth, we cannot claim with complete assurance that all Raman light was removed. The excellent sideband blocking characteristics of the filter make it extremely unlikely that vibrational Raman scattering was transmitted to a measurable extent. On the other hand, pure rotational Raman lines, for which $\rho_v = \frac{3}{4}$, are only slightly shifted from the central Rayleigh line. Typical separations of adjacent rotational lines are of the order of several Ångstroms.* Although the transmission coefficient of the interference filter decreased rapidly to either side of 6943Å, it does not necessarily follow that the rotational Raman light was sufficiently diminished. Unfortunately, the necessary cross sections for rotational Raman scattering are not available, thus precluding a calculation of their effect in our experiments with N_2, H_2, D_2, and N_2O.

Consequently, it can only be claimed with assurance that these measurements represent new upper limits for the true Rayleigh depolarization ratios. However, the fact that Weber and colleagues measured for nitrogen $\rho_v = 0.60$, a value negligibly different from ours, is a strong

*It is interesting to note an advantage of performing a scattering experiment in the red portion of the spectrum: the spacing between adjacent Raman lines is 2.5 times greater for 6943Å ruby light than for the 4358Å Hg line. Thus the rotational spectrum is further spread out with the result that a filter of given bandwidth is considerably more effective in the red.

indication that Raman scattering had no important effect in our experimental results. It thus follows that more than representing upper limits, our measured values probably differ from the actual depolarization ratios by only experimental error.

It is interesting to note that while the competition of Raman scattering was of paramount concern in the measurements just described, it had no effect on the depolarization measurements conducted with spherically symmetric scatterers. The noble gases do not Raman scatter and methane has no pure rotational* Raman spectrum.[4,31]

The results for helium, argon, xenon, and methane appear in the second half of Table 5.3. In helium and argon, no depolarization could be observed to respective confidences of 3×10^{-3} and 4×10^{-5}.** To the best of our knowledge, both of these numbers are approximately one order of magnitude lower than any others that have been measured elsewhere,[19,33,38,51] thus supporting the contention that spherically symmetric scatterers do not, in themselves, measurably depolarize.

Xenon and methane, on the other hand, displayed nonzero depolarizations. We are convinced that these depolarizations are real and not instrumental. The effects of the imperfection of the polarization state of the incident beam and the nonzero extinction coefficient of the analyzer have been removed. Errors such as those due to impurities,

*The vibrational Raman scattering of methane is sufficiently removed from 6943Å to have been very strongly attenuated by the interference filter.

**The difference between the two confidence levels is the result of the much smaller σ_{ZZ} scattering cross section of helium.

misalignment of the polarization analyzer, and convergence of the incident beam have been analyzed and shown to be too small to account for the measured depolarizations. Finally, there is the overwhelming fact that no anisotropy in the scattering of argon and helium was detectable with precisely the same experimental arrangement. Had there been some important instrumental depolarizing effect, it should have manifested itself in these measurements as well.

In vainly attempting to explain the measurements with xenon, we performed the calculation outlined in Section 2.3. The prime value of the analysis appears to be in its negative result: away from resonance, the effect of nuclear spin in causing depolarization is negligible.

Subsequent to the performance of this calculation, we were fortunate to discover the work of Kielich,[26] who has treated the effects of real gas behavior on Rayleigh scattering. Although at STP conditions the departure from the ideal gas approximation in most gases is too small to be observable in Rayleigh scattering, our success in reducing spurious light has apparently enabled us to detect it in the depolarized scattering from xenon and methane.

Kielich's quasi-classical treatment of the problem involves a virial expansion of a quantity which governs the anisotropy of the scattering (and corresponds to the cross section that has been defined as σ_{zx}). Since the polarizability tensor is diagonal for a spherically symmetric scatterer, the first virial coefficient of the expansion vanishes. However the second coefficient is finite due to the polarizing effect of

intermolecular forces. Kielich succeeded in obtaining an analytical expression for the coefficient by assuming a Lennard-Jones (6-12) intermolecular potential. Suitably rearranging his results and keeping only the dominant term, we can show:*

$$\rho_v \simeq \frac{2\pi}{5}\left(\frac{\lambda}{2\pi}\right)^4 \sigma_{zz} N_o \frac{H_6(y)}{r_o^3 y^4}$$

where r_o and y are parameters of the Lennard-Jones potential, r_o being the intermolecular distance at which attractive and repulsive potentials are equal and

$$y = 2\left(\frac{\epsilon^*}{kT}\right)^{1/2}$$

Boltzmann's constant is k, the gas temperature is T, and ϵ^* is the negative value of the potential energy minimum. Values of the function $H_n(y)$ may be found tabulated by Buckingham and Pople.[9]

Employing experimental values for the Lennard-Jones (6-12) parameters r_o and ϵ^*, as tabulated by Hirschfelder, Curtis, and Bird,[25] we have computed ρ_v for helium, argon, xenon, and methane, as indicated in Table 5.4. The differences in the computed depolarizations result mainly from the σ_{zz} cross sections, as the quantity $H_6(y)/r_o^3 y^4$ is a relatively insensitive function of the gas identity. For purposes of further discussion, these values and the known σ_{zz} cross sections have been used to calculate σ_{zx} values for each gas, which are compared with

*The seemingly significant wavelength dependence of this equation, due to the λ^4 term, is removed when it is recalled that σ_{zz} varies as $1/\lambda^4$. Thus the true wavelength dependence is only that due to the slight dispersion of the refractive index μ.

our actual measurements.

TABLE 5.4

THEORETICAL AND MEASURED SCATTERING ANISOTROPIES FOR SPHERICALLY SYMMETRIC PARTICLES

Gas	$\rho_v x10^5$ (Calculated)	$\sigma_{zx} x10^{33}$ (Calculated)	$\sigma_{zx} x10^{33}$ (Measured)
He	.045	.0013	≤ 7.5
Ar	1.27	2.35	≤ 7.5
CH_4	2.25	10.1	58.0
Xe	5.19	59.1	177.0

The minimum cross section detectable above the spurious light background was approximately $7.5x10^{-33}$ cm^2. It is clear that the (theoretical) anisotropic cross sections of helium and argon are too small for us to have observed any depolarization, which indeed was the case. On the other hand, theory indicates that σ_{zx} for each of the other two gases is sufficiently large to have allowed the measurement of nonzero depolarizations in our experiments. Although the quantitative agreement with theory is rather poor, the fact that we observed the predicted finite depolarizations is certainly significant. The Kielich calculation is clearly an approximation, and it is not at all surprising that only order of magnitude agreement was obtained. Other theoreticians, including Buckingham and Stephen[10] and Theimer and Paul,[59] have also recognized that real gas effects can cause assemblies of spherically symmetric scatterers to depolarize. However no theory of sufficient rigor has yet been proposed for which more than qualitative agreement with experimental results is possible.

Although the departure from ideal gas behavior is the most plausible explanation for all of our experimental results with spherical scatterers, recent indications that xenon may form Xe_2 molecules,[52,63] even at STP conditions, suggest the interesting possibility that a portion of the measured depolarization was due to scattering from these diatomic molecules. Shardanand's[52] results indicate that at one atmosphere and 25°C the number density of Xe_2 should be approximately 1.4×10^{17} (or 0.55% of the density of Xe atoms). Conservatively assuming the cross section of Xe_2 to be the same as that of Xe and the depolarization ratio to be 1%, one-third of our measured depolarization may have been due to scattering from the molecules. However, until there is conclusive proof that the Xe_2 molecule exists, this must remain speculation.

CHAPTER VI

CONCLUSION

By virtually eliminating the effects of spurious light, this experiment has been able to study with unprecedented detail the possible depolarization of spherically symmetric scatterers. The inability of the experiment to detect any anisotropy in the scattering from argon and helium while measuring finite, though very small, depolarization ratios for xenon and methane is most tenably explained in terms of departures from ideal gas behavior.

New values have been obtained for the depolarization ratios of hydrogen, nitrogen, and nitrous oxide, and arguments have been presented for the conclusion that the lower measured depolarizations were due to experimental reduction (and possible elimination) of Raman scattering effects.

Absolute cross sections for Rayleigh scattering in various gases have been measured and found to agree with calculated values to within experimental error. In addition, the angular dependence of Rayleigh scattering in nitrogen has been studied as a function of the polarization states of both incident and scattered radiation, and agreement with Rayleigh theory has been demonstrated.

The lack of close agreement between our measured depolarizations for xenon and methane and the predictions of current real gas theories points out the need for further theoretical efforts in this direction.

It is possible that depolarization measurements with spherically symmetric scatterers could yield interesting information regarding the features of gas dynamics and intermolecular interactions. However a more accurate theory is required to both analyze the results of such investigations and to suggest new experiments.

It would certainly be of interest to construct a modified scattering chamber capable of being filled to pressures of approximately 20 atmospheres. Then the direct dependence of depolarization on number density, as predicted by Kielich's theory, could be tested with xenon and methane. It would furthermore be interesting to determine at what pressure the departure from ideal gas behavior is sufficiently great to cause argon to depolarize measurably. It would probably also be instructive to investigate the apparently less marked temperature dependence of depolarization in xenon and methane, particularly if the temperature range available was sufficiently wide.

Perhaps some of the interesting mechanisms of intermolecular interactions could be brought out by studying a mixture of, for example, helium and xenon. Certainly more theoretical work would be necessary to interpret the results of such an experiment.

The question of the possible existence of Xe_2 molecules could probably be answered by a spectroscopic analysis of the scattering from xenon gas. If indeed Xe_2 molecules are formed, their Raman spectrum would be unique and should be identifiable.

APPENDIX A

CALCULATION OF PARAMETER γ

In order to measure absolute scattering cross sections, it is necessary to know the scattering volume viewed by the detection optics and the effective solid angle subtended by the detector. In this experiment, these were solely determined by the rectangular collimators in the observation port, as the last one was the limiting aperture of the detection system.

A generalized picture of the scattering process is depicted in Fig. A.1. A parallel beam of photons is incident on a homogeneous collection of particles of number density N_o. The number of photons scattered from an element of volume δV located at position $\underline{r}$ into elemental solid angle $\delta\Omega$ about direction $\underline{\Omega}$ is $n(\underline{r})N_o\sigma(\underline{\Omega})\delta\Omega$ where n is the number of photons/cm^2 at $\underline{r}$. In order to determine the total number of photons scattered into limiting aperture "A," it is necessary to integrate over all solid angles permitted by the geometry of the collimators and over all volume viewed by the detection optics:

$$n_{sc} = N_o \int_{\text{Volume}} d^3r\, n(\underline{r}) \int_{\substack{\text{Solid}\\ \text{Angle}}} \delta\Omega\, \sigma(\underline{\Omega}) \qquad \text{(A.1)}$$

The angular dependence of the scattering cross section varies so slightly over the small angular view permitted by the collimating aper-

tures that it may be removed from the integral:*

$$n_{sc} = N_o \sigma(\underline{\Omega}) \int d^3r \, n(\underline{r}) \, d\Omega(\underline{r}) \qquad (A.2)$$

where

$$d\Omega(\underline{r}) \equiv \int \delta\Omega \qquad (A.3)$$

The computation of Eq. (A.3) requires specific information regarding the experimental arrangement, as is shown in Fig. A.2 (in which no attention has been paid to scale accuracy). A coordinate system (X,Y,Z) is centered on the limiting rectangular aperture "A," which was $2s_1$ in height and $2s_2$ in width. The closest aperture to the scattering volume (denoted "B") was of identical geometry and was located at Z = L.** A second coordinate system (x,y,z) is positioned at the center of δV, which is located at (X,Y,Z) with respect to the first system.

We now consider the scattering through an element of area dxdz, in the plane of aperture "A" and located at (x,y,z) from the scattering volume. The elemental solid angle becomes:

$$\delta\Omega = \frac{\sin\xi \, \sin\nu \, dx\,dz}{(x^2 + y^2 + z^2)}$$

*We have performed a series of computations which included the angular variation of the cross section and found that removal of the cross section from the integral involved negligible error except for the case of transverse scattering of horizontally polarized light by particles having a very low depolarization ratio.

**Observe that the two intermediate apertures, also of the same dimensions, play no role in this geometrical analysis. However their actual collimating effect of virtually eliminating forward scattering from the edges of the first aperture was of crucial importance in the experiment.

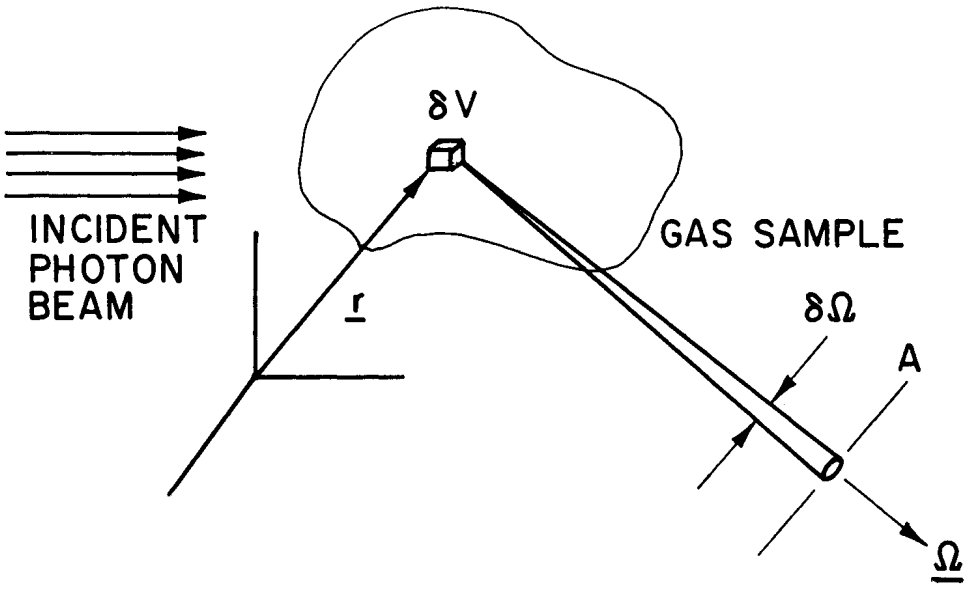

Fig. A.1. Schematic of general scattering process.

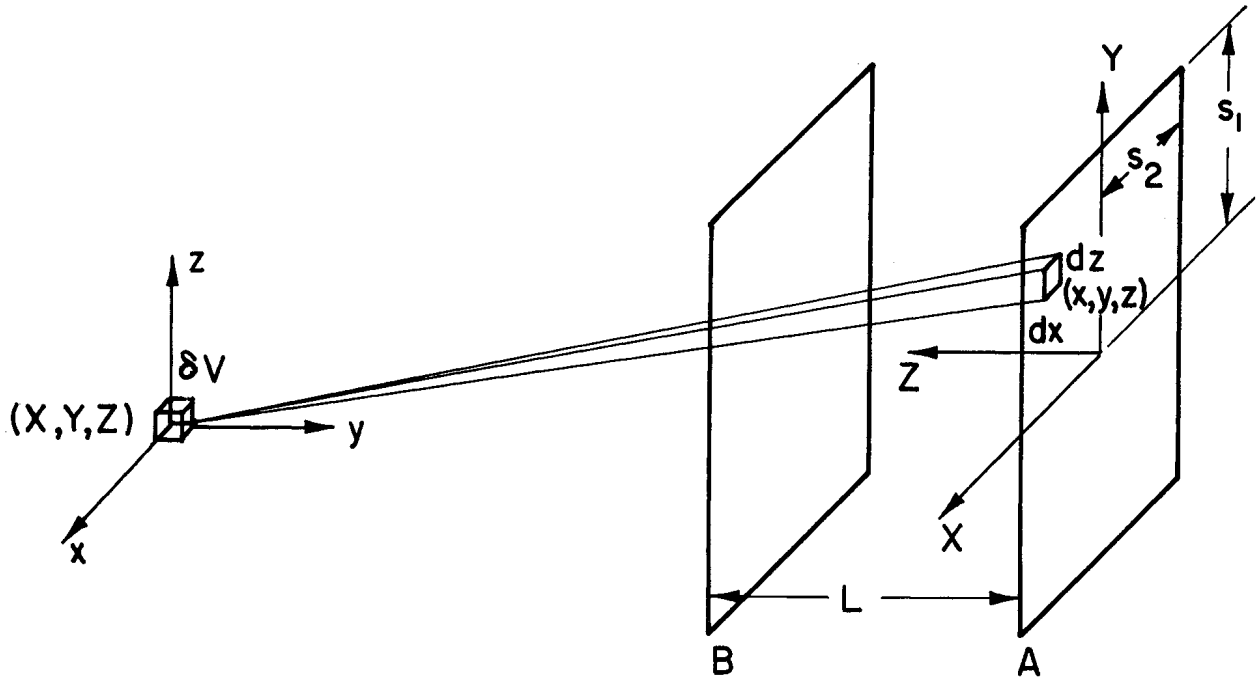

Fig. A.2. Schematic of rectangular apertures for solid angle calculation.

where ξ and ν are the indicated polar and azimuthal scattering angles. Expressing these angles in terms of rectilinear coordinates,

$$d\Omega = \iint dx\, dz \, \frac{Z_1}{(x^2 + Z^2 + z^2)^{3/2}} \tag{A.4}$$

where it has been noted that y = Z.

The solid angle is a function of position, and as may be seen from the geometry of Fig. A.2, three separate calculations must be performed These are for the following regions:

$$\begin{aligned} &\text{(a)} \quad X \geq s_2 \\ &\text{(b)} \quad s_2 \geq X \geq -s_2 \\ &\text{(c)} \quad X \leq -s_2 \end{aligned} \tag{A.5}$$

Since the diameter of the laser beam was less than the aperture height ($2s_1$), the condition on Y is always: $-s_1 \leq Y \leq s_1$. For condition (a), when aperture B "shadows" a portion of the last aperture:

$$d\Omega_a = \int_{-(X-s_2)}^{-(X-s_2)\frac{Z}{Z-L}} dx \int_{-(Y+s_1)}^{(s_1-Y)} dz \, \frac{Z_1}{(x^2 + Z_1^2 + z^2)^{3/2}} \tag{A.6}$$

The limits on both x and z integrations have been determined purely on the basis of geometric optics. Unfortunately the integrals cannot be performed exactly; however binomial expansions may be employed and only the leading term(s) retained. Corrections to the leading term are of order $(s_i/Z)^2$, which were less than 10^{-3} for the experimental conditions. Consequently to a very good approximation:

$$d\Omega_a \simeq \frac{2s_1}{Z_1^2}\left[\frac{s_2(2Z_1 - L) - L\bar{X}}{Z_1 - L}\right] \qquad (\bar{X} \geq s_2) \quad (A.7)$$

The solid angle integrals for conditions (b) and (c) may be calculated similarly:

$$d\Omega_b = \int_{-(\bar{X}+s_2)}^{s_2-\bar{X}} dx \int_{-(Y+s_1)}^{s_1-Y} dz \; \frac{Z_1}{(x^2 + Z_1^2 + z^2)^{3/2}} \qquad (A.8)$$

$$d\Omega_b \simeq \frac{4 s_1 s_2}{Z^2} \qquad (s_2 \geq \bar{X} \geq -s_2)$$

and

$$d\Omega_c = \int_{-\frac{(\bar{X}+s_2)}{(Z-L)}Z_1}^{-\bar{X}+s_2} dx \int_{-(Y+s_1)}^{s_1-Y} dz \; \frac{Z_1}{(x^2 + Z^2 + z^2)^{3/2}} \qquad (A.9)$$

$$d\Omega_c \simeq \frac{2s_1}{Z^2}\left[\frac{s_2(2Z - L) + L\bar{X}}{Z_1 - L}\right] \qquad (\bar{X} \leq -s_2)$$

The equation for n_{sc} now is:

$$n_{sc} = n_{sc}^{(a)} + n_{sc}^{(b)} + n_{sc}^{(c)} \qquad (A.10)$$

where, for example

$$n_{sc}^{(a)} \equiv N_o \sigma(\Omega) \iiint_{(a)} n(\underline{r})\, d\Omega_a(\underline{r})\, d^3r \qquad (A.11)$$

The calculation of these integrals for an arbitrary direction of laser beam travel in the XZ plane requires a new coordinate system (u,v,w). As shown in Fig. A.3, its origin is located at $(0,0,R_o)$ with respect to the (X,Y,Z) coordinate system, and the u-axis, which coincides with the direction of laser beam travel, is rotated an angle α with respect

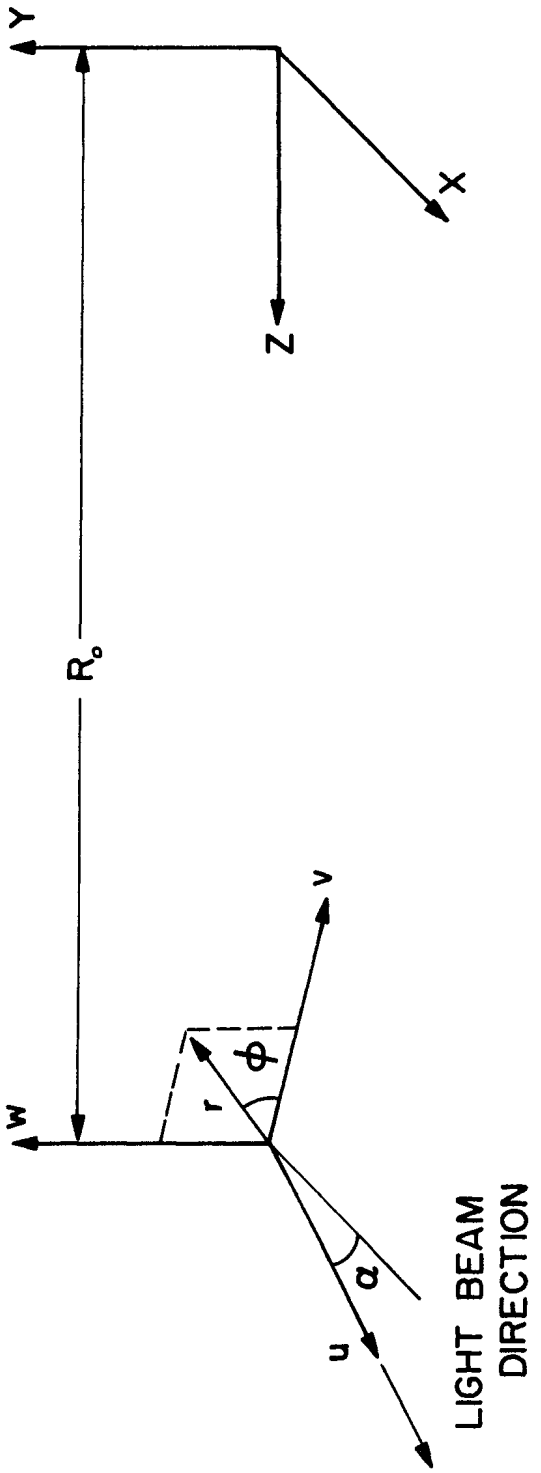

Fig. A.3. Schematic of coordinate systems used for calculations of n_{sc}.

to the X axis. Consequently the two systems are connected by:

$$\begin{aligned} X &= u\cos\alpha + v\sin\alpha \\ Y &= w \\ Z &= R_o + u\sin\alpha - v\cos\alpha \end{aligned} \tag{A.12}$$

The integrals of (A.10) are most conveniently evaluated if a cylindrical coordinate system (r,ϕ,u) is employed, where:

$$v = r\cos\phi \quad ; \quad w = r\sin\phi \tag{A.13}$$

So:

$$\begin{aligned} X &= u\cos\alpha + r\cos\phi\sin\alpha \\ Y &= r\sin\phi \\ Z &= R_o + u\sin\alpha - r\cos\phi\cos\alpha \end{aligned} \tag{A.14}$$

The following assumptions are now employed:

(a) The incident light beam is parallel and well-collimated. This neglects the actual convergence of the laser beam through the scattering volume; however a separate analysis has demonstrated that convergence error was negligible in this experiment.

(b) The medium through which the beam travels is optically thin, and hence n is independent of the coordinate u. For gases of the type studied in this work, this is an excellent assumption.

(c) The beam is of uniform intensity across a circular cross section. This assumption somewhat simplifies the analysis. It may be

easily demonstrated that the final results for n_{sc} are independent of beam shape and intensity distribution as long as the beam height is less than $2s_1$.

Summarizing, the light beam is assumed to be contained in a cylindrical envelope of radius r_o and to be of uniform intensity. Consequently, $n(r,\phi,u)$ is:

$$n(r,\phi,u) = \begin{cases} C & r \leq r_o \\ 0 & r > r_o \end{cases} \qquad \text{(A.15)}$$

Employing this assumption and substituting Eqs. (A.7) and (A.14) into (A.11), $n_{sc}^{(a)}$ becomes:

$$n_{sc}^{(a)} = 2N_o\sigma(\Omega)s_1 C \int_0^{r_o} r\,dr \int_0^{2\pi} d\phi$$

$$(x)\int_{u_1}^{u_2} du \frac{s_2(2R_o + 2u\sin\alpha - 2r\cos\phi\cos\alpha - L) - L(u\cos\alpha + r\cos\phi\sin\alpha)}{(R_o + u\sin\alpha - r\cos\phi\cos\alpha)^2(R_o + u\sin\alpha - r\cos\phi\cos\alpha - L)} \qquad \text{(A.16)}$$

The lower limit u_1 of the u-integration is determined by the intersection of the cylindrical light beam with a plane passed through the $X = s_2$ edges of the two defining apertures, and the upper limit u_2 is determined by the intersection of the cylinder with a plane passed through the $X = -s_2$ edge of aperture "A" and the $X = s_2$ edge of aperture "B." Thus for u_1:

$$\frac{X}{s_2} = 1$$

which may be solved:

$$u_1 = \frac{1}{\cos\alpha}(s_2 - r\cos\phi\sin\alpha) \qquad \text{(A.17)}$$

Similarly for u_2:

$$-\frac{X}{s_2} + \frac{2Z}{L} = 1$$

or

$$u_2 = \frac{s_2(2R_0 - L) - r\cos\phi(L\sin\alpha + 2s_2\cos\alpha)}{L\cos\alpha - 2s_2\sin\alpha} \qquad (A.18)$$

The evaluation of the integrals of (A.10) is a very tedious, but straightforward task. We will leave many of the details to the interested reader, and briefly outline the method employed. Since the integrals of (A.16) cannot be performed analytically, the first term in the denominator is expanded in powers of $1/R_0$:

$$n_{sc}^{(a)} \simeq \frac{2N_0\sigma s_1 C}{R_0^2}\int_0^{r_0} dr \int_0^{2\pi} d\phi \int_{u_1}^{u_2} du \, \frac{a_1 u + a_2}{a_3 + u\sin\alpha}$$

$$\times\left[1 + \frac{1}{R_0}(2r\cos\phi\cos\alpha - 2u\sin\alpha) + O\left(\frac{1}{R_0}\right)^2\right] \qquad (A.19)$$

where

$$\begin{aligned} a_1 &\equiv (2s_2\sin\alpha - L\cos\alpha) \\ a_2 &\equiv s_2(2R_0 - L) - r\cos\phi(2s_2\cos\alpha + L\sin\alpha) \\ a_3 &\equiv R_0 - L - r\cos\phi\cos\alpha \end{aligned} \qquad (A.20)$$

First considering the leading term only:

$$\begin{aligned} I_1 &\equiv \int_0^{r_0} r\,dr \int_0^{2\pi} d\phi \int_{u_1}^{u_2} du \, \frac{a_1 u + a_2}{a_3 + u\sin\alpha} \\ &= \int_0^{r_0}\int_0^{2\pi} r\,dr\,d\phi \, \frac{1}{\sin\alpha}\left[-\left(a_2 - \frac{a_1 a_3}{\sin\alpha}\right)\ln\left(1 - 2\frac{s_2}{L}\tan\alpha\right) + a_1(u_2 - u_1)\right] \end{aligned} \qquad (A.21)$$

where it has been observed that $\int_0^{2\pi} d\phi \cos\phi = 0$. Performing the remaining angular and radial integrations and using the expressions given above for a_1, a_2, a_3, u_1, u_2:

$$I_1 = -\frac{\pi r_o^2 L}{\sin\alpha}\left[s_2 + (R_o - L)\operatorname{ctn}\alpha\right]\left[\ln\left(1 - \frac{2s_2}{L}\tan\alpha\right) + \frac{2s_2}{L}\tan\alpha\right]$$

Expanding the logarithm and keeping terms in the expansion to $O(1/L^2)$, the integral becomes:

$$I_1 \simeq \frac{2\pi r_o^2 s_2^2 (R_o - L)}{L\cos\alpha}\left[1 + \frac{s_2}{R_o - L}\tan\alpha + \frac{4s_2}{3L}\tan\alpha + O\left(\frac{1}{L}\right)^2\right] \tag{A.22}$$

Returning to Eq. (A.19) and now considering the terms which are of order $1/R_o$, we must compute the following integral:

$$I_2 \equiv \frac{2}{R_o}\int_0^{r_o} r\,dr \int_0^{2\pi} d\phi \int_{u_1}^{u_2} du\, \frac{a_4 u^2 + a_5 u + a_6}{a_3 + u\sin\alpha} \tag{A.23}$$

where

$$\begin{aligned} a_4 &\equiv -a_1\sin\alpha \\ a_5 &\equiv r a_1 \cos\alpha\cos\phi - a_2\sin\alpha \\ a_6 &\equiv r a_2 \cos\alpha\cos\phi \end{aligned} \tag{A.24}$$

After the u integration is performed, I_2 breaks up into three parts:

$$I_2 \equiv I_{21} + I_{22} + I_{23} \tag{A.25}$$

where

$$I_{21} = \int_0^{r_o} r\,dr \int_0^{2\pi} d\phi \left(-\frac{a_4 a_3}{\sin^2\alpha} + \frac{a_5}{\sin\alpha} \right)(u_2 - u_1)$$

$$I_{22} = \int_0^{r_o} r\,dr \int_0^{2\pi} d\phi \left(-\frac{a_4 a_3^2}{\sin^3\alpha} + \frac{a_5 a_3}{\sin^2\alpha} - \frac{a_6}{\sin\alpha} \right) \ln\left(1 - \frac{s_2}{L}\tan\alpha\right) \qquad \text{(A.26)}$$

$$I_{23} = \int_0^{r_o} r\,dr \int_0^{2\pi} d\phi \; \frac{a_4}{2\sin\alpha} (u_2^2 - u_1^2)$$

Using the expressions for a_1, a_2, a_3, a_4, a_5, u_1, and u_2, and performing the angular integrations, these are:

$$I_{21} = -4\pi s_2 L \int_0^{r_o} r\,dr \frac{\left[(R_o - L)\cos\alpha + s_2 \sin\alpha\right]^2}{\sin\alpha\cos\alpha(L\cos\alpha - 2s_2\sin\alpha)}$$

$$-2\pi s_2 \int_0^{r_o} r^3 dr \; \frac{2s_2 + L\tan\alpha}{L\cos\alpha - 2s_2\sin\alpha}$$

$$I_{22} = \frac{-2\pi L(R_o - L)}{\sin^2\alpha} \int_0^{r_o} r\,dr \left[(R_o - L)\cos\alpha + s_2\sin\alpha\right] \ln\left(1 - \frac{2s_2}{L}\tan\alpha\right)$$

$$I_{23} = 4\pi s_2^2 \int_0^{r_o} r\,dr \; \frac{R_o(R_o - L) + s_2\tan\alpha(L - s_2\tan\alpha)}{L\cos\alpha - 2s_2\sin\alpha}$$

$$+2\pi s_2 \int_0^{r_o} r^3 dr \; \frac{L\tan\alpha + s_2(1 - \tan^2\alpha)}{L\cos\alpha - 2s_2\sin\alpha} \qquad \text{(A.27)}$$

Peforming the radial integrations, adding I_{21}, I_{22}, and I_{23} tegether, and rearranging, I_2 becomes:

$$I_2 \approx \frac{4\pi r_o^2 s_2^2 \tan\alpha}{\cos\alpha} \frac{(R_o - L)}{L} \left[-\frac{s_2}{3}\left(\frac{2R_o + L}{LR_o}\right) \right.$$

$$\left. + \frac{s_2^2}{R_o}\tan\alpha \left(-\frac{20}{3L} - \frac{1}{R_o - L} + \frac{4R_o}{L^2} \right) + O\left(\frac{s_2}{R_o}\right)^3 \right]$$

$$- \frac{4\pi r_o^2 s_2^2}{\cos\alpha} \left[\frac{r_o^2}{4\pi R_o \cos^2\alpha} + O\left(\frac{r_o}{L}\right)^3 \right] \qquad \text{(A.28)}$$

Now combining I_1 and I_2, we have:

$$n_{sc}^{(a)} \simeq \frac{4\pi v_o^2 C N_o \sigma(\Omega) s_1 s_2^2 (R_o - L)}{R_o^2 L \cos\alpha} \left[1 + \frac{s_2}{R_o L} + \tan\alpha \right.$$

$$\left. + \frac{4 s_2}{3L} \tan\alpha - \frac{2 s_2 (2R_o + L) \tan\alpha}{3 R_o L} + O\left(\frac{s_2}{R_o}\right)^2 \right] \tag{A.29}$$

The calculations of $n_{sc}^{(b)}$ and $n_{sc}^{(c)}$ follow the same procedures, with the following results:

$$n_{sc}^{(b)} = 4 N_o \sigma(\Omega) C s_1 s_2 \int_0^{r_o} r\,dr \int_0^{2\pi} d\phi \int_{-(r\cos\phi\sin\alpha + s_2)/\cos\alpha}^{(s_2 - r\cos\phi\sin\alpha)/\cos\alpha} du$$

$$(x) \left(\frac{1}{R_o + u\sin\alpha - r\cos\phi\cos\alpha} \right)^2 \tag{A.30}$$

or

$$n_{sc}^{(b)} \simeq \frac{8\pi r_o^2 C N_o \sigma(\Omega) s_1 s_2^2}{R_o^2 \cos\alpha} \left[1 + O\left(\frac{s_2}{R_o}\right)^2 \right] \tag{A.31}$$

and

$$n_{sc}^{(c)} = 2 N_o \sigma(\Omega) s_1 C \int_0^{r_o} r\,dr \int_0^{2\pi} d\phi \int_{-(r\cos\phi\sin\alpha + s_2)/\cos\alpha}^{-\frac{s_2(2R_o - L) + r\cos\phi(L\sin\alpha - 2s_2\cos\alpha)}{L\cos\alpha + 2 s_2 \sin\alpha}} du$$

$$(x) \frac{s_2(2R_o + 2u\sin\alpha - 2r\cos\phi - L) + L(u\cos\alpha + r\cos\phi\sin\alpha)}{(R_o + u\sin\alpha - r\cos\phi\cos\alpha)^2 (R_o + u\sin\alpha - r\cos\phi\cos\alpha - L)} \tag{A.32}$$

or

$$n_{sc}^{(c)} \simeq \frac{4\pi r_o^2 C N_o \sigma(\Omega) s_1 s_2^2 (R_o - L)}{R_o^2 L \cos\alpha} \left[1 - \frac{s_2}{R_o - L} \tan\alpha \right.$$

$$\left. - \frac{4 s_2}{3L} \tan\alpha + \frac{2 s_2 (2R_o + L) \tan\alpha}{3 R_o L} + O\left(\frac{s_2}{R_o}\right)^2 \right] \tag{A.33}$$

In adding $n_{sc}^{(a)}$ and $n_{sc}^{(c)}$ together, the first order correction terms cancel, leaving only second and higher order correction terms (in the parameter s_2/R_o). We have more fully investigated the importance of the second order terms and have found they contribute a total correction of less than 1%. Consequently, to reasonable accuracy:

$$n_{sc} = N_o n_1 \gamma \sigma(\Omega) \tag{A.34}$$

where

$$\gamma \equiv \left(\frac{4 s_1 s_2}{R_o^2}\right)\left(\frac{2 s_2 R_o}{L \sin\Theta}\right) \tag{A.35}$$

and n_1 is the total number of incident photons ($\pi r_o^2 C$). It is evident that $4s_1s_2/R_o^2$ is the nominal solid angle of scattering $d\Omega_s$. Furthermore, $2s_2R_o/L \sin\Theta$ can be identified as the effective length of beam viewed by the detection.*

*The scattering angle Θ is related to α by $\Theta = \alpha + \frac{\pi}{2}$.

REFERENCES

1. R. Ananthakrishnan, Proc. Ind. Acad. Sci. 2, 133 (1935).

2. R. Ananthakrishnan, Proc. Ind. Acad. Sci. 2, 153 (1935).

3. D. Kent Anderson, Phys. Rev. 137, A21 (1965).

4. S. Bhagavantam, Nature 130, 740 (1932).

5. S. Bhagavantam, The Scattering of Light and the Raman Effect, Chemical Publishing Company, Brooklyn, N. Y., 1942.

6. M. Born, Optik, Julius Springer, Berlin, 1933.

7. G. Breit, Revs. Mod. Phys. 4, 504 (1932); 5, 91 (1933).

8. N. Bridge and A. Buckingham, J. Chem. Phys. 40, 2733 (1964).

9. A. D. Buckingham and J. A. Pople, Trans. Faraday Soc. 51, 1173, 1179 (1955).

10. A. D. Buckingham and M. Stephen, Trans. Faraday Soc. 53, 884 (1957).

11. J. Cabannes, Comptes Rendus 160, 62 (1915).

12. J. Cabannes, Ann. der Phys. 15, 5 (1921).

13. J. Cabannes and J. Granier, J. de Phys. 4, 429 (1923).

14. J. Cabannes, La Diffusion Moleculaire de la Lumiere, Les Presses Universitaires de Paris, 1929.

15. E. V. Condon and G. H. Shortley, The Theory of Atomic Spectra, University Press, Cambridge, 1964.

16. T. C. Damen, R.C.C. Leite, and S.P.S. Porto, Phys. Rev. Letters 14, 9 (1965).

17. J. Daure, Comptes Rendus 180, 2032 (1925).

18. Alan DeSilva, University of Maryland, private communication.

19. F. R. Dintzis and R. S. Stein, J. Chem. Phys. 40, 1459 (1964).

REFERENCES (Continued)

20. P.A.M. Dirac, Proc. Roy. Soc. (London) 114, 710 (1927).

21. R. Gans, Ann. der Phys. 65, 97 (1921).

22. T. V. George, L. Goldstein, L. Slama, and M. Yokoyama, Phys. Rev. 137, A369 (1965).

23. Andrew Guthrie, Vacuum Technology, John Wiley and Sons, New York, 1963.

24. T. H. Havelock, Phil. Mag. 3, 158, 433 (1927).

25. Joseph O. Hirschfelder, Charles F. Curtiss, R. Byron Bird, Molecular Theory of Gases and Liquids, John Wiley and Sons, New York, 1954.

26. S. Kielich, Acta. Phys. Polonica 19, 149 (1960).

27. Hans Kopfermann, Zeits. fur Physik 87, 460 (1934).

28. H. A. Kramers and W. Heisenberg, Zeits. fur Physik 31, 681 (1925).

29. Landolt-Börnstein Zahlenwerte and Funktionen aus Physik, Chemie, Astronomie, Geophysik, und Technik, II Band, 8 Teil, Optische Konstanten, Springer-Verlag, Berlin, 1962.

30. R.C.C. Leite, R. S. Moore, S.P.S. Porto, and J. E. Ripper, Phys. Rev. Letters 14, 7 (1965).

31. M. Lewis, Phys. Rev. 41, 389 (1932).

32. André Massoulier, Comptes Rendus 251, 358 (1960); 255, 1093 (1962).

33. André Massoulier, J. de Phys. 24, 342 (1963).

34. C. A. Mead, Phys. Rev. 110, 359 (1958).

35. Albert Messiah, Quantum Mechanics, North Holland Publishing Company, Amsterdam, 1964.

36. Charlotte E. Moore, Atomic Energy Levels, Vol. 3, Circular of the National Bureau of Standards 467, 1958.

37. S. Parthasarathy, Ind. J. Phys. 7, 139 (1932).

REFERENCES (Continued)

38. S. Parthasarathy, Ind. J. Phys. 25, 22 (1951).

39. C. M. Penney, Phys. Rev. Letters, 14, 423 (1965).

40. C. M. Penney, Doctoral Thesis, The University of Michigan, 1965.

41. G. Placzek, Rayleigh-Streuung und Raman Effekt, Handbuch der Radiologie, Vol. 6, Part 2, Akademische Verlagsgesellschaff, 209 (1934); English Transl. UCRL-Trans-526(L).

42. S.P.S. Porto, J. Op. Soc. Am. 56, 1585 (1966).

43. C. V. Raman and K. S. Rao, Phil. Mag. 46, 426 (1923).

44. C. V. Raman, Ind. J. Phys. 2, 387 (1928).

45. K. R. Ramanathan, Proc. Roy. Soc. (London) 107, 684 (1924).

46. I. R. Rao, Ind. J. Phys. 2, 61 (1927).

47. Lord Rayleigh, Phil. Mag. 41, 447 (1871).

48. Lord Rayleigh, Phil. Mag. 47, 375 (1899).

49. Lord Rayleigh, Phil. Mag. 35, 373 (1918).

50. M. Rotenberg, R. Bivins, N. Metropolis, and J. K. Wooten, Jr., The 3-J and 6-J Symbols, MIT Press, 1959.

51. A. Rousset, Comptes Rendus 204, 1725 (1937).

52. Shardanand, Phys. Rev. 160, 67 (1967).

53. L. Silberstein, Phil. Mag. 33, 92, 215, 521 (1917).

54. M. V. Smoluchowski, Bull. Acd. Soc. Cracovie 218 (1916).

55. R. J. Strutt, Proc. Roy. Soc. (London) 94, 453 (1918).

56. R. J. Strutt, Proc. Roy. Soc. (London) 95, 155 (1919).

57. R. J. Strutt, Proc. Roy. Soc. (London) 98, 57 (1920).

58. O. Theimer, Phys. Rev. Letters 13, 622 (1964).

REFERENCES (Concluded)

59. O. Theimer and R. Paul, J. Chem. Phys. 42, 2508 (1965).

60. H. Volkmann, Ann. der Phys. 24, 457 (1935).

61. Robert D. Watson and Maynard D. Clark, Phys. Rev. Letters 14, 1057 (1965).

62. Alfons Weber, Sergio P. S. Porto, Leonard E. Cheesman, and Joseph J. Barrett, J. Op. Soc. Am. 57, 19 (1967).

63. P. G. Wilkinson, J. Quant. Spectry. Radiative Transfer 6, 823 (1966).